12-20-2009

Enhancement of the Properties of Polymer by using Carbon Nanotubes

Wai-Yin Tam
University of New Orleans

Enhancement of the Properties of Polymer by using Carbon Nanotubes

A Dissertation

Submitted to the Graduate Faculty of the
University of New Orleans
in partial fulfillment of the
requirements for the degree of

Doctor of Philosophy
in
Engineering and Applied Science

by

Wai-Yin Tam

BEng.(Hon), The Hong Kong Polytechnic University, 2000
MEng., The Hong Kong Polytechnic University, 2000

December, 2009

ACKNOWLEDGEMENTS

I would like to thank for my chief supervisor Prof. David Hui for his intellectual guidance, support and patience throughout the research project in all these years. I am grateful to have opportunity to work with him, and able to adapt to the scientific world under his supervision. Besides, I would like to thank Prof. Hui for offering me graduate research assistantship and the possibility to travel and visit other research centers and facilities and attend the ICCE conference. The warmest thanks go to his wife, Ms. Shun-Ying Hui for her care and deep involvement during my study in US.

I am appreciative and thankful to my department head, Prof. Paul Herrington, for his valuable suggestions and helps regarding my enrollment and financial problems in the University of New Orleans (UNO). Without his help, I would have a lot of difficulties in returning to UNO and have my dissertation defense. Additionally, I would like to thank for the support and guidance from the lecturers in the faculty and staff of the Mechanical Engineering Department at UNO during my course of studies. I am especially grateful to Dr. Kazim M. Akyuzlu, Dr. Paul Schilling, Ir. Robert H. Lipp, Dr. Melody Verges, Dr. Salvadore Guccione, Dr. Ram V. Mohan, and Ms. Deborah B. Duzac for all that they have taught me and all the help they offered. Moreover, special thanks to Prof. Dongming Wei from Department of Mathematics for his assistance and encouragement during my learning in UNO. His kindness and patience in teaching have led me to overcome a lot of obstacles during my studies and able to enjoy the fun in learning.

I would also like to express my deepest gratitude towards my co-supervisor Dr. Alan Lau, the Associated Professor of Mechanical Engineering Department in The Hong Kong Polytechnic University, for his advices, encouragement, patience and gentleness during my time in Hong Kong. Without his enthusiasm and guidance, this research project and dissertation would never have been completed. Thanks for his understanding and support during my difficult time with family; I am able to move on again in my research studies. His passion and perspective also helped me to find my direction in work and push me towards scientific achievement.

I would like to extend a great deal of thanks to my peers and my colleagues, Dr. Alan's group, for cooperation and support every time when I have complexities. I have broadened the way of thinking in research through fruitful discussions with them. Special thanks to my colleague, Ms. Karen Cheung, who is always willing to provide valuable opinions to me on my works and family issue. I appreciate the friendship with her.

I am also indebted to the technicians, Mr. Jeremy Yeung of Material Research Center and Mr. C.N. Tang of Mechanical Engineering Department in The Hong Kong Polytechnic University. Their assistances in using the equipments and useful suggestions on my experiments are indispensable for the accomplishments of my work.

Finally, I would like to utter my immense gratitude to my family for their understanding and support. Sincere thankfulness to my parents for letting me continue my studies and never want me to give up even our family was in a bad situation during my research time in Hong Kong.

TABLE OF CONTENTS

LIST OF FIGURES

LIST OF TABLES

ABSTRACT

The outstanding properties of carbon nanotubes (CNTs) have stimulated a large number of researches to explore the potential of using them as reinforcement in polymer composites. Although many studies have reported the enlighten improvement of the materials properties by using CNTs as reinforcement, there are no promising and optimal results have been concluded to date. This thesis aims at studying the mechanical properties on thermoset polymer, Epoxy, by employing a small amount of carbon nanotubes as reinforcement. Two different types of nanotube-based composites are prepared i.e. a raw single-walled carbon nanotube (SWNT) composites and a functionalized single-walled carbon nanotube (FSWNT) composite. Chemical functionalization on SWNTs with carboxyl functional group (COOH) aims at modifying the end caps of nanotubes, so to provide covalent bonding of SWNTs to the polymer matrix during manufacturing of composite systems. Different weight percentages (wt %) of each type of SWNTs are added into the composite system. Standard test methods are performed on these nanotube composite systems and satisfactory results were achieved when the weight percentages of both types of SWNTs increased. Through the comparison between two systems (raw SWNTs and FSWNTs), the FSWNT reinforced composite is found to provide a better improvement on the mechanical properties as compared with the SWNT reinforced system. The integrity of both composite systems is examined by using Scanning Electronic Microscopy (SEM). The SEM images of the composites indicated the derivation in wetting and bonding between the nanotubes (both SWNTs and FSWNTs) and epoxy resin, and the FSWNTs provide an eminent dispersion when compared with the SWNTs in the composite system. Moreover, thermal testings are employed to further investigate the interfacial interaction between the nanotubes and the polymer matrix.

Molecular Dynamics (MD) simulations are also carried out to investigate the structural change of a SWNT under different temperature-controlled manufacturing environments. Swivel of the SWNT was noticed as the temperature increased. Such alteration in structure form can provide physical interlocking between SWNT and its surrounding polymer system. Thus, its overall mechanical and thermal properties can be enhanced.

Keywords: Single-walled carbon nanotube, functionalized single-walled carbon nanotube, nanotube based composites, mechanical properties, thermal properties, molecular simulation.

CHAPTER 1

INTRODUCTION

1.1 MOTIVATION AND SCOPE

For centuries, scientists have been looking for new ways to improve the living standard of mankind. Their continuous innovations on different infrastructures such as bridges, aircrafts, power plants, have shortened the distance between people living in the world. Although many innovated ideas and technologies have been introduced, traditional materials for example, steel and polymer, are not sufficient to be used to meet those performance designed. Thus, the development of new types of materials is urged. In order to achieve this goal, much research has been carried out which aims at improving the properties of traditional materials by being reinforced with different substances. Advanced composite materials are, therefore, invented to overcome incapabilities of existing materials for the engineering applications nowadays.

In this century, advanced composite materials have become more and more popular for different industrial applications due to their attractive performances. Over the past decades, advanced reinforced polymer composites have been tremendously used as primary structural components in a wide range of engineering applications varying from small sport utilities such as the shaft of a golf club, to large infrastructures. Their outstanding properties like high specific strength to weight ratio, superior thermal and corrosion resistance, transparency to radiation, make them appreciated by those economic important applications

in which high performance, light weight, less production cost and high manufacturing rate are strongly deserved.

Among all substances used as reinforcements in advanced composite materials, carbon nanotube (CNT) has been claimed as a new star for this purpose. Since the discovery of CNT by S. Iijima in 1991 [1], scientists have devoted all their energies to study the possibility of applying the CNT in our daily living. At the nanoscale, the unique form of CNT exhibits excellent mechanical and physical properties with its Young's modulus above 1 TPa, elastic strain as high as 5% [2,3]**,** failure strength of about 150GPa [4], and exceptional resilience has been reported. These superior properties of CNT combined with its low density make it an ideal substance as reinforcement for advanced composites and provide the opportunities to produce a new type of strong and light weighted material. Due to its brilliant potential in applications, CNT based composites are proposed to be used as a major reinforcing material in different fields, especially in the space industry. Recently, the National Aeronautics and Space Administration (NASA) has been putting a lot of efforts in developing nanotube based composites in future human spaceflight [5]. The results obtained from experiments in fabricating and testing of these composites showing attractive mechanical properties improvements. Apart from this, CNT based composites are also promoted as the tensile element in the tether design of space elevator project from NASA, in which a CNT composite rope can reach stationary orbits of satellites [6, 7]. Construction would be a vast project: a tether would have to be built of a material that could endure tremendous stress while also being light-weight, cost-effective, and manufacturable in great quantities. CNT technology shows a great promise to meet this intention as materials currently available can not be able to meet these requirements.

Though CNTs are believed to be the major focus in the following decades, the specialties of CNT have not yet all being discovered. CNTs are found to agglomerate easily due to the high Van der Waals interactions arise from each nanotube [8]. This agglomeration not only causes poor dispersion of CNTs in polymer matrix, but also incurs slippage among CNTs [9], which results in poor load transfer inside resultant composites. Besides, the interfacial bonding between CNTs and polymer matrix also plays an important role in controlling the properties of CNTs composites under different loading conditions. Any impoverished bonding between media would cause failure in load transfer within the composite. These uncertainties in producing CNT-reinforced composites make CNT as a challenge to be fully utilized by the industry.

This research work aims at investigating the mechanical properties of polymer by employing CNTs as reinforcement. Single-walled carbon nanotube (SWNT) is the major interest as the reinforcement in the work while epoxy is chosen as the matrix due to its high availability in the market and is commonly adopted by engineering industry. Additionally, functionalization on SWNT is performed to examine its effect in dispersion and load transfer ability in the matrix. Molecular Dynamics (MD) simulation is applied to study the structural change of the SWNT during the temperature variation in the composite manufacturing process.

1.2 CARBON NANOTUBE

1.2.1 Background

In the mid of 1980s, Smalley, Koroto and co-workers at Rice University [10] discovered a new form of carbon, buckminsterfullerene C_{60}. This cage-like structure (often referred as “buckyball”) is composed of 60 carbon atoms bonded in hexagon and pentagon arrangement. Since its discovery, different forms of fullerenes have been observed such as C_{70} and C_{84} molecules. Carbon nanotubes being a member of the fullerene family were first observed by a Japanese electron microscopist S. Iijima of NEC in 1991. These nanotubes are long tubular fullerene where the walls of the tubes hexagonal carbon layers with graphite structure and the ends are closed with hemisphere of the C_{60} structure (Figure 1.1). Since then, nanotubes have been the focus of researches worldwide causing intense amount of investigations and predictions on the structure and properties of the nanotubes.

Carbon nanotubes can be divided into two categories; Single-walled carbon nanotube (SWNT) and Multi-walled carbon nanotube (MWNT) [4, 11, 12]. Also, these nanotubes can have different graphization and orientation providing them with singular characteristics.

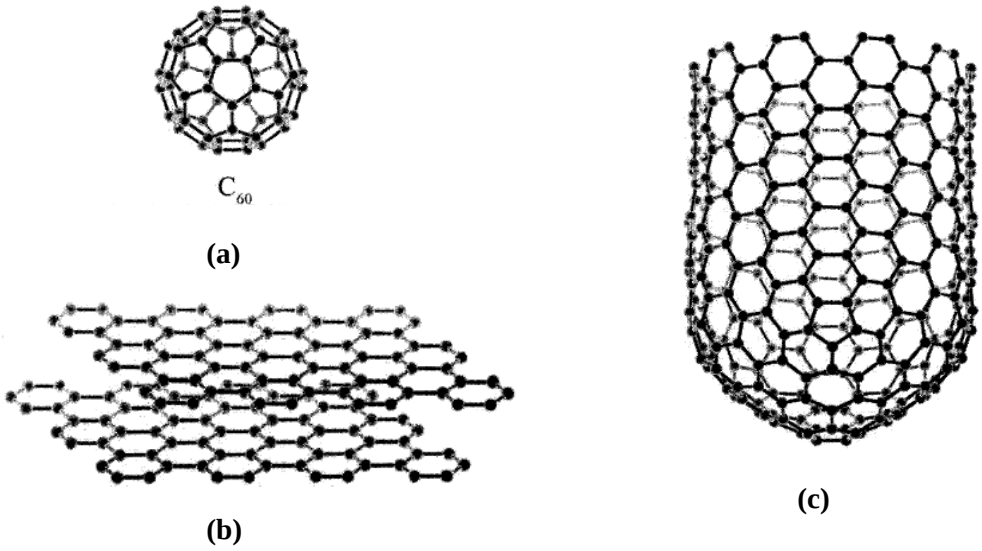

Figure 1.1 Various forms of carbon structure. (a) buckminsterfullerene C_{60}, (b) the graphite layers and (c) Nanotube with end closed with hemisphere of the C_{60}. [11]

1.2.2 Basic of Carbon Nanotube

Carbon nanotube can be visualized as a graphite sheet that has been rolled into a seamless tube. Various geometrical structures [13] can be obtained by changing the rolling direction. This difference in atomic arrangement together with the morphology, the diameter and length of the tube causing the CNTs exhibit totally diverse properties even in the same condition.

In general, CNTs can be divided into three main groups, armchair, zig-zag and chiral, depending on the tube charity. In order to characterize the chirality of CNTs, the chiral vector C_h and the chiral angle θ are employed.

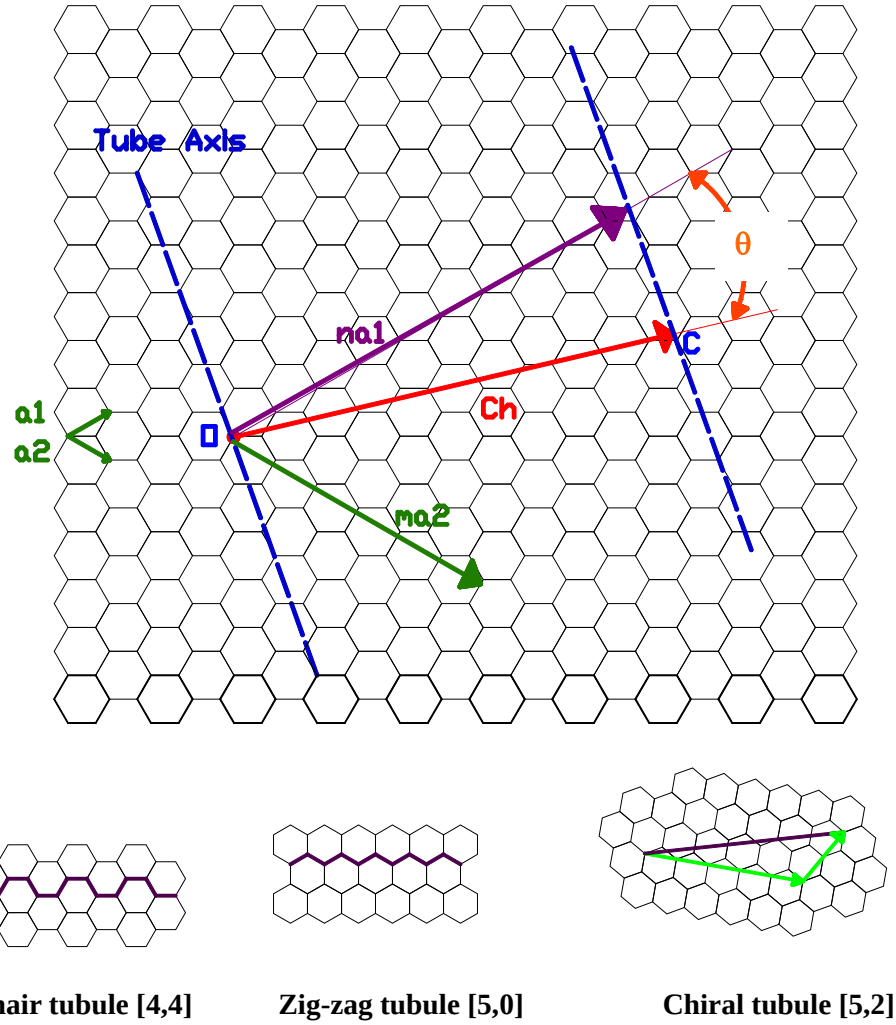

Figure 1.2 Illustration demonstrating how the nanotube is defined on a two dimensional graphene sheet.

In figure 1.2, it shows a two-dimensional graphene sheet with the indication of the chiral vector C_h and the chiral angle θ. This chiral vector can be defined as a line connected between two crystalographically equivalent sites O and C on the graphite structure. This vector can be considered as a roll-up vector and can be described by the formula [14]

$$C_h = n a_1 + m a_2$$

where the value (n,m) is the lattice translation indices and a_1, a_2 is the unit vector of the hexagonal lattice. The chiral angle is the measured angle between the chiral vector and the vector with indices (n,0). The two limiting cases exist when the chiral angle is at 0^o and 30^o.

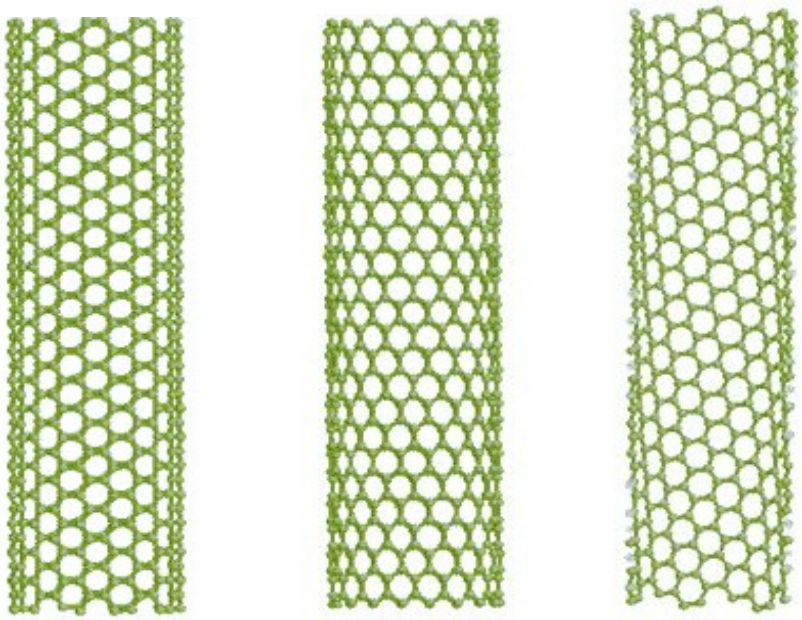

Figure 1.3 Schematic structures of SWNTs (a) A (10,10) armchair nanotube (b) A (12,0) zig-zag nanotube and (c) A (7,16) chiral tube.

The type of CNTs is highly depended on the chiral angle. When the angle is equal to 0^o, the CNT is defined as zig-zag nanotube with indices (n,0). On the other hand, if the angle is equal to 30^o, the CNT is defined as armchair nanotube with indices (n,n). For those nanotubes with angle other than 0^o and 30^o , ($0^o < \theta < 30^o$), are defined as chiral nanotube with indices (n,m). The schematic structures of nanotubes are shown in figure 1.3. Besides, the diameter of CNTs can be determined through the formula of chiral vector once those parameters are known. Table 1 summarizes the equations and parameters required for defining the geometry of the SWNT [15]:

Table 1.1 Parameters of carbon nanotubes [15]

Geometrical Parameter	**Symbol**	**Formula**	**Value**
Length of the Carbon Bond	$a_{c\text{-}c}$		1.42 Å
Length of unit vector	a	$a = \sqrt{3}\, a_{c-c}$	2.64 Å
Unit vectors	a_1, a_2	$a_1 = \left(\frac{\sqrt{3}}{2}, \frac{1}{2}\right) a$ $a_2 = \left(\frac{\sqrt{3}}{2}, -\frac{1}{2}\right) a$	In (x, y) coordinates
Chiral vector	C_h	$C_h = n a_1 + m a_2$	n, m are integers
Circumference of nanotube	L	$L = \lvert C_h \rvert = a\sqrt{n^2 + nm + m^2}$	$0 \le \lvert m \rvert \le n$
Diameter of nanotube	D	$d = \frac{L}{\pi} = a\,\frac{\sqrt{n^2 + nm + m^2}}{\pi}$	
Chiral Angle	θ	$\sin\vartheta = \frac{n+m}{2\sqrt{n^2 + nm + m^2}}$ $\cos\vartheta = \frac{2n+m}{2\sqrt{n^2 + nm + m^2}}$ $\tan\vartheta = \frac{\sqrt{3}\, m}{2n+m}$	$0 \le \theta \le 30°$

The chirality of CNTs is found relating to its material properties. CNTs can either be metallic or semi-conducting according to the chirality of tube [16], thus any changes in the chirality will strongly influence the electronic properties of nanotubes. Besides, mechanical properties of the CNTs rely on the chirality are also investigated. Robertson et al. [17] has

computed the strain energy of nanotubes by continuum elastic model and they found that the nanotubes exhibit softly behavior in small radius and chiral angle.

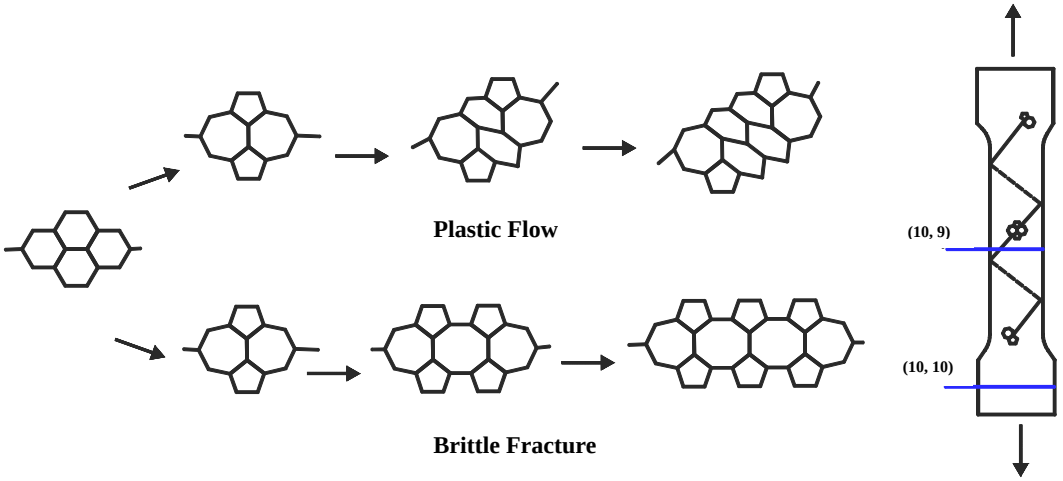

Figure 1.4 Schematics drawing of carbon nanotube undergoes Stone-Wales transformation during tensile condition. The transformation may result in plastic deformation of nanotube or causing brittle fracture due to crack initiation. The formation of Stone-Wales transformation introduces necking in the nanotube causes the diameter of the nanotube to alter stepwise [20].

Yakobson and co-workers [18, 19] pointed out that the CNTs are significantly resilient and able to sustain extreme strain with no signs of brittleness through simulations. Though the influence on CNTs due to its chirality is small, they claimed that the Stone-Wales transformation is one of the major reasons causing plastic deformation under tension. The Stone-Wales transformation is energetically favored as the initial defect-formation mechanism under tension. It involves rotation of a single C-C bond in the hexagonal lattice, and two neighboring pentagon-heptagon pairs are formed. Figure 1.4 shows a schematic proposed by Yakobson [20] on the transformation pathways of CNTs under tension. Besides, according to the theoretical prediction, Nardelli et al. [21] ascertained that the Stone-Wales transformation would result in ductile fracture for armchair nanotubes.

Apart from the chirality, the properties of CNTs are also highly depended on its variety; SWNT and MWNT. Each type of nanotubes has their own particular properties making them widely adopted in different applications. As mentioned, carbon nanotube is a graphene sheet rolled-over into a cylinder. It has diameter varies from 0.7-10nm, with the majority of SWNTs having diameters <2nm, and aspect ratio as high as 10^5 (aspect ratio is the ratio of length to diameter). These nanoscopic dimensions allow nanotubes to have large surface areas, which can enhance the interaction between the nanotube and polymer when CNTs are adopted as a reinforcing agent in polymer matrix. However, nanotubes can vary in size and are not always cylindrical in shape. It is found that the larger the nanotube, the more easy for them to bend due to its own weight.

On the other hand, MWNTs consist of numerous concentric SWNTs of varying diameter held together by weak Van der Waals forces. The tubes are separated by a distance of 3.4Å [13], which is slightly higher than the interplanar spacing in graphite. Besides, the interplanar bonding between the nanotubes is very weak compared to in-plane bonding. The diameter of MWNTs is of the order of 30nm [8, 22], it can range anywhere between 10 to 100nm, and MWNTs were actually the first type of nanotubes being discovered [1]. Figure 1.5 shows the transmission electron microscopy (TEM) analysis on crystal structures of carbon nanotubes including SWNT and MWNT with five layers (left), two layers (middle) and seven graphene layers (right).

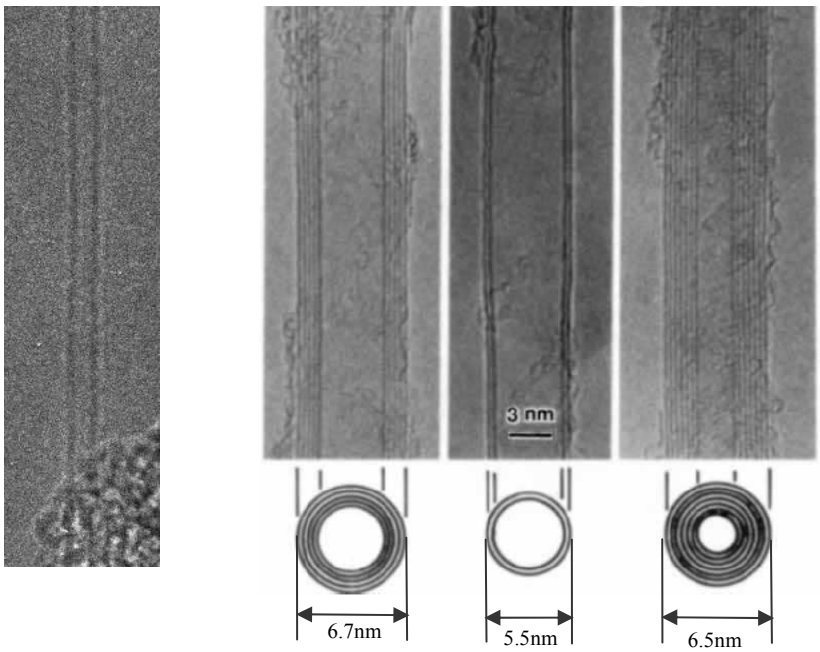

Figure 1.5 TEM Observations on microtubules graphitic carbon. (a) Single-walled carbon nanotube [23] and (b) multi-walled carbon nanotubes with different numbers of graphene layers [1].

It is observed that nanotubes are commonly found as ropes of several (20-100) nanotubes [24]. These ropes are bundles of tubes packed together in an orderly manner. CNTs in these ropes are usually of uniform diameter and are weakly coupled by Van der Waals forces. It is also noticed that the individual SWNTs packed into a closed-packed triangular lattice with lattice constant of about 17Å as indicated in figure1.6. Besides, Gao et al. [25] shown that the density, lattice parameter, and interlayer spacing of the ropes is dependent on the chirality of the tubes in the mat.

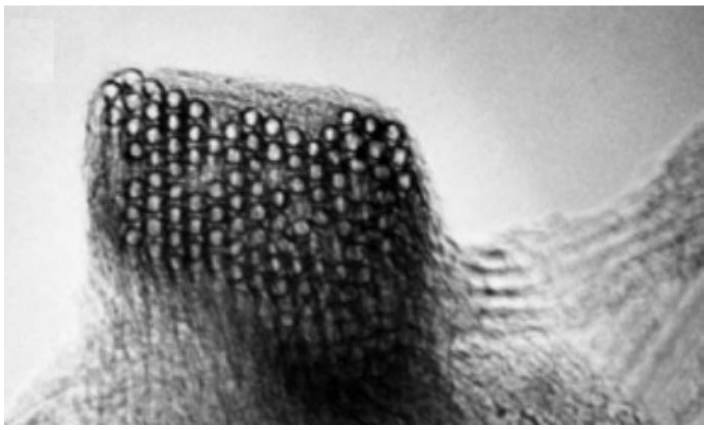

Figure 1.6 TEM image of the cross-section of a rope of SWNTs, which are with uniform diameter around 1.4nm and packed in a triangular lattice. [24]

1.2.3 Synthesis of Carbon Nanotube

Since the discovery of carbon nanotubes, scientists have been searching for an efficient method which not only able to produce nanotubes with high purity and uniformity, but also can be operated at fast speed. Different synthesis methods are introduced to achieve this purpose, however, the production of nanotubes are seriously influenced by the parameters such as pressure and temperature. Any changes in those parameters may lead to poor fabrication of nanotubes. Nowadays, the most common adopted synthesis methods for single- and multi-walled carbon nanotubes includes Direct Current Arc Discharge [1, 26-28], Laser Ablation [29-31] and Chemical Vapor Decomposition (CVD) [32-36]. Although there are various synthesis methods for nanotubes manufacturing, each method has their own advantages and drawbacks. All these factors become the critical steps for industries when they decide which production method of nanotubes can fulfill their own needs the most.

1.2.3.1 Direct Current Arc Discharge

In 1991, Iijima [1] first observed MWNTs synthesized from direct current arc discharge technique. And a year later, Ebbesen and Ajayan [37] achieved to produce a macroscopic quantity of MWNTs at the gram level through an improved arc discharge technique. In general, the arc discharge technique involves the use of two opposing graphite rods as the electrodes separated a few millimeters apart. Electricity is running across the electrodes in a helium atmosphere, resulting in the vaporization of the electrode and the creation of hot plasma cloud. And the nanotubes are obtained from the re-condensation of hot plasma. During which, the nanotubes form only on the negative electrode, where the current flows. The voltage is about 20V while the temperature maintains at 2000-3000^{o}C [38].

The yield from this technique is up to 30 percent by weight and it able to produce both SWNTs and MWNTs with length up to 50 micrometer [39]. Netherless, the diameter of the nanotube is ranged from 2nm to 20mm. However, the products are normally tangled and deposited in random sizes, and coexistence of nanotubes with different chirality is found in the product.

1.2.3.2 Laser Ablation

Laser ablation technique has been widely used since the invention of high temperature superconductors. Similar to arc-discharge, this high energy process involves the vaporization of a graphite target in a hot temperature chamber with 4000-5000^{o}C [40] and the sweeping of inert gas (e.g. argon) across the chamber. The corresponding materials are allowed to deposit onto the cooler surface of the chamber or react with any catalysts (e.g. Cobalt-nickel) to assist the growth of nanotubes.

This synthesis technique is recognized as an efficient tool to produce SWNTs according to Thess [24]. And it has a yield over 70 percent of the volume of material with mostly the armchair type of SWNTs. The length and the diameter of the nanotube can be controlled through the variation of parameters like reaction temperature and catalyst composition. Moreover, the alignment of the growth nanotube can be achieved by using a cobalt coat silica plate. [41].

1.2.3.3 Chemical Vapor Decomposition

The carbon nanotubes were first formed by chemical vapor decomposition (CVD) in 1993. The motivation of develop this gas-phase technique was initiated by the limitation on the sample volume of nanotubes produced by the arc discharge and laser ablation techniques. Moreover, subsequent purification steps are required to separate the nanotubes from unwanted by-products in these two processes.

During CVD, carbon nanotubes are formed through the decomposition of a carbon-containing gas. The continuous supply of this gas acts as a carbon source for the growth of nanotubes. The final products obtained from this process can reach relatively high purity and thus the subsequent purification steps can be minimized. Smalley and co-workers [42] described a refined CVD process named HiPco (High-pressure conversion of carbon monoxide) for the large scale production of SWNTs with excellent purity. This gas-phase production process of SWNTs uses carbon monoxide (CO) as the carbon source under the operating temperature between 800-1200^{o}C. And by applying the pressure up to 10 atm, the disproportionation of CO molecules has been increased and thus enhances the growth of SWNTs. Apart from carbon monoxide, hydrocarbon gases are also employed as the carbon source in the CVD process to produce both SWNTs and MWNTs [43-46]. This process

involves the use of catalyst materials, which heat up to 500-1000^{o}C in a tube furnace, and the hydrogen gas as flowing media through the reactor. During which, the hydrogen molecules catalyzed by the transition metal are dissociated, and the carbon atoms are dissoluted and saturated in the metal nanoparticle. As the result, nanotubes would grow from the hydrocarbons, and with the amorphous carbon which may deposit on the surface of the nanotubes during the process. Though this type of CVD techniques may have impact on the purity, the nanotubes are allowed to grow on wide range of substrates at a lower operating temperature.

While having a promising advantage for industrial scale deposition in terms of its price/unit ratio, CVD are also able to synthesize vertically aligned carbon nanotubes with controlled diameter and length. Ren et al. [35] was the first to achieve the growth of straight, aligned carbon nanotube arrays using the substrates coated with catalyst. In the process, ammonia gas is used as the catalytic gas while acetylene gas is used as the carbon source as shown in figure 1.7(a). Electric field is utilized for the generation of plasma and a carbonized tungsten filament is employed to assist the dissociation of the reactive gases and supplies heat to the substrate. By varying the potential of electric field, the orientation of the carbon nanotubes can be controlled. Additionally, the graphitization and length of carbon nanotube can be regulated through altering the operating temperature and time while the diameter of it can be managed by adjusting the thickness of the catalyst. This type of CVD process using plasma as a gravity media is called as plasma-enhanced chemical vapor deposition (PECVD).

During PECVD, the plasma can be excited not only by direct current, but also by microwave frequency source. Bower and coworkers [47] showed that carbon nanotube can grow with vertical alignment in the microwave plasma-enhanced CVD (MPEVCD). The

alignment of nanotubes is resulted from the self-bias imposed on the substrate surface from the microwave plasma. Fan et al. have obtained ordered MWNT structures by CVD catalytically patterned substrates [48-50]. During CVD growth, squared iron patterns on porous silicon substrates are applied to allow the MWNTs self-assemble into aligned structures. These regularly positioned arrays of nanotube towers exhibit very sharp edges and corners with no nanotubes branching away from the blocks. The MWNTs inside each block are well aligned along the directional perpendicular to the substrate surfaces (figure 1.7(b)).

Apart from the synthesis of aligned MWNTs, growing SWNTs into structure with well controlled orientation is found to be possible by the similar method. Franklin et al. [51] found that ordered SWNTs could be directly grown by catalytically patterned substrates with methane as the flowing media. Suspend SWNTs networks with directionality on substrates containing lithographically patterned silicon pillars have been grown. Catalyst materials are transferred onto the tops of the pillars by the contact printing selectively. The methane employed in the CVD together with the substrates leads to the formation of practically ordered network from the suspended SWNTs as shown in figure 1.8.

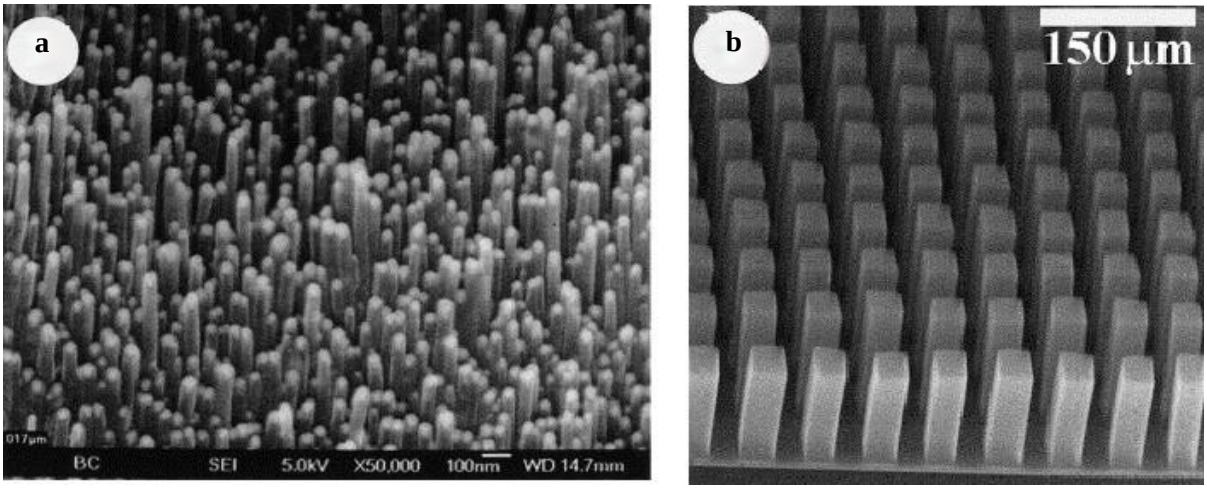

Figure 1.7 Aligned MWNTs synthesized by CVD methods on different substrates. (a) An oriented MWNTs grown on a glass substrate [47]. The cylindrical rods in the image are the MWNTs with the diameter in the order of tens of nanometer, which are grown perpendicular to the substrate. (b) Self-oriented MWNTs array is shown. The MWNTs are synthesized perpendicular to the substrate and closely packed into a tower-like structure [48-50].

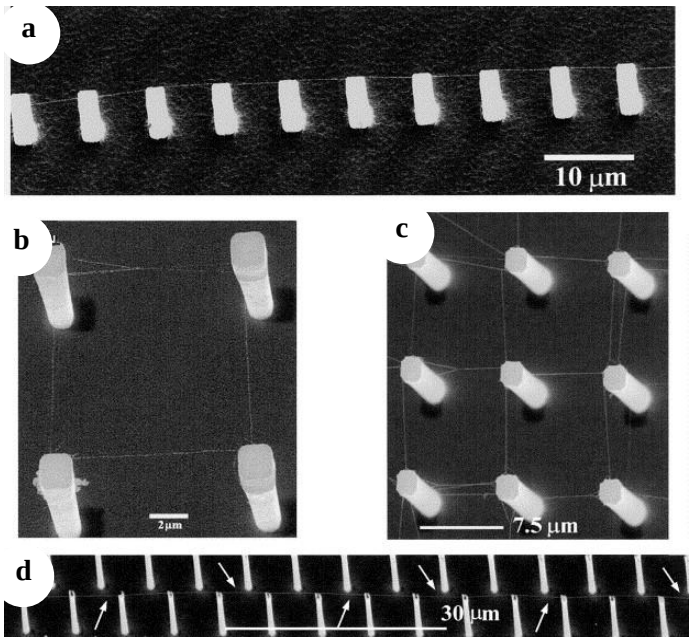

Figure 1.8 Self-directed grown of suspended SWNTs. (a) The suspended SWNTs are grown on a row of silicon pillars. The white post-like objects are the silicon pillars and the line-like structures linking the posts are SWNTs. (b) A squared formed from suspended SWNTs. (c) A square networks of suspended SWNTs. (d) The silicon pillars are linked by a long SWNT. These results demonstrate the ability of the growth of ordered SWNTs network through the self-assembled method, which could be employed into the fabrication of electronic devices [51].

Nanotubes have the orientations directed by the pattern of the pillars and served as the nucleus on the top of the pillars, where the CNTs start to grow. The passage of methane gas keeps the nanotube floating and waving in the reactor since the flow velocity near the bottom surface is much lower than that at the level of the tower tops. The difference of flow velocity prevents the SWNTs from being wedged by the bottom surface and the nearby towers provide fixation point for the growth of nanotubes. Thus, if the waving SWNTs contact adjacent towers during the process, the tube-tower Van der Waals interactions will catch the nanotubes and hold them aloft. This CVD method is able to produce SWNTs with length up 0.2 micrometer.

When comparing with the other nanotubes synthesis method, the CVD has the advantages of growing nanotube with high quality and large quantity, and allowing the growth of nanotubes in specified locations and with greater purity. Also, CNTs can be grown directly onto substrates or onto bulk-supported catalyst. The growth direction and orientation of nanotube can be controlled with electromagnetic field and the diameter can be adjusted by altering the size of catalytic nanoparticles used. All these factors make CVD more welcomed by the industries.

1.2.4 Characterization of Carbon Nanotube

Carbon nanotubes are unique for their approximately perfect cylindrical shape of seamless graphite, nano-scale diameter, and high aspect ratio. These materials are found to be much stronger than steel, with high flexibility and only one-sixth the weight of the steel. Their outstanding properties make them favored in different application. However, the exact values of these properties vary from study to study due to the variations in the

micro-structures of nanotubes formed from different synthesize methods. Thus, before they can be widely utilized today, it is important to understand their properties in different means.

1.2.4.1 Mechanical Properties

Carbon nanotubes have extraordinary mechanical properties and SWNTs are even claimed to be the strongest of any know fibers [4, 11]. However, direct measurements on this nano-scale structures and it composites are challenged. It is because there is complete lack of micro-mechanical characterization techniques for direct properties measurements, high limitations on sample size, difficulty in controlling the alignment and distribution of CNT, erratum of data obtain from indirect measurements, also inadequacy in test specimen preparation technique.

In order to obtain the properties of nanotubes, researchers have developed different novel methods for measurement. Treacy and co-workers [52] have examined the Young's modulus of MWNTs via the thermal vibration. Measurements of the elastic properties of the nanotubes were performed by using Atomic Force Microscope (AFM) together with the TEM. They concluded that the elastic modulus obtained from this direct measurement has the value of 1.8$\pm$0.9TPa. Wong et al. [53] used a scanning force microscope to bend MWNT which was fixed at one end mechanically. By evaluated the force-displacement relation of bending obtained from the experiments, a value of 1.26TPa was achieved for Young's modulus and the bending strength was measured to be be14.2 $\pm$ 8GPa. However, with similar approach, Poncheral et al. [54] found that its elastic modulus was below 1TPa by measuring the vibration of nanotubes in an electrical field.

Single-walled carbon nanotubes tend to arrange into a rope with close-packed stacking. Salvetat et al. [55] reported that the SWNTs ropes grown by the arc discharge method has an elastic modulus of about 1TPa, while those synthesized through the CVD of hydrocarbon provided a modulus with magnitude smaller by one to two orders. The SWNTs ropes were depositing onto a membrane having 200nm pores and the tip of AFM was used to bend them in the middle. The results showed that only highly ordered and well graphitized CNTs have stiffness comparable to graphite, meanwhile those synthesized by CVD are weaker due to the defects occurred inside the nanotube.

Yu et al. [56] has also demonstrated the use of AFM to measure the mechanical properties of MWNTs in the SEM. The MWNT was attached to the AFM tips at the ends and loaded under tension (figure 1.9). The AFM tip was used to stretch the MWNT till it broken, and also used as the force sensor to determine the actual force applied onto the nanotube. According to the stress-strain analysis from experiments, they concluded the elastic modulus of nanotubes ranged from 270 to 950GPa and the tensile strength is varied from 11 to 63GPa. Besides, it also observed that the outer layer of nanotubes rupture at the tensile limit and slides over the inner tubes. This implied the tubes within the MWNT are held by comparatively weak Van der Waals forces and the shear strength between the layers is small. Also, the maximum value of strain could be achieved to about 12% at failure. Further insight into the mechanical properties of SWNT ropes was investigated by Yu and co-workers [57]. They assumed that the outermost tube packed in the ropes carried the applied load throughout the experiments. The calculated elastic moduli are in the range of 320 to 1420GPa and the tensile strength varies from 13 to 52GPa.

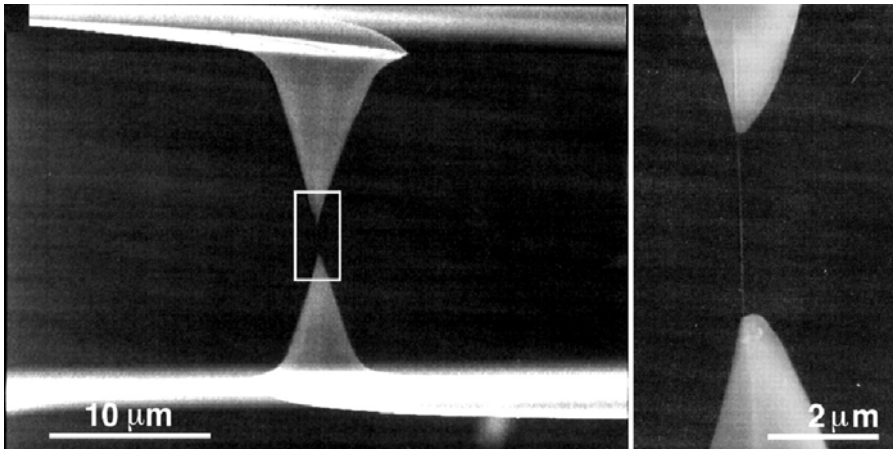

Figure 1.9 The SEM image of a MWNT attached to the AFM tips during the tensile testing [56].

Though the experimental studies show attractive behaviors of CNTs, the value of those mechanical properties were still diverse. In order to get a better picture of CNTs, plenty of theoretical analyses have been performed, so to validate the results obtained from experiments.

Overney et al. [58] were the first to evaluate the nanotube properties by atomistic simulation. Nanotubes with various number of carbon atom (100, 200 and 400 atoms) were used to study its low frequency mode and structural rigidity. They concluded that the nanotube exhibit the highest value of bending rigidity among all the presently available materials. Lu [59] studied the elastic properties of SWNT using an empirical lattice dynamics model, which has been successfully applied in evaluating the phonon spectrum and elastic properties of graphite. From the prediction, the elastic modulus is found to be about 1TPa, the shear modulus is closed to 0.45TPa and the bulk modulus is approximately equal to 0.74TPa which are comparable to those of diamond. Moreover, they concluded that the elastic modulus of nanotube is insensitive to its size and chirality. Apart from this, Lu has also studied the mechanical behavior of SWNT ropes through simulation. Each rope has 100-500 uniform SWNTs which were packed in hexagonal order. The results showed that the SWNTs

rope is very anisotropic in its elastic properties-soft on basal plane and stiff along the axial direction. Also, the predicted elastic moduli of ropes are about 0.6TPa. Hernandez et al. [60] preformed calculations by using similar approach. Nevertheless, they obtained the Young's modulus of 1.24TPa which is slightly higher than the value evaluated by Lu.

Popov et al. [61] studied the elastic modulus of SWNTs, with triangular crystal lattice, analytically based on a force constant lattice dynamics model. Calculations were executed on nanotubes with different chirality and they inferred the elastic modulus, bulk modulus and poisson's ratio are strongly depended on the tube radius. The bulk modulus reaches a maximum value of 38GPa for the SWNTs crystal with radius about 0.6nm. However, the works from Vaccarini and co-workers [62] obtained a different result. They examined the effect of SWNTs structure and chirality on the elastic properties, and found that the chirality of CNT only produces insignificant effect on the tensile modulus. On the other hand, among all 3 types of CNT, the chiral tube is the one shown an asymmetric torsional behavior. Nardelli et al. [21] have used molecular dynamics simulations to study the mechanical performance of nanotubes under uniaxial tensile loading and different temperature conditions. They reported that, under the tensile loading, the armchair nanotubes could release its excess strain through the formation of Stone-Waals defects. Under this condition, the stretched CNT could provide the strain more than 5%. Apart from this, they also concluded that all nanotubes exhibit brittle behaviors in a high strain at low temperature situation; however, the armchair nanotube would behave completely ductile at low strain and high temperature condition. Yakobson et al. [18, 63, 64] studied the inelastic behavior of nanotubes by using a realistic many-body Tensoff-Benner potential and molecular dynamics simulations. The results showed that the CNT would reversibly switch into morphological pattern when subjected to large deformations. Furthermore, by employing the molecular

dynamics simulations, both SWNTs and MWNTs exhibit large breaking strain (~30 to 40%) at different temperature even though they might have dissimilar chirality.

Multi-walled carbon nanotubes consist of numerous concentric SWNTs which are held together by weak Van der Waal force. Ruoff et al. [65] derived the tensile and bending stiffness constants of MWNTs in terms of the known elastic properties of graphite. Also, they pointed out that, different than conventional carbon fiber and graphite, the thermal expansion of MWNTs is practically isotropic. Ru [66, 67] has used a continuum shell and multi-shell elastic models to study the buckling behavior of MWNT under uniaxial compressive loading. They reported that the effect of interlayer displacements in MWNT could not be neglected although the Van der Waals forces are not strong. The results showed that MWNTs are extremely resilient, and could sustain a large strain without the sign of brittleness, plasticity or atom arrangement. Kolmogorov and co-workers [68] studied the interlayer interactions in double-walled nanotubes. They found that a smooth solid-solid interface can be achieved due to the tightly restricted geometry of MWNT. The energetic barrier to interlayer sliding in defect-free nanotubes can be comparable to that for a single unit cell of crystalline graphite. Additionally, Lu [59] used the empirical lattice dynamics model to determine the elastic properties of MWNTs, which formed by single-layer tubes. The results indicated the effect of chirality and tube structure has no influence on the elastic properties. And the Van der Waals forces within the layers have trifling effect to both tensile and shear stiffness.

1.2.4.2 Electrical Properties

The electrical properties of carbon nanotubes have been thoroughly explored so far both in theory and in experiment. Lot of studies has been reported carbon nanotubes exhibit different electronic manners under different conditions, and can also be affected by mechanical deformation. Understanding these behaviors would be helpful in applying nanotubes in today's design.

As describe in previous section, nanotube can be considered as a hexagonal lattice of carbon atoms that has been wrapped up into a seamless cylinder. Due to the electronics structure of graphite, it is revealed that carbon nanotubes also exhibit the electrical characteristics, that is, they can possess metallic or semi-conducting behavior based on the chiral angle that the graphite sheet is rolled. This finding was being reported in numerous of studies.

Mintmire and White [69] used both empirical and first-principal techniques to examine the helical symmetry for the electron structure of nanotubes. They reported the nanotube diameter and chirality would have serious influence on the electronic properties. These properties are unique specified by the chiral vectors, thus any change in this vector would greatly alter the conducting characteristics of nanotubes. Same results were obtained by Dresselhaus's group [70] and Saito et al. [13]. Figure 1.10 shows a two-dimensional graphene sheet together with the vector specified the chiral nanotube and the metallic status of nanotubes at specified indices (n,m).

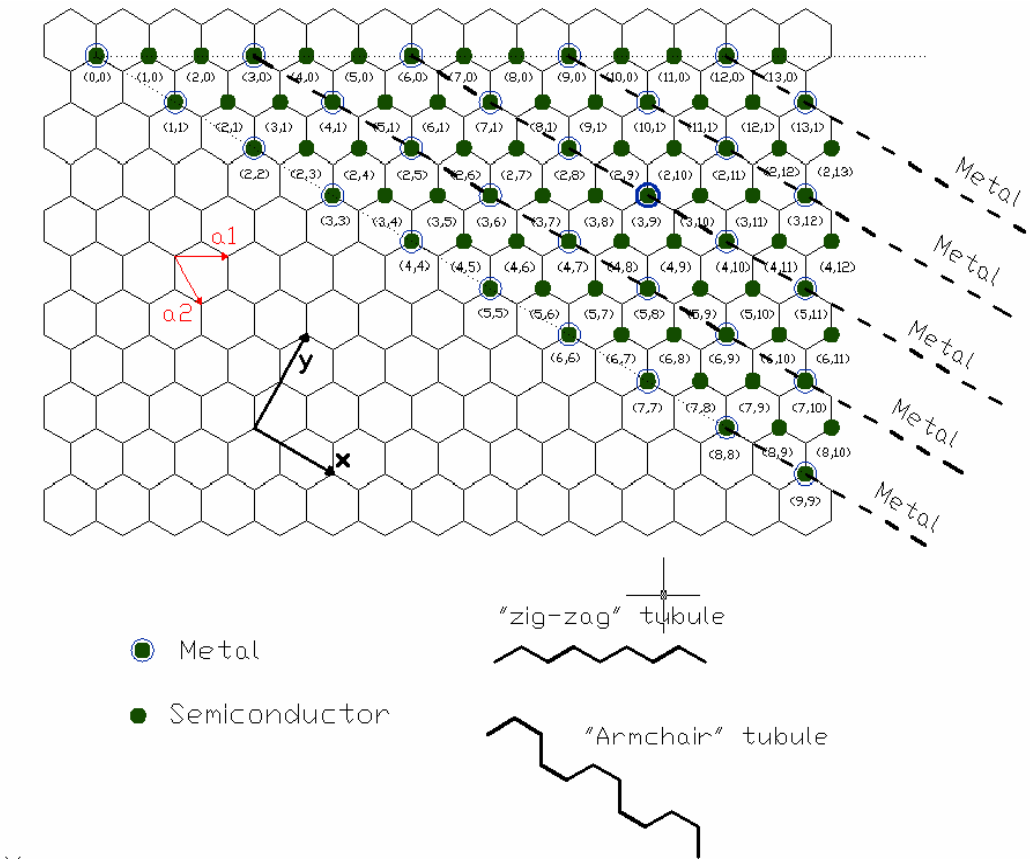

Figure 1.10 The two-dimensional graphene sheet shows the metallic and semi-conducting behavior of nanotubes.

Stroscio et al. [71] have investigated that armchair nanotube (n,n) has energy bands crossing the Fermi level and thus possess metallic behaviors. Netherless, for the rest of nanotubes with chiral indices (n,m) and (n,0), they may refer to metallic or semi-conducting group according to the relation n-m = 3p (where p is an integer). When the value obtained is a multiple of 3, the nanotube is expected to be metallic. On the other hand, if n-m ≠ 3p, the nanotube are concluded as semi-conducting materials and having an energy band gap in the order of 0.5eV. Also, this band gap is highly dependent on the nanotube diameter and can be determined by $E_{gap} = \frac{2\gamma_o a_{c-c}}{d}$ where γ_o, a_{c-c} and d denoted the C-C tight-binding overlap energy, the nearest neighbor c-c distance and the diameter of nanotube. As refer to the equation, it is known that the energy band gap would be decreased by increasing the diameter

of nanotube. Odom et al. [72] obtained the same result of semi-conducting properties of carbon nanotubes calculated by the above formula. And they suggested that a small band gap would exist at the Fermi level in metallic nanotube. Although nanotubes give delighted properties, the growth of nanotube currently provides a wide range of different geometrics. Researchers are seeking improvements so that the specified types of nanotubes can be produced.

Liber's and Dekker's group [16, 72] studied the atomic structure of SWNTs with scanning tunneling microscope (STM). They found that the results obtained from the experiments are greatly agreed with the theoretical predictions. The armchair SWNTs are metallic with a finite density of states at Fermi level, and semi-conducting chiral tubes have energy band gap with zero density of states inside the gap. While SWNTs can be considered a metallic or semi-conducting, MWNTs also have a slight variation to the SWNTs. Since most MWNTs are composed of concentric SWNTs, the electronic properties of MWNTs would be the net results obtained from SWNTs, therefore MWNTs are metallic opposed to SWNTs.

Due to the amazing reveal of electronic properties from nanotubes, they are soon have been utilized in the transport of electricity. Tan's [73] and Bockrath's group [74] were the first to carry out the measurement of individual metallic SWNT. They reported that the nanotubes samples have high resistance on the order of megaohms chiefly due to poor metal-tube contact. Also, nanotubes were found to act as quantum wires, and its capacitance scale linearly with the inverse of its length. This coherent electronic transport can even be maintained through these wires up to distance of at least 140nm. Later, lot of efforts has been put on the tube-tube electrical transportation of the nanotubes at different contact position [51,

75, 76]. In this configuration, the atomic structures in contact regions are important and the resistance of contact is highly dependent on the nanotubes structure and chirality. The results showed that by using two nanotubes to create a cross-junction, high conductance in this area can be achieved when two tubes are in-registry and commensurate, where atoms from one tube are placed on top of another. However, the resistance of such junction is highly susceptible to the applied force or pressure.

Franke et al. [77] have investigated the conductance of nanotube by Scanning probe microscopy (SPM). They concluded that the nanotube behaves as a ballistic conductor with quantum behavior. The conductance of the nanotubes is found to be $1/12.9k^{-1}$, where $G_o = 2e^2/h$ (here e is the electron charge and h is the Plank constant). Furthermore, the current density in the nanotubes is able to reach the value greater than 10^7 A/m^2. Collians et al. [39] has compared the conductance of nanotubes with that of copper. They concluded that a bundles of nanotubes could conduct about 1 billion A/m^2 while, copper wires would saturated at 1 billion A/m^2 instead. Furthermore, Thess et al. [24] measured the resistivity of ropes of metallic SWNTs directly with a four-point technique. And they reported the rope of nanotubes has a resistivity in the order of 10^{-4}cm at 300K. Wei and co-workers [78] studied the current-carrying capacity of MWNTs under high current densities. They found that the nanotubes could carry current density up to $10^9 - 10^{10}$ A/m^2 and remain stable at higher temperature.

On the other hand, mechanical deformation was also found to influence the electrical properties of nanotubes. Nardelli et al. [79] reported that the conductance of armchair SWNT was found to change slightly under small bending angles. Later, Rochefort and co-workers [80, 81] claimed that, through simulation, the electrical conductance of an armchair SWNTs

can lower by up to ten-fold when the bending angle reached 45^{o}. Besides, Tomber et al. [82] has carried out experiments on conductance of SWNTs due to the deflection. They concluded that the conductance decreases by a factor of 2 at ~5^{o} bending angle (strain ~0.3%), and decreases more severely by two orders of magnitude at a bending angle ~14^{o} (strain ~3%). However, it would recover as the applied force removed.

1.2.4.3 Thermal Properties

Apart from mechanical and electrical properties, the thermal conductivity and expansion of carbon nanotubes are also fundamentally interesting and technologically crucial. Though intensive researches on those values of nanotubes have been carried out, the exact values of these factors are still widely disputed. However, there are some basic parameters are found to have influence on these values such as temperature, large phonon modes, current, and vacancy concentration.

For the materials composed of the same element, carbon atom, diamond has the thermal conductivity about 1000-2600 W/m.K while graphite has the value of 120 W/m.K at 100^{o}C. Hone et al. has [83] reported the thermal conductivity of carbon nanotubes is temperature dependent and almost in linear relationship. They also revealed the thermal conductivity of a rope of nanotubes at room temperature can range between 1800-6000 W/m.K. Che and co-workers [84] found that the thermal conductivity of an armchair nanotube could reach 2980 W/m.K by numerical calculation. Kwon et al. [85] carried out the molecular dynamics simulations to examine the thermal conductivity of nanotubes and also its dependence on temperature. They reported that the value of conductivity could approach as high as 6600 W/m.K at room temperature, and this result confirms well with that predicted by Hone. However, the temperature dependence is found to be non-linear as compared to that

obtained by Hone. Fujii et al. [86] performed a measurement on the thermal conductivity of a SWNT using a suspended sample-attached T-type nanosensor. They concluded that the thermal conductivity of a carbon nanotube at room temperature increases as its diameter decreases, and exceeds 2000 W/m.K for a diameter of 9.8 nm. Also, the temperature dependence of the thermal conductivity for a nanotube with a diameter of 16.1 nm appears to have an asymptote near 320 K.

On the other hand, Kim et al. [87] used a micro-fabricated suspended device to measure the thermal conductivity of a MWNT. The found that the nanotube has a thermal conductivity more than 3000 W/m.K at room temperature and its dependence on temperature exhibits a peak at 320 K. Zhang and Li [88] studied the dependence of thermal conductivity of SWNT on chirality, isotope impurity, tube length and temperature by non-equilibrium molecular dynamics method with accurate potentials. They reported that the thermal conductivity is insensitive to the chirality and the isotope impurity could reduce the thermal conductivity up to 60% and change the temperature dependence behavior. Moreover, they also found that the tube length dependence of thermal conductivity is different for nanotubes of different radius at different temperatures.

When accounting for the important factors which influence the thermal properties of nanotubes, the coefficient of thermal expansion (CTE) is claimed to be a critical parameter that must not be disregarded. The values of mechanical properties, e.g. elastic modulus, are found to be lowered at high temperature because the materials has been weakened and caused change in structure. Such change at high temperature is quantized by property termed coefficient of thermal expansion. Yosida [89] investigated the lattice constant of SWNTs bundles in the temperature ranged from 290 to 1600K by X-ray diffraction (XRD). The

results showed that the lattice constant shrank over the whole temperature range. And the CTE was found to be negative in the same temperature range under the assumption that the tube axis expansion is similar to the in-plane expansion of graphite. Similar approach was adopted by Suematsu et al. [90] to study the CTE of SWNT bundles. And they obtained the values of $(-0.15 \pm 0.2) * 10^{-5} K^{-1}$ for the tube diameter and $(0.75 \pm 0.25) * 10^{-5} K^{-1}$ for triangular lattice constant.

Raravikar and co-workers [91] determined the temperature dependence of SWNTs on the radial breathing mode Raman frequency through molecular dynamics simulations. In the model, two armchair type of SWNT, (5, 5) and (10, 10), were adopted. And the results indicated that the curvature effect from nanotube causes the radial CTE to be smaller than the axial one. Besides, the nanotube with smaller diameter is found to present a larger radial and axial CTE than the one with larger diameter. Meanwhile, the CTE values are found to decrease with increasing tube diameter, and would become negative and reach that of graphite when the tube diameter turns into a big value. Apart from this, studies on the temperature dependence of elastic modulus are also performed. The results showed that the temperature and elastic modulus are linearly but inversely proportional. And the CTE value due to the change in elastic modulus was about $7 * 10^{-5} /K^{-1}$.

Kwon, Berber and Tomanek [92] studied the thermal contraction of carbon fullerenes and nanotubes through molecular dynamics simulations with ab-initio density function. They reported that the nanotubes exhibit contraction in both longitudinal and volumetric way up to a temperature of 800 K, after which the anharmonicities in the vibration result in an overall thermal expansion. The maximum CTE is found to occur at 400K in longitudinal side meanwhile it is happened at 400K when accounted for volume. In addition, the tube is

reported to exceed its initial length when the temperature reaches above 1300 K. Also, the length contraction is revealed to be affected by the bending, twist and pinch modes whereas the pinch mode dominates the volumetric contraction.

Analytical model to examine the dependence of CTE of SWNT on temperature and chirality was developed by Jiang et al. [93]. They found that the value of CTE of nanotube is positive at higher temperatures, but become negative at low and room temperature. Besides, bases on the model of armchair nanotube, the radial thermal expansion is found to be greater than the axial one, while the result is vice versa for the model of zig-zag nanotube. When focused on the thermal expansion in the radial and axial direction, it is revealed that the chirality has no influence on the radial CTE, but show a significant impact on the axial CTE. Moreover, the value of CTE of nanotube is found to vary as the diameter increased to 400 K. During which, the CTE of armchair nanotube is changed from positive to negative value, whilst that of zig-zag nanotube is altered from less negative to more negative.

1.2.5 Functionalization of Carbon Nanotube

The functionalization of carbon nanotubes aims to modify, chemically or otherwise, the surface in a controlled manner, which would lead to enhancements in structural or electronic of the materials. When carbon nanotubes applied as reinforcement into polymer, its interfacial bonding with the polymer matrix becomes a crucial issue for the load transfer within the composite. Chandra et al. [94] has observed that the thermo-mechanical transfer between fiber and matrix in conventional composites is influenced by both chemical and mechanical bonding. While chemical bonding arise from the formation of new phases, mechanical bonding occurs by interlocking of asperities. Apart from these two types of bonding, there is a third type of bonding that contributes to the load transfer mechanism,

which is Van der Waals bonding. Inside the nanotube based composites, these three types of bonding are considered to be the main transfer mechanism of load, and which governed the final properties of the composites. To ensure the nanotube based composites maintain sufficient strength, the nanotube must be well bonded to polymer interface. However, employing nanotubes as filler is challenging as they are difficult to disperse and dissolve in any organic and aqueous medium. Due to the strong attractive long-ranged Van der Waals interaction, nanotubes tend to aggregate and form ropes. Because of these highly entangled networks structures, the polymer matrix exhibits difficulties to penetrate into the nanotube structures.

In order to obtain a homogenous dispersion and achieve the full potential of nanotubes, two different possessing methods are introduced – physical/mechanical and chemical methods. The physical method implies the physically separation of the nanotube from each others. Meanwhile, the chemical technique implies the modification of the tube surface by surfactant or chemical treatment. Chemical treatments are always preferred in producing nanotube based composites. During which, the nanotube surface would be modified chemically and letting different chemical functional groups attached to its surface. These functionalized nanotubes not only would improve its dispersion throughout the solvent/the host composite material, but also improve the interfacial strength chemically due to the cross-linking created between the nanotubes and polymer matrix. Therefore, in turn, causing an enhancement in load transfer ability in the composites. Currently, there are several techniques widely adopted to modify the surface of carbon nanotubes. These techniques include solution oxidation method, sidewall functionalization, fluorination and high energy radical bombardment.

1.2.5.1 Solution oxidation method

Solution oxidation method [95-108] is the first method developed for chemical modification. Since this method does not require any particular equipment, it has been widely used for nanotube surface modification. Strong chemicals, such as concentrated HNO_3, $KMnO_4$, HF, are used in this method to oxidize the carbon atoms on the surface of nanotube. During the oxidation process, the carbon atoms at the end of the nanotube will be excited by the chemicals and causing its hybridization to alter, which allow other atoms or molecules to react with the excited atoms to form functional groups such as carboxyl or hydroxyl. The concentration of functional groups on the surface is found to be controlled successfully by using phase transfer catalyst to assist the process [109]. Though solution oxidation method is the simplest technique used for nanotube surface modification, the activation energy of carbon atoms at the end of functionalized nanotube is found to be lower than that of carbon atoms on the side wall because C-C bond is more serious deformed at the end. Besides, time consuming and chemical waste created during the process make this method unfavor to commercialize.

1.2.5.2 Sidewall functionalization

Since the solution oxidation method will only able to oxidize the end atoms on the surface of nanotube and leave the sidewall untouched, therefore, further modification is required to functionalize the sidewall of carbon nanotubes. In this method [110-117], carbon nanotubes and proper amount of aniline are mixed together with a magnetic stirrer. And Isoamyl nitrite is then added to the mixture to give the reactive arenediazonium species. The whole is heated to 60 ºC and vigorously stirred. In this way, the organic species would attach to the sidewall of carbon nanotubes by covalent reaction and serve as functional groups.

Although this method provides a solvent free condition, it involves the reactive and unstable chemicals which are not favor for storage and environment.

1.2.5.3 Fluorination [56-63]

Fluorination of carbon nanotubes occurs when fluorine atoms are made to covalently bond to the sidewalls of a nanotube. In order to achieve this propose [118-125], nanotubes are reacted with He diluted HF gas in the hot chamber, which is about 150-250^{o}C, for about 10 hours. Fluorine atom will attach to the surface of nanotubes and can be easily substituted by other function groups through further chemical reaction. This method is totally solvent free as it takes place in gas phase and easily acquired as the reaction can be run on large quantities of nanotubes. However, the evolution of hydrogen fluoride gas (HF) may happen due to the high processing temperature [126], and additional reaction has to be involved to substitute the fluorine atom, thus increases the complexity of the process.

1.2.5.4 High energy radical bombardment

Apart from the chemical method, physical method has also been developed for the purpose of modification. Researches [127-129] employed oxygen ion and argon ion as working radials and applied electrical field to accelerate the working radials to certain energy level. The accelerated ions were then utilized to bombard the surface of carbon nanotubes in the chamber. The carbon atoms on the surface would absorb the energy from radials and react with oxygen ions to form functional groups. This method is highly efficient and provides a solvent free condition. However, the high energy ions in bombardment process may cause damage to the structure of carbon nanotubes which leads to the degradation in the properties of nanotubes.

1.2.6 Carbon Nanotube Composites

Since discovered from 1991, carbon nanotubes have been studied extensively and claimed as a promising new material in the coming centuries. Their superior properties have motivated many researchers to investigate the possibility of using nanotubes as nanosensor, nanoindentator, field emission, and panel display materials. As a consequence, there has been recent interest in the development of advanced composites with carbon nanotube. Although nanotubes have much attractive properties as compared to any existing fiber, which shown in Table 1.2, the excellent properties of reinforcement doesn't necessarily translate to the delighted properties of composites. Challenges like homogeneous dispersion in solvent and supporting media, alignment of filler in the load directions, and interconnectivity with matrix must be considered in order to obtain heterostructures with enhanced properties. Therefore, the processing techniques for manufacturing nanotube based composites become an important issue and must be carefully designed.

Currently, there are three main types of sample preparation methods that would partially overcome the problems in dispersion and adhesion, and they are solvent solution mixing, melt mixing and in-situ polymerization.

Table 1.2 Mechanical Properties of different fibers [130] (All fiber properties, except carbon nanotube, are obtained form the reference [130])

Reinforcement (Fibers)	Young's Modulus (GPa)	Tensile Strength (GPa)	Density (g/cc)
C-Glass	-	3.31	2.56
S-Glass	81.3	3.44	2.62
E-Class	88.9	4.58	2.5
Kevlar	83-190	2.8-4.1	1.45
Carbon	230-320	3.3-6.8	1.7-1.9
Ceramic Oxides	69-380	1.38-3.4	2.5-4
SiC	400	3.9	3.0
Boron	400	3.6	2.5
Carbon Nanotube	~1000	~60	~1.3

1.2.6.1 Solvent solution mixing

Solvent solution mixing method [131-135] provides the advantage through low viscosity, which facilitates the mixing and dispersion of carbon nanotubes. In general, the nanotubes are first dispersed with chemical solvent with the help of high energy process such as magnetic stirring, shear mixing and ultrasonication. After dispersing nanotubes into the solvent, the polymer will be added into the mixture with further agitation. This final mixture will then be placed in a mold at the room temperature or a heat environment for evaporating the solvent and curing. The time period for curing will be relied on the polymer employed during composite manufacturing. For thermoplastic composite, curing will happen in a short time once it allows cooling down from the hot operating condition. However, for thermoset

composite, depending on the curing temperature, it may require different time interval to complete the curing process.

Due to the simplicity in processing, this method has been widely adopted in composite making. Schadler et al. [136] manufactured the nanotube based composite with solvent solution mixing method. It is reported that the composite, which made from epoxy and 5 wt% of MWNT, has an improvement in tensile modulus from 3.1GPa to 3.71GPa while that in compression modulus from 3.63GPa to 4.5GPa. Mora and co-workers [137] also fabricated the carbon nanotube fiber composite with the same method. They found that the composite has enhancement in both tensile and compressive properties. In the tensile side, the composite of epoxy with 27% nanotube fiber has the elastic modulus changed from 1.2GPa to 18.8GPa whilst the tensile strength increased from 43MPa to 253MPa. Meanwhile, in the compressive way, the composite of epoxy with 14% nanotube fiber has the stiffness improved from 1.2GPa to 10GPa and the yield strength gained from 40MPa to 130MPa.

1.2.6.2 Melt Mixing

Melt-mixing is a process normally applied for thermoplastic composites. This method [138, 139] makes use of the softening properties of the thermoplastic to disperse the carbon nanotubes in the polymer matrix. Conventional processing techniques, such as extrusion, internal mixing, injection molding and blow molding, are employed in the method due to their simplicity and availability in the industries. This method has the advantages of contaminants and solvents free, however, the dispersion of nanotubes is comparatively poor than the other two methods. During the process, the viscosity of polymer remains at high level even its melting point is reached thus prevents the nanotubes from separation. In order to disperse the nanotube into polymer matrix, high shear mixing is employed to overcome the

high viscosity of nanotube-polymer mixture. Though shear mixing is the most preferable driving force in such a high operating temperature environment, the ability of carbon nanotubes to withstand such high shear force is still under investigation. An optimization of processing parameters is required to produce a well dispersion of nanotube whilst diminish the possibility of polymer degradation.

The improvement of mechanical properties of nanotube based composites by melt mixing method various from study to study. Jin et al. [140] obtained 130% improvement in elastic modulus of composite made with PMMA and 17wt% MWNT. Potschke and co-workers [141] examined the composite of polycarbonate with 15wt% MWNTs and they found that there is only a 30% improvement in elastic modulus. However, Kearns et al. [142] found that nanotubes would function more efficient when applied as reinforcement in the draw-out type of composite. By adding 1 wt% of SWNT into polypropylene, it is revealed that the elastic modulus would have 55% enhancement.

1.2.6.3 In Situ Polymerization

In situ polymerization method [143-148] is aimed to improve the dispersion and integration between phases. In general, there are two different techniques to carry out this polymerization for the production of nanotube based composites. Traditionally, carbon nanotubes are dispersed in the monomers via sonication to produce homogenous solution. Initiator or hardening agent is then added to the solution to initialize the polymerization. During the process, the polymerized materials would constrain the nanotube and prevent them from aggregation. There are numerous polymers, such as polystyrene, epoxy and PPV, which make to of this technique to produce nanocomposites. The latest type of in situ polymerization is named electropolymerization method. During the process, carbon

nanotubes, which are in the form of array or film, will be applied as electrode. Monomers like pyrrole, aniline in the cell will be absorbed, deposited on the surface of nanotubes and polymerized via external electric field. Finally, nanocomposite will be obtained after certain period of time. This method is normally employed for those polymers with monomers in gas phrase, like polyethylene, polypropylene and polyvinylchloride. For the other type of polymers with different form of monomers, the traditional in situ polymerization should be applied.

This method provides a better dispersion for nanotube as the reinforcement and matrix are obtained in molecular scale. Velasco-Santos et al. [149] fabricated composite of PMMA with 1 wt% of MWNTs through in situ polymerization. They concluded that the elastic modulus of the composite is improved from 1.5 to 2.5GPa. Also, the tensile strength is increased from 30MPa to 50MPa. Besides, using the same approach, Putz and co-workers [150] investigated the composites of PMMA with extremely low volume fraction, $8x10^{-5}$, of SWNT. They reported that the elastic modulus of the composite is increased from 0.3GPa to 0.38GPa through the measurement of DMA. This result is comparable to the one obtained from the rule of mixtures for long, well-aligned carbon nanotubes.

1.2.6.4 Processing and Characterization of Nanotube Based Composites

Many researches developed carbon nanotube based composite for electrical and thermal applications. The studies done with the mechanical area of nanotubes have far fewer then those in the electrical and thermal fields. Here, the review on recent works in this area has been present together with the discussion on the challenges arises in the development of nanotube based composites.

As mentioned earlier, the fabrication of nanotube based composites is highly relied on the dispersion of nanotubes in the polymer matrix, and the interaction between them. Any variations in these issues will influence the final properties of nanocomposites. Shaffer and Windle [151] studied the nanotubes as reinforcement of solution based composites. By employing Dynamic-Mechanical Thermal Analysis (DMTA) measurement on nanocomposite with nanotubes weight fraction up to 60%, they reported that the storage modulus of the composite is increased from 6GPa for neat polymer to 12GPa for 60 wt% composite. Analysis through the theory developed for short fiber composites, they obtained the nanotube elastic modulus and effective length of 150MPa and 35nm, respectively. However, these calculated values are much lower than the value reported for individual nanotube.

Using similar approach, Cadek et al. [152] fabricated the MWNT/PVA and MWNT/PVK composites with various volume fractions of nanotubes. They found that the elastic modulus is increased from 7GPa to 12.6GPa with 0.6 vol.% MWNT in PVA and 2GPa to 5.6GPa with 4.8 vol.% in PVK. Also, through the measurement of Differential Scanning Calorimetric (DSC), they observed that the PVA crystallinity increases linearly with the nanotube content while PVK remains the same. This indicated that the difference in reinforcement may create a crystalline interface for PVA composites, but an amorphous one for PVK composites. The results implied the possibility that stress transfer may be maximized by the existence of an ordered interface as pointed out by Frankland et al. [153]. Apart from this, Haggenmueller and co-workers [154] prepared the SWNT/PMMA composite fibers via solution mixing, followed by melt mixing and then melting spinning. They reported that the mechanical properties of the composite fibers enhance with increasing nanotube content and drawing ratio. The elastic modulus of fibers are found to alter with draw ratio to some extent, on the other hand, the yield strength has a significant improvement

with the draw ratio. The yield strength is found to improve about 20% with the addition of 8wt% of SWNT and about 15% with SWNT adding up to 5wt%.

When processing the nanocomposites, addition of surfactant and chemical modification of nanotubes are found to have certain impacts on the properties of the final product. Gong et al. [155] fabricated nanotube based composite through curing mixing of nanotubes with epoxy resin in the presence of surfactant. The results showed that for the composite produces with surfactant and 1wt% nanotubes, its elastic modulus is improved by more than 30% and the glass transition temperature is increased from 63^{o}C to 88^{o}C. Netherless, for the composite fabricated without the aid of surfactant, its elastic modulus and glass transition temperature has only exhibited some moderate variation. They concluded that the addition of surfactant can improve the dispersion of nanotubes and modify the interaction of the nanotubes with the polymer matrix.

Paiva et al. [156] studied the composites of SWNT and a crystalline PVA using solvent solution technique, and both pure and functionalized SWNTs are used as reinforcement in this work. The results showed that the yield strength and elastic modulus are increased 55% with the 5wt% functionalized SWNT/PVA composites. The yield strength of 2.5wt% functionalized SWNT/PVA improves 17% over the neat PVA while that of 2.5wt% pure SWNT/PVA is degraded 5% from the neat PVA. Yu and co-workers [157] also prepared the functionalized SWNT/polyimide composite film with the solvent solution method, which followed by sonication, spin coating and oven drying. From the results, they concluded that the elastic modulus and the tensile strength of composite with 0.3wt% SWNT has been increased by 18% and 5 % while that of composite with 1wt% SWNT has been improved by 90% and 9%. Meanwhile, the value of elongation-to-break has been lowered from 4.5% to

4.1% and 2.6, respectively, which showing that the addition of SWNT into polyimide would enhance the properties of the polymer, but at the same time would increase its brittleness.

Though the results of nanotube based composites give delighted properties improvement, the control of the nanostructure of carbon nanotubes in the final product is still not yet achieved. Also, there is no optimal conclusion can be drawn for different nanotube based composites. The measured properties of nanocomposites are found to vary from study to study, and these values are known to be highly relied on the type of polymer and processing methods apply. The interfacial interaction, which knows as the critical factor for load transfer inside the nanocomposites, has been studied thoroughly to obtain the finest solution. In order to achieve this purpose, different assessment techniques are introduced as to obtain the better answer for this.

Qian et al. [8, 158] characterized carbon nanotube/polystyrene composites. They reported that the elastic modulus and tensile strength of the nanocomposite has been increased by 42% and 25%, respectively, with addition of 1wt% of nanotubes. The load transfer ability between nanotube and polystyrene was studied with TEM. Through the images obtained from TEM, they concluded that the nanotube-polymer interface is operative well into the plastic deformation regime of the composite. Also, the failure of the composites is mainly caused by the debonding at the nanotube-polymer interface, and the rest is caused either by sword-in sheath mechanism or transverse shear.

Wanger and co-workers [159] studied the stress-induced fragmentation of MWNT/Urethane composite films. With the aid of TEM, they found that the fragmentation phenomenon is caused by either process-induced stress resulting from curing of polymer or

tensile stress generated by polymer deformation and transmitted to the nanotube. According to the Kelly-Tyson model, they concluded that the nanotube-polymer interfacial shear stressing on the order of 500MPa and up, which is an order higher than that of conventional advanced composites. Lourie et al [160] investigated the buckling and collapse of MWNT/epoxy composite. They reported that the nanotubes are under substantial high compressive stress due to the shrinkage of an epoxy matrix after curing. Bent and loop shapes of buckled nanotubes are observed under the inspection of TEM. And this sharp turn formed in the buckled nanotubes causes the outer surface of the nanotubes to sustain a high flexural strength. Later, this result was confirmed by Hadjiev et al. [161]. They showed that the residual stress of less than 70 MPa exist on the embedded nanotubes due to the shrinkage of epoxy in the curing process.

Apart from the TEM, Raman spectroscopy is another widely used technique to examine the stress transfer and the strain of nanotube composite[136,162,163]. Cooper et al. [163] prepared composite specimens by applying a carbon nanotube/epoxy mixture onto the surface of an epoxy beam. Raman spectroscopy was applied to study the stress transfer inside the composite during the four-point bending test. The results showed that the Raman spectra shifted downward to a lower wavenumber which indicated the surface strain of the composite is increased. Besides, they also reported that the effective modulus of SWNT based composite could be over 1 TPa and that of the MWNT composite could be about 0.3 TPa. Schadler et al. [136] also studied the behavior of MWNT/epoxy composites with Raman Spectroscopy. They found that, although both tensile and compressive moduli of the nanocomposite are improved, the significance of such enhancement in the modulus of tensile is much lower than that of compressive. Through the results of Raman spectroscopy, they observed only a shift in compression and none in tension. They concluded that the load

transfer in MWNTs during tension is negligible due to the fact that the inner tubes are sliding within the outer tubes, thus the load is not able to transfer efficiently inside the composite system. Similar results were drawn by Ajayan and co-workers [9], they investigated the fracture behavior of SWNT/epoxy composite loaded axially in tension and compression. They reported that the shifts of Raman peaks in both tensile and compressive studies are not significant. The results indicated that the interfacial interaction between nanotubes and matrix is poor, which mostly caused by the sliding of nanotubes inside the rope.

Even with the improved dispersion and interfacial adhesion, the performance of nanotube based composites may not be the same as in expectation. This is because the orientation of nanotubes has a significant impact on the overall properties of the nanocomposite. In order to fully utilize the carbon nanotubes as reinforcement, the control of nanotubes distribution must be studied carefully. Jin and co-workers [164] fabricated the aligned nanotube composites with mechanical stretching. X-ray analysis has been carried out to examine the orientation and degree of alignment of nanotube inside the composite. They found that the degree of nanotube alignment could be varied with the stretching ratios, regardless of the composite thickness. Haggenmueller [154] used the melting spinning method to produce a well-aligned SWNT based composite fibers. Later, Vigolo and co-worker [165] further developed this spinning method by dispersing the nanotubes in surfactant followed by recondensing the nanotubes in the stream of polymer solution to form macroscopic fibers and ribbons. They found that the nanotubes are oriented along the axis of the ribbons through the SEM, and the nanotube fiber exhibits the characteristics of high flexibility and resistance to torsion when this fiber was made into a knot. More recent method for nanotube alignment is applying magnetic or electric field during the production of nanocomposites. Due to the electronic characteristic of carbon nanotube, it is found that

nanotube would able to response to the magnetic/electric field. Walters et al. [166] made use of this characteristic and achieved an aligned membrane of SWNTs by introducing the SWNT suspension into the magnetic field. The nanotubes suspension is found to align, and filtered in the magnetic field and finally able to form as an aligned nanotube membrane.

1.3 OUTLINE OF THE THESIS

The primary goal of this work is to investigate the enhancement of mechanical properties of polymer by employing carbon nanotubes as reinforcement. Chapter 1 provides a broad review in recent advances in carbon nanotubes and their composites, examining the works regarding the nanotubes structures, processing methods, properties characteristics and also the achievement of their composites. Chapter 2 describes the composite preparation methods adopted in this research and also the experimental techniques employed to study the mechanical properties of nanotube based composites. Chapter 3 presents the experimental results of nanotube based composites obtained from various testings, and also a detailed discussion regarding the results would be followed. Chapter 4 focus on the molecular modeling of carbon nanotube, which aims to examine the structural change of carbon nanotube during the temperature variation. Finally, brief conclusion about this work is drawn in Chapter 5 and the possible future work is also mentioned.

CHAPTER 2

SAMPLE PREPARATION AND INVESTIGATION METHODS

Two fundamentals for any experiment in condensed matter physics are a sample and an instrument with which to measure it. The success or failure of an experiment is ultimately determined before the first set of data is acquired. Any inadequate set of experiments during groundwork will result in completely unrelated results. This includes proper handling and preparation of samples and verifying that all instrumentation is in proper working order. The hours invested in developing a reliable experimental procedure can eliminate weeks of wasted operational time.

This chapter will focus on the preparation method applied to fabricate the carbon nanotube composites and also the investigation methods adopted to study the mechanical properties of these composites. The single-walled carbon nanotubes were employed as reinforcement in the nanocomposites in this work. Both purified and functionalized SWNTs were used in this study so to examine the effect of surface modification on nanotube dispersion and adhesion. The chemical processes for functionalizing the nanotubes were kept as simple as possible in order to fulfill the requirement for future industrial application. The improvement in properties of polymer due to the embedded SWNTs, and in the surface interaction between the nanotubes and polymer matrix due to the functionalization were studied through various experiments and characterization.

2.1 MATERIALS AND SAMPLE

2.1.1 Single-Walled Carbon Nanotubes

The SWNTs used in this study were obtained from Shenzhen Nanotech Port Company Limited (NTP), synthesized by chemical vapor deposition in a furnace with flowing methane gas as the carbon source. These nanotubes with hollow morphology have diameter less than 2nm, length varied from 5 to 15 μm, and purity of 90%. Figure 2.1 shows the micrograph of SWNTs obtained by the CVD process from NTP Company.

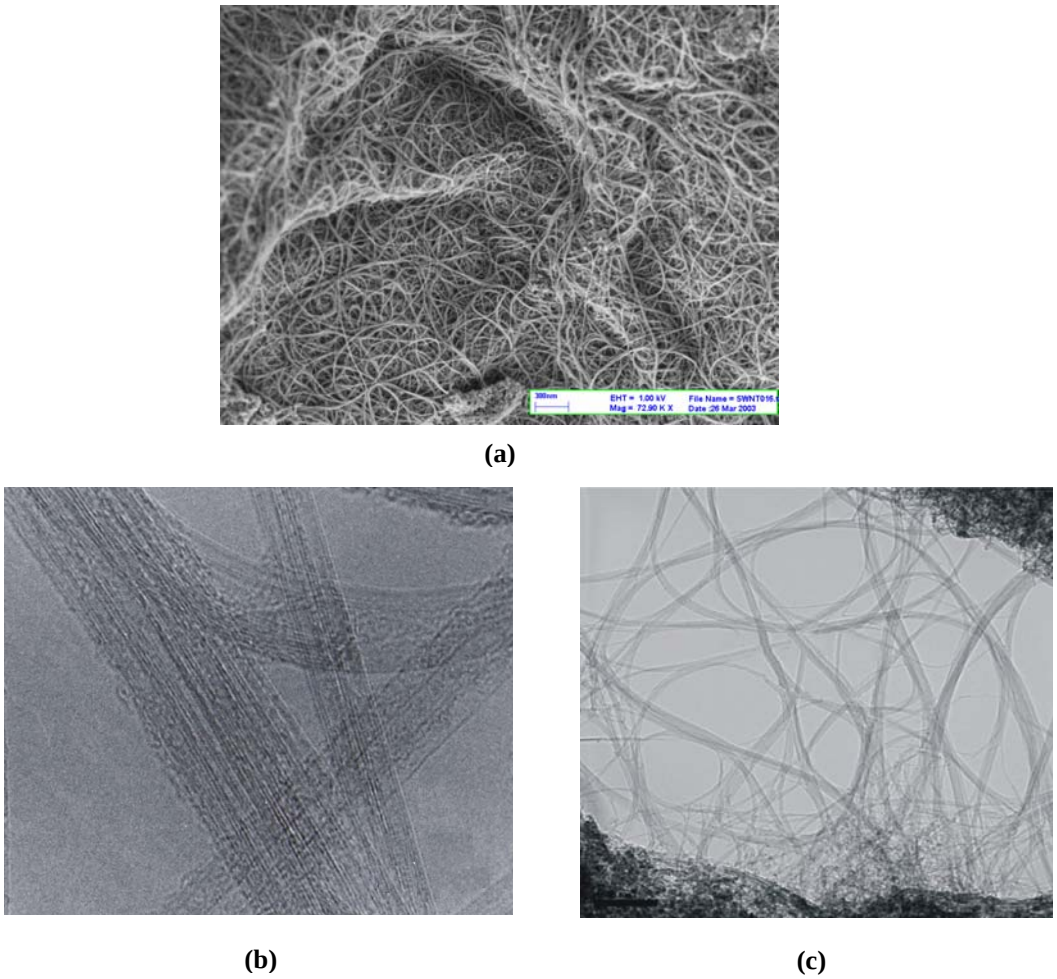

(a) **(b)** **(c)**

Figure 2.1 The micrographs of SWNTs synthesized by NTP Company. (a) SEM image of nanotube showing large agglomerates. (b) and (c) TEM images showing the variation in nanoscale morphology of nanotubes [167]

Figure 2.1(a) is a SEM image of bulk nanotubes showing large agglomerates. These agglomerates were resulted from the entanglement of carbon nanotubes and, which caused significant obstruction toward achieving a homogeneous dispersion of nanotubes in a composite. Apart from the agglomeration of nanotubes, Figure 2.1 (b) and (c) are the TEM images of the SWNTs showing the variation in size of the nanotubes as received.

According to the specification from the NTP Company, the nanotubes have purification about 90%. In order to confirm such high purification, thermogravimetric analysis (TGA) was performed to ensure the impurities (e.g. amorphous carbon) were kept in a minimum value. It is important to control the amount of these impurities, which were created during the nanotube synthesis, inside the nanotube bundles since the existence of impurities would influence the interaction between the polymer matrix and nanotubes, thus lower the final properties of the nanocomposite. In order to carry out the experiment, a Setaram Labsys TG-DTA/DSC system was employed to perform the thermal analysis. The samples were heated from 25^{o}C to 1100^{o}C at a rate of 10^{o}C/min in air. The result (figure 2.2) showed that the sample weight (wt%) of nanotubes decreased gradually during the heating process and reached the minimum value of ~9.1%. This implied that the existence of amorphous carbon was not significant enough to cause oxidation and the total impurities only contributed about 9.1% of the entire weight of nanotubes sample. These nanotubes were then used directly as the purified reinforcement in the nanocomposite in this study.

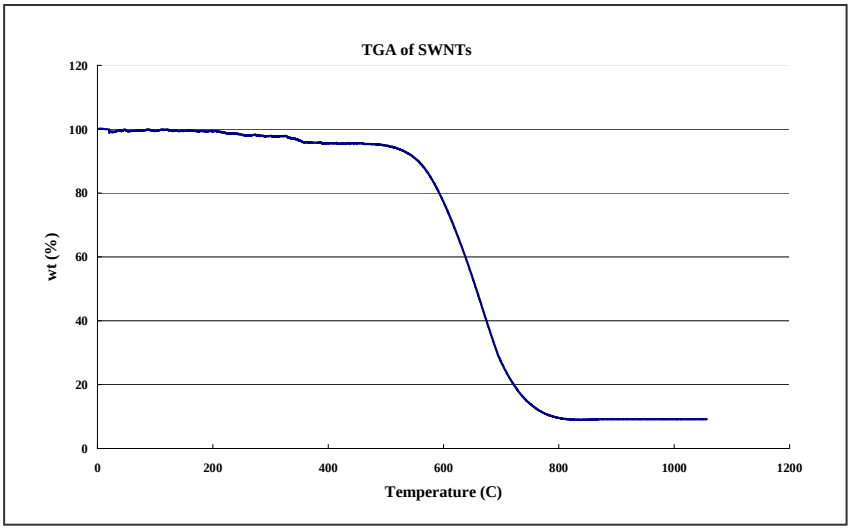

Figure 2.2 TGA curve of SWNTs as received from NTP

2.1.2 Functionalization of SWNTs

As mentioned in previous section, both purified and functionalized SWNTs were incorporated into polymer as reinforcement. The functionalization of nanotube was aimed to enhance the interfacial interaction between nanotubes and polymer matrix. This process can be initiated by oxidizing the nanotube with different chemical agents. In this work, the SWNTs were oxidized with a mixture of sulfuric acid and nitric acid in the ratio of 3:1 in volume, (H_2SO_4 with concentration 98%; HNO_3 with concentration 70%). SWNTs were suspended in this solution followed by sonication (ultrasonic bath 240W, 50~60kHz) for 3 hours to modify the nanotubes. These modified SWNTs would have the functional group COOH (carboxylic group) attached at the ends. Hydrochloric acid (HCL) was then added to the suspended mixture of nanotube to ensure the modified nanotubes were molecularly perfect and chemically clean. The acidic nanotube mixture was washed thoroughly with distilled water and NaOH solution [168]; this process was repeated until a neutral solution was obtained. The acid-treated nanotubes were filtered off using double layer of 0.2μm millipore membrane. The SWNTs were then dried under vacuum at room temperature.

The functionalization method which was adopted to attach the carboxylic group chemically to the ends of SWNT is shown in figure 2.3. Although the end sides of the nanotube were chemically modified, the mechanical properties of nanotubes would not be altered as it is governed by the tube body instead of the end cap of the nanotubes. These functionalized nanotubes were used as one of the reinforcements throughout this study, so to investigate the load transfer ability of the functionalized carbon nanotube based composites.

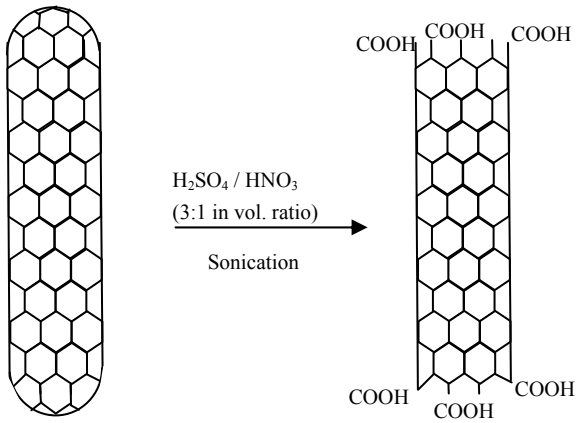

Figure 2.3 Functionalization of carbon nanotube

2.1.3 Dispersion of SWNTs

As mentioned in previous section, carbon nanotubes are easily to form aggregates which behave differently in response to a load when compare with individual nanotubes. In order to take the full advantages of nanotubes as reinforcement in composites, the aggregates need to be broken up and the nanotubes should be dispersed throughout in the polymer to avoid stress concentrations which will degrade the properties of the nanocomposites.

Sonication is one of the main techniques for dispersing the nanotubes. During the fabrication of composites, sonication is widely adopted to blend the nanotubes with chemical

solvent and surfactant, followed by the addition of the well dispersed nanotubes solution into the soften polymer which undergoes further sonication afterwards. The aim of sonication is not to enhance the nanoscale dispersion of nanotubes within the polymer matrix, but rather to assure that the nanotubes are dispersed on the microscale. The microscale dispersion of nanotubes ensures the nanotubes are completely embedded into the polymer after evaporation of solvent.

There are large variation of solvents can be used for this mixing process and the most commonly applied solvents include acetone, ethanol, toluene, chloroform, tetrahydroduran, dimethylformamide (DMF) and sodium dodecyl sulfate (SDS). Many researches have already reported that the delighted properties of composites produce with the above solvents. However, on the other hand, the use of solvents was also found to have significant impacts on the properties of the composites. Lau and co-workers [169] examined the effect due to the solvent on the nanocomposites. They found that the solvent effect on SWNTs are in the order of DMF>ethanol>acetone while the mechanical performance of SWNT/Epoxy composites are in the reverse order. This result indicated the unsuitable selection of solvent for composites processing would induce serious problems in the final properties of the composites.

2.1.4 Polymer

The model nanocomposite system is composed of an Epoxy polymer matrix reinforced with CVD grown SWNTs. The epoxy applied in this study is a commercially available Araldite GY 251 epoxy resin DGEBA (diglycidylether of bisphenol A) together with the hardener, Ciba HY 956 ethane-1,2-diamine hardener. Their chemical structures are shown in figure 2.4.

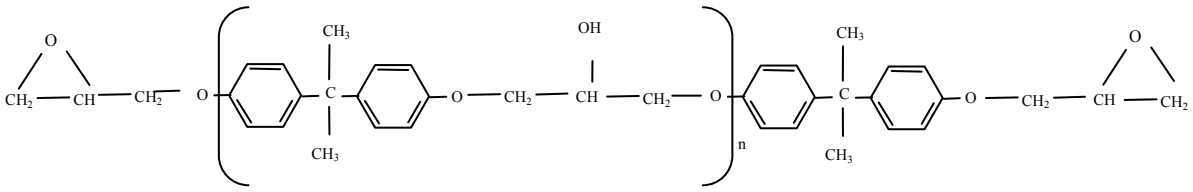

(a)

$$H_2N - CH_2 - CH_2 - NH_2$$

(b)

Figure 2.4 Chemical structures of (a) Epoxy Resin and (b) Hardener

2.1.5 Composite Fabrication

In order to investigate the effect on polymer due to the addition of carbon nanotubes, both pure polymer and nanotubes based composites were fabricated. During the processing SWNT/Epoxy composite, the solution-solvent mixing method, as described in section 1.2.6.1, was initially employed for dispersing the SWNTs in the mixture. However the final nanocomposites were found to exhibit an undeserved phenomenon which was unsuitable for mechanical property testings, hence the fabrication of procedures of nanotubes has been modified to omit the solvent usage. The details regarding the processing procedures will be discussed in the following section. Furthermore, various weight percentages, i.e. 1%, 2%, 3%, 4%, 5%, of SWNTs and FSWNTs were introduced for manufacturing the composite, thus to study the mechanical improvement of polymer due to the application of nanotubes.

2.1.5.1 Solution Solvent Mixing Process

The solution solvent mixing process was the first method attempted for making SWNT/Epoxy composites in this study. The SWNTs, either purified or functionalized, were suspended into the solvent for 1 hour through sonication. Acetone was employed as the required solvent in this process as its influences on composites are the least when compares to others. The first sonication was aimed to degglomerate the nanotube bundles in the solvent and to produce a well suspended SWNT solution. This mixture was then mixed with epoxy resin (Araldite GY251) for the second sonication which last for 2 hours.

The overall time for two consecutive sonication processes was set to be 3 hours because the sonication time was found to have remarkable effect on the chemical structure of the nanotubes [170]. It is reported that longer the sonication time, more the regular graphene sheets of carbon nanotubes would be converted into amorphous carbon layers. The sonication time for such conversion was observed to begin between 3 and 4 hours. Therefore, in order to prevent the formation of amorphous carbons, which would affect the final properties of the nanotube based composite, the maximum allowable sonication time was set to be 3 hours in this study.

During sonication, the nanotube/epoxy resin mixture was heated up to 75^{o}C to reduce the viscosity of the solution mixture and thus enhanced the nanotube dispersion. Moreover, as the boiling point of acetone, i.e. 60^{o}C, is much below than the heating temperature, the solvent is allowed to evaporate from the mixture. The heating procedure is critical during the fabrication of composites as the low viscosity of polymer at high temperature would increase the penetration of nanotubes into the polymer, thus a better dispersed nanotubes-polymer mixture could be obtained. The suspension from sonication was then degassed in a vacuum

chamber for 5 minutes to get rid of the air bubbles that may occur during the sonication process. Long degassing process is not recommended since nanotubes would start agglomerating in the mixture once they leave the hot sonication environment. Also, the solution mixture after the degassing process could remain at relatively high temperature ~65^{o}C; hence the viscosity was able to stay in a low value which allowed a better mixing process with hardener afterwards.

Hardener (HY 956) was added immediately into the mixture at the resin to hardener ratio of 5:1 right after the degassing step and with stirring followed. The SWNT/Epoxy solution was then injected into a silicon rubber mold which would place into the oven at 80^{o}C for 12 hours to complete the curing process. Figure 2.5 shows one of the silicon rubber molds used in this study. Since different experimental setup used in this work required different sample (in size and shape), the nanotube based composites was processed and prepared to meet all necessary experimental conditions and requirements of applied investigation methods. The samples obtained from the mold after completion of curing were kept in the desiccators, with temperature 22 ^{o}C and humidity 45%, for one week to ensure the samples were completely cured and eliminated the thermal stressed created inside the samples during their transmission from high temperature 80^{o}C to room temperature 22^{o}C after curing.

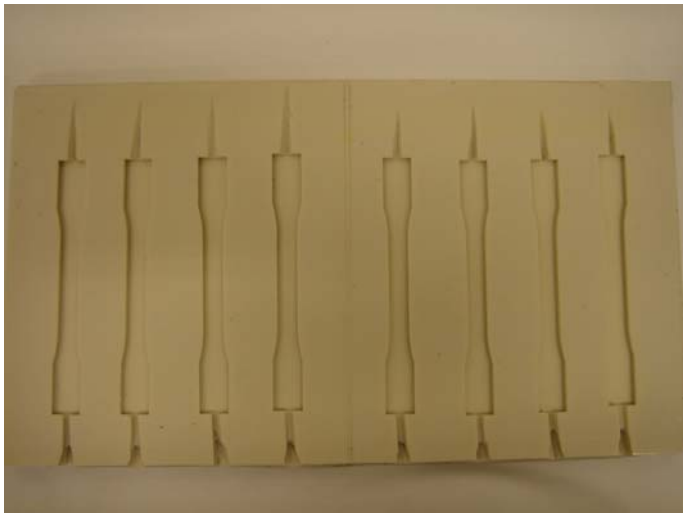

Figure 2.5 Silicon rubber mold for producing the dumbbell shape specimen.

The pure epoxy specimens were processed in the same way as above, except no solvent was added during the process as no dispersion of particles was required. The epoxy resin was first sonicated for 3 hours in the hot water bath, and then followed with the degassing and the hardener mixing procedures. The rest of the processes were similar as mentioned before.

The nanotubes based composite samples fabricated by this method were found to exhibit certain problems. For those nanocomposites with the 1–3% weight percentage of nanotubes (SWNT or FWNT) showed ductile behavior while composites with 4-5% weight percentage of nanotubes (SWNT or FWNT) found difficulties in curing. On the other hand, pure epoxy samples were in rigid condition which was the same as indicated in the manufacturer's specification. The problems occurred in the specimens were accounted for the existence of solvent inside the composite. In order to eliminate the effect due to the solvent, the composites manufacturing process was modified to omit the usage of solvent. The

nanotube based composites were fabricated in the same way as produced the epoxy specimens, and the nanotubes were added and sonicated directly with the epoxy resin in a hot bath for 3 hours at the beginning. Figure 2.6 shows the pure epoxy and nanocomposite specimens obtained through this method.

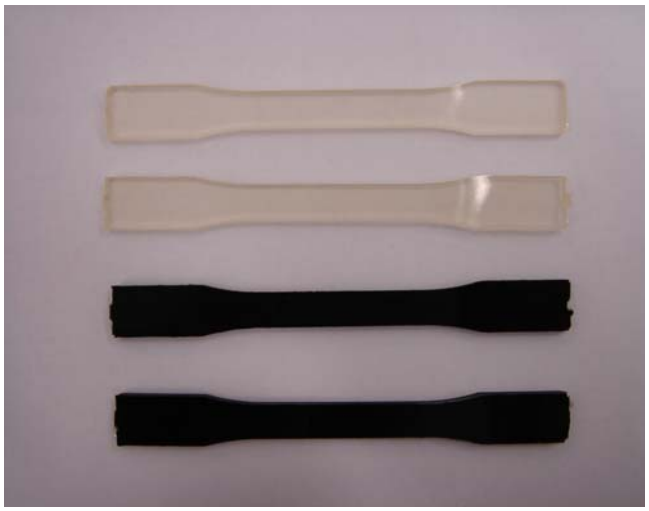

Figure 2.6 Pure Epoxy and SWNT/Epoxy specimen obtained from the silicon rubber mold.

2.2 EXPERIMENTAL TECHNIQUES

The enhancement of mechanical properties of the composites due to the addition of nanotubes and the improvement of interfacial interaction induced by functionalized SWNTs over the pure SWNTs were characterized utilizing various experimental techniques including tensile property test, flexural property test, microhardness test, impact test, dynamic mechanical analysis, thermogravimetric analysis, and scanning electron microscopy. The general description of the experimental setups used in this study, as well as the conditions and parameters of each experiment, are purposed in the following sections.

2.2.1 Tensile Property Test

Tensile property test is a measure to evaluate the resistance of the specimen to elongate under axial loading until it fails. In this work, tensile property tests were performed according to the standard ASTM D-638 at room temperature 22^{o}C and mean relative humidity 60% by using the MTS Alliance RT/50 tensile testing machine (figure 2.7) with a crosshead speed of 1mm/minute together with an extensometer (MTS 632 24f-50) having 25mm gauge length. The tensile specimens were of dumbbell shaped with dimension 84mm x 6.5mm x 3mm (figure 2.6) and were clamped to the sample holder vertically.

During the experiment, a uniaxial loading was continually applied on the specimen until such time as failure occurs. This test was performed here to calculate the Young's modulus, tensile strength, and strain at break of the materials. The Young's modulus is a very important factor which is measured in mega Pascal (MPa), moreover, it is a measure of the stiffness of a given material. It is defined as the ratio, for small strain, of the rate of change of stress with strain. This can also be experimentally determined from the slope of a stress-strain

curve created during tensile property tests conducted on a sample of the material. A low modulus means that the material would be flexible while a high modulus indicates the structure would be stiff and inflexible.

Figure 2.7 MTS Alliance RT/50 tensile machine and extensometer.

Theoretically, the Young's modulus of materials is expressed as follows:

$$Young's\ Modulus\ E = \frac{Applied\ Stress\ \sigma}{Strain\ \varepsilon} = \frac{F / A_o}{\Delta l / l_o} \tag{2.1}$$

where

F = applied force on the sample, N

A_o = the original cross-sectional area through which the force is applied, mm^2

Δl = the amount by which the length of the sample changes, mm

l_o = the original length of the sample, mm.

Meanwhile, the tensile strength of a material is the maximum amount of tensile stress that it can be subjected before failure and is defined as

$$\begin{aligned} \textit{Tensile Strength } \sigma_{\max} &= \frac{\textit{Maximum Applied Force } F_{\max}}{\textit{Original Cross – Sectional Area } A_o} \\ &= \frac{F_{\max}}{A_o} \end{aligned} \tag{2.2}$$

2.2.2 Flexural Property Test

The flexural property test provides measures to the behaviors of materials subjected to simple beam loading including the flexural modulus (modulus of elasticity in bending) E_f, flexural stress σ_f, flexural strain ε_f and the flexural stress-strain response of the material. In this study, flexural property tests were carried out according to the standard ASTM D-790 at room temperature 22^{o}C and mean relative humidity 60% by using the MTS Alliance RT/50 tensile testing machine (figure 2.7) together with the 3 point bending fixture (figure 2.8). The specimen was placed on a support span and the downward loading was applied on the center by the loading nose producing three points bending at the rate of 0.495mm/min. The parameters for this test e.g. the speed of loading required for the test were defined through the above standard.

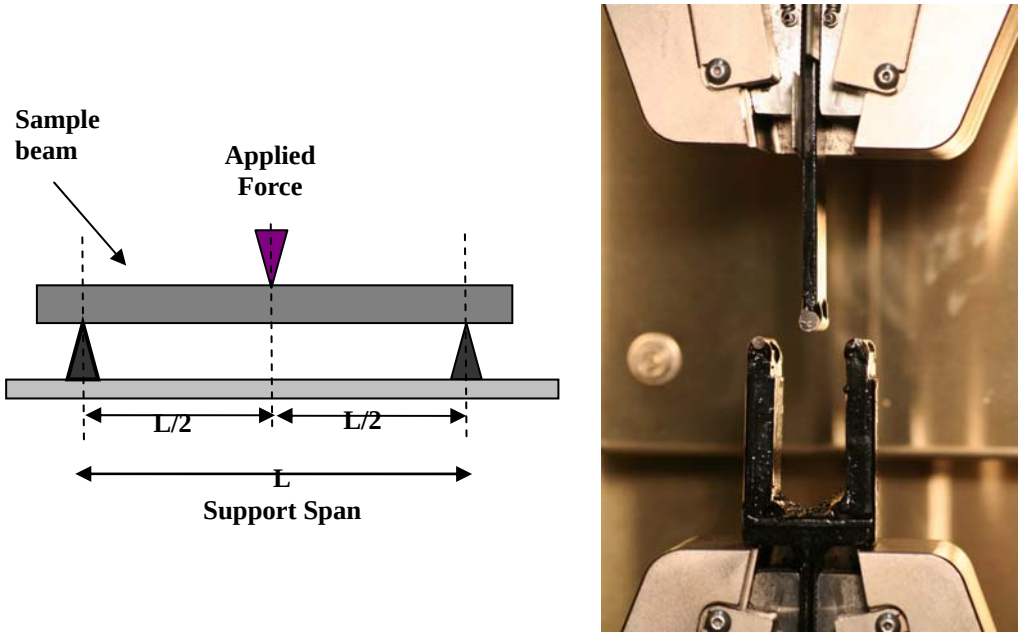

Figure 2.8 Flexural Property Test with 3 point loading

A flexure property test produces tensile stress in the convex side of the specimen and compression stress in the concave side. Flexural strength is defined as the maximum stress in the outermost fiber and is calculated at the surface of the specimen on the convex or tension side. Flexural strain is referred to the fractional change in length of an element of the outer surface of the specimen while flexural modulus is an indication of a material's stiffness when flexed and can be calculated from the slope of the stress-deflection curve.

The specimens adopted in this test were rectangular in shape with dimension 70mm x 6.5mm x 3mm. The flexural parameter and results of the tests can be evaluated through the definitions from the ASTM standard, which are shown as follows:

(1) The crosshead motion of the machine

$$R = \frac{Z\ L^2}{6\ d} \tag{2.3}$$

(2) The flexural stress sustained by the sample

$$\sigma_f = \frac{3\ P\ L}{2\ b\ d^2} \tag{2.4}$$

(3) The flexural strain induced by the sample

$$\varepsilon_f = \frac{6\ D\ d}{L^2} \tag{2.5}$$

(4) The flexural modulus of the sample

$$E_f = \frac{L^3 m}{4 b d^3} \tag{2.6}$$

where

R = rate of crosshead motion, mm/min

L = support of span, mm

d = depth of beam, mm

Z = rate of straining of the outer fiber which is equal to 0.01 mm/mm/min according to ASTM D790

σ_f = flexural stress sustained by the sample, MPa

P = load at a given point on the load-deflection curve, N

b = width of beam test, mm

D = maximum deflection of the beam, mm

ε_f = flexural strain provided by the beam, MPa

m = slope of the tangent to the initial straight-line portion of the load-deflection curve, N/mm

2.2.3 Izod Impact Test

Impact testing techniques were established to ascertain the fracture characteristics of materials. The basic characteristics of an impact test are that stresses are applied by subjecting the test piece to a sudden blow. In this work, the pendulum type of impact test, Izod impact test, was used to investigate the influence on the property of fracture strength by the addition of nanotube into the epoxy. The experiments were carried out according to the standard ASTM D 256 in the room with temperature 22^{o}C and mean relative humidity 60%. Besides, all the specimens having the dimension of 64 x 6.5 x 3mm were produced for measuring the impact properties of the materials.

The standard test for this test method requires a specimen made with a mild notch. The notch produces a stress concentration that increases the probability of a brittle, rather than a ductile, fracture. In order to introduce the required notch onto the specimens, the motorized notch cutter machine from International Equipments was utilized. The notch prepared by the cutter has the cutting angle 45^{o} with the radius of curvature at the apex of 0.25mm and with the ratio of 5 between the depth of specimen and that of notch. Figure 2.9 shows the notch cutter machine employed in the experiment and the schematic drawing of the notch produced by the machine on the prepared specimen.

Figure 2.9 The Notch Cutter Machine from International Equipments [171] and the schematic drawing of the prepared specimen.

All the specimens were kept in the conditioning situation, which was the same of the testing condition, for 40 hours after notching and prior to testing. This procedure is aimed to release the thermal stresses induced during cutting operation and bring the specimen in equilibrium. The impact test machine adopted in this experiment was the Analogue Izod/Charpy Impact Tester from International Equipments (figure 2.10(a)). During the Izod impact test, the specimen was clamped by the vises as a vertical cantilever beam as indicated in figure 2.10(b). The pendulum would then release from it highest position and strike the specimen through a single swing of the pendulum. The line of initial contact was a fixed distance from the specimen clamp as well as from the centre line of the notch and was on the same face as the notch. The impact tester would then provide the fracture energy required to break the specimen.

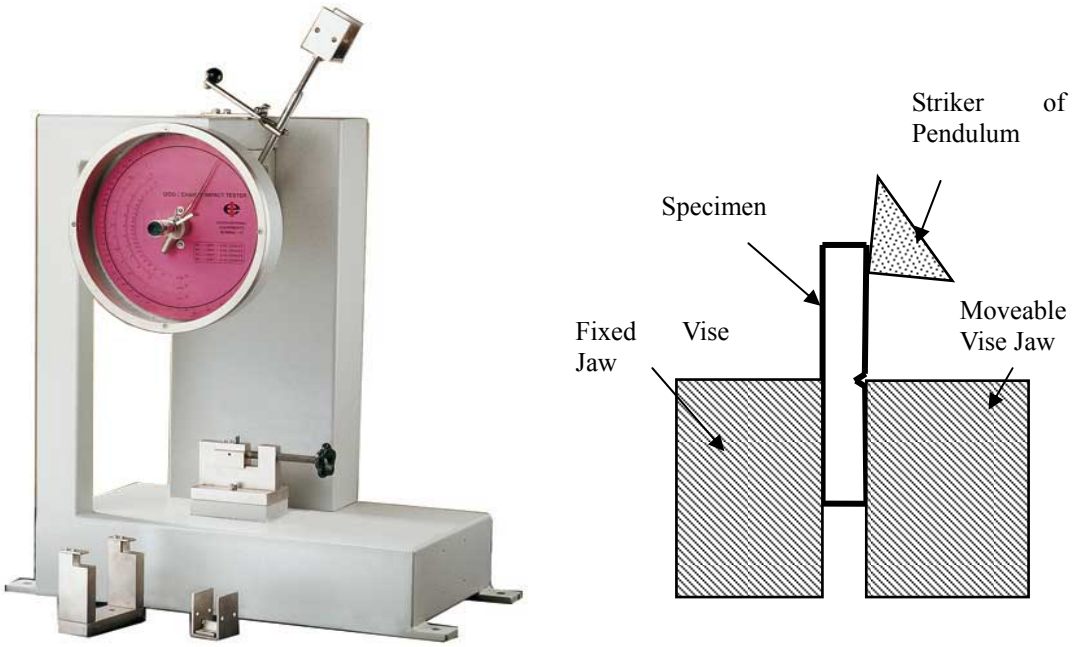

Figure 2.10 (a) The Analogue Izod/Charpy Impact Tester from International Equipments [171] and (b) the schematic drawing of the specimen positioning.

According to the standards, the results of all the test methods are reported in terms of energy absorbed per unit of specimen width or per unit of cross sectional area under the notch. For relatively brittle materials having fracture energy less than 27J/m, which is the fracture propagation energy is small in comparison with the fraction initiation energy; the toss correction must be carried out. The toss correction (energy to throw the free end of the broken specimen) obtained in Izod test is only an approximation of toss error, since the rotational and rectilinear velocities may not be the same during the re-toss because store stresses in the specimen may have been release as the kinetic energy.

Furthermore, there are four possible types of failures during the impact test:

1. Complete Break – A break where the specimen separates into two or more piece

2. Hinge Break – An incomplete break, such that one part of the specimen cannot support itself above the horizontal when the other part is held vertically

3. Partial Break – An incomplete break that doesn't meet the definition for a hinge break but has fractured at least 90% of the distance between the vertex of the notch and the opposite side.

4. Non-Break – An incomplete break where the fracture extends less than 90% of the distance between the vertex of the notch and the opposite side.

2.2.4 Microhardness Test

Hardness is a measure of scratch resistance and rebound resilience, but for polymer it is taken to refer to a measure of resistance to localized plastic deformation (e.g. a small dent or a scratch). The mode of deformation under an indentor is a mixture of tension, shear, and compression, and hardness is by no means a fundamental property. The results achieved from the hardness test are highly depended on the indentor geometry and the degree of indentation as well as the time of indentation after the measurement is made.

In order to examine the improvement in the property of composites, the microhardness machine, Future-tech micro-hardness tester (model FM-7E, figure 2.11(a)), was adopted to perform the experiments. The whole process was relied on the standard ASTM E-384 and was carried out in the condition of 22^{o}C room temperature and 60% mean relative humidity. The dimension of specimens was the same as used in the tensile test and all specimens were polished to obtain a smooth and flat enough surface for indentation. Moreover, the hardness value of the specimen was taken as the average of six indentations which were made randomly on the specimen. The indentor utilized in this experiment was a square-based pyramidal-shaped diamond with face angles of 136°. The indentor force adopted was 100-gram force and the dwell time was 15 seconds during the indentation. Figure 2.11 (b) shows the dent made through the microhardness machine. The unit and magnitude of the hardness are defined by Vickers hardness (Hv), and was determined by measuring the average diagonal length, d (mm), of the indentation mark on the specimen surface.

$$H_v = \frac{8\,F\,\sin(\theta/2)}{\left[\,(d_1 + d_2)/2\,\right]^2} \tag{2.7}$$

where

F = loading force, g-f

θ = face angle of a pyramidal diamond indenter, 136^{o}

d_1, d_2 = are the two diagonal lengths of the indentation, μm

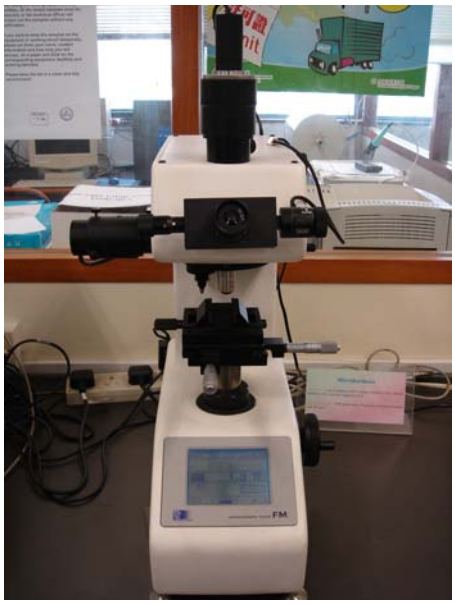

(a)

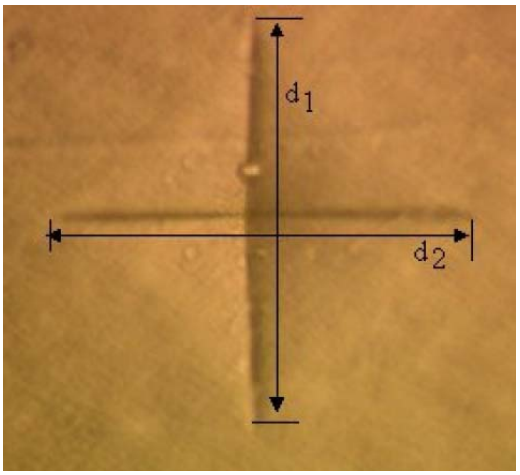

(b)

Figure 2.11 (a) Future-tech FM series micro-hardness testing machine and (b) indention mark

2.2.5 Dynamics Mechanical Analysis

Dynamics mechanical analysis (DMA) is an efficient method of determining the material's viscoelastic behavior and developing structure-property relationship. It is able to measure the modulus (stiffness) and damping (energy dissipation) properties through the application of periodic stress. The effects on composites by adding different weight percentage of purified/functionalized carbon nanotubes were studied though this technique. The specimens for dynamics mechanical analysis were prepared to dimensions of 50 x 6.5 x 3mm. The testing was conducted in a dual-cantilever bending geometry on a Dynamic Mechanical Analyser (Perkin Elmer Diamond DMA Lab System) and in the room with temperature 22^{o}C and mean relative humidity 57%. Figure 2.12 shows the Dynamic Mechanical Analyser and the dual-cantilever bending geometry employed in the experiment. In addition, during the analysis processing, time scans were run from approximately 25^{o}C to 220^{o}C at a heating rate of 2^{o}C/min with frequencies 1 Hz.

(a)

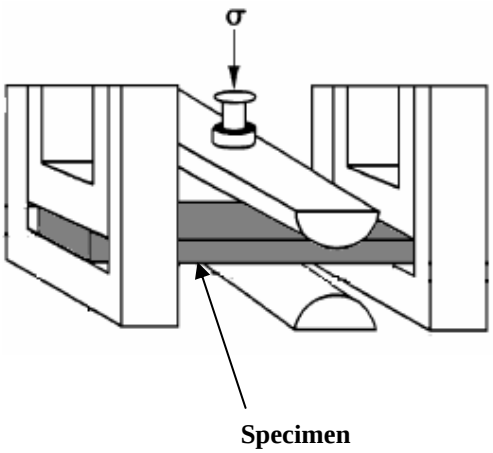

(b)

Figure 2.12 (a) Dynamic Mechanical Analyser and (b) the dual-cantilever bending geometry employed in the experiment.

Due to the differences in composition, materials would response differently when subjected to sinusoidal stress in the dynamics mechanical analysis. For a perfectly elastic material, the stress and strain are perfectly in phase as strain is directly proportional to stress, however, for a perfectly viscous fluid, the strain will lag behind by a phase angle of 90^{o}. For a polymeric material, the response to a variable load is a combination of elastic and viscous response, i.e. they show elasticity to some extent and also flow to some extent and the strain lags behind the stress by phase angle δ. Thus, polymeric materials are also named as viscoelastic materials. Figure 2.13 shows a common response of stress and strain with time for a polymeric material.

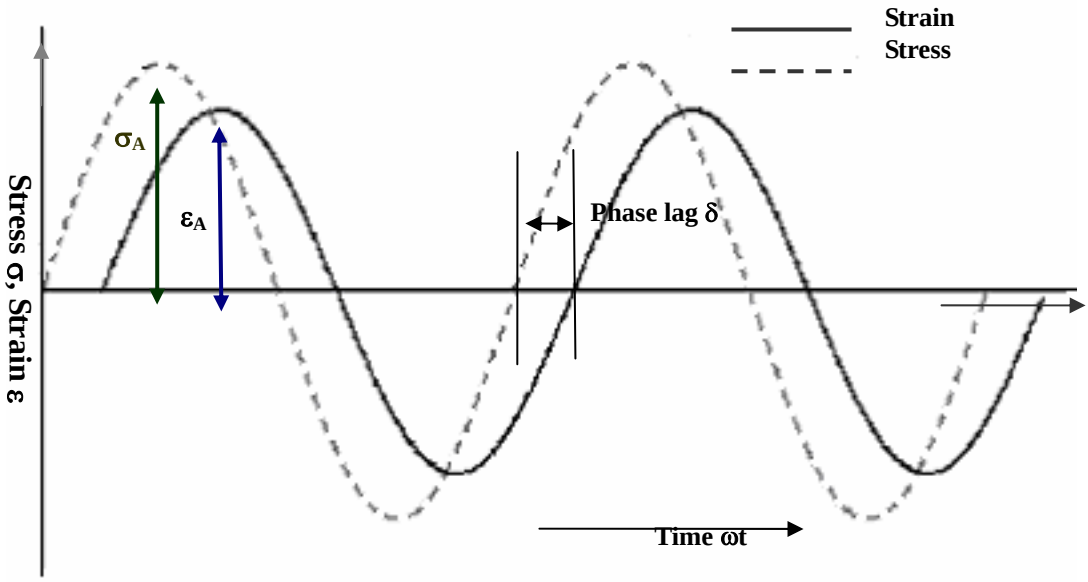

Figure 2.13 Stress-strain response of a polymeric material.

Because of the differences in response, the results obtained from dynamic mechanical analysis are always applied to characterize the viscoelastic behavior of the material under investigation. The complex viscosity, complex modulus, storage (elastic) modulus, loss modulus are the most common properties can be acquired from the analysis and their relationships are shown as follows:

(i) The complex modulus E* is the ratio of the stress amplitude to the strain amplitude and represents the stiffness of the materials. It is composed of the storage modulus E' (the real part) and the loss modulus E" (the imaginary part)

$$E^*(\omega) = E'(\omega) + iE''(\omega) \tag{2.8}$$

Its magnitude is in term in MPa and can be evaluated as

$$\left|E^*\right| = \frac{\sigma_A}{\varepsilon_A} = \sqrt{\left[E'(\omega)\right]^2 + \left[E''(\omega)\right]^2} \tag{2.9}$$

(ii) The storage modulus E' represents the stiffness if a viscoelastic material and is proportional to the energy stored during a loading cycle. Besides, it is generally equal to the elastic modulus for a single, rapid stress at low load and reversible deformation. Its expression is written as

$$E'(\omega) = E^*(\omega)\cos\delta \tag{2.10}$$

(iii) The loss modulus E" is defined as being proportional to the energy dissipated during one loading cycle. It represents energy lost during the process and is a measure of vibrational energy that has been converted during vibration and that cannot be recovered. Its expression is defined as

$$E''(\omega) = E^*(\omega)\sin\delta \tag{2.11}$$

(iv) The loss factor tan δ is the ratio of loss modulus to storage modulus. It is a measure of the energy lost, expressed in terms of the recoverable energy, and represents mechanical damping or internal friction in viscoelastic system. A high value of tan δ implies a material has a high, nonelastic strain component, while a low value of tan δ indicates one that is more elastic. Also, the maximum of this ratio represents the material's glass transition temperature T_g [155, 172] and it expression is indicated as

$$\tan\delta = \frac{E''(\omega)}{E'(\omega)} \tag{2.12}$$

(v) The complex viscosity η* is the tendency of a material to flow. A similar relationship, as in the complex modulus, is used to define this value. In dynamics mechanical analysis, the complex viscosity η* is also separated into two components; the stored viscosity η' and loss viscosity η". And it is evaluated from:

$$\eta^*(\omega) = \eta'(\omega) + i\eta''(\omega) \tag{2.13}$$

where $\eta'(\omega) = \frac{E''(\omega)}{\omega}$ is the real part and $\eta''(\omega) = \frac{E'(\omega)}{\omega}$ is the imaginary part of the complex viscosity.

2.2.6 Thermogravimetric Analysis

Thermogravimetric analysis (TGA) is a branch of thermal analysis, which examines the mass change of a sample as a function of temperature in the scanning mode or as a function of time in the isothermal mode. Thermal events like melting, crystallization or glass transition do not change the mass of the sample but there are some very important exceptions which include desorption, absorption, sublimation, vaporization, oxidation, reduction and decomposition. TGA is used to characterize the decomposition and thermal stability of materials under variety of conditions and to examine the kinetics of the physico-chemical processes occurring in the sample. The mass change characteristics of a material are strongly dependent on the experimental conditions. Factors such as sample mass, volume, shape and nature of sample holder, nature and pressure of the atmosphere in the sample chamber and the scanning rate all have important influences on the characteristics of the recorded TGA curve. TGA is useful to distinguish one polymer from the other on the basis of oxidation or decomposition curves. Moreover, this technique is commonly used to compare the behavior of polymer with and without additives.

In this study, the thermogravimetric analysis was employed to investigate the purity of the carbon nanotubes purchased from Shenzhen Nanotech Port Company and also the enhancement of thermal stability of the composites due to the application of SWNT and FSWNT as the reinforcement. The thermal experiments were carried out with the instrument, Setaram Labsys TG-DTA/DSC system, in the room with temperature 22^{o}C and relative humidity 55%. Figure 2.14 shows the Setaram Labsys TG-DTA/DSC system used for the thermal analysis.

Figure 2.14 Setaram Labsys TG-DTA/DSC system.

The thermogravimetric analyzer is a low volume, high temperature computer controlled oven. During the heating process, the sample will decompose or evolve in the oven and causing a change in its temperature and mass. Such changes in the sample will be monitored and recorded by the thermocouple and electrobalance which were built-in the thermal system. The data obtained from the process provides important information on the decomposition and thermal stability of samples and also the kinetics of the physico-chemical processes occurring in them. The sample that use for the thermogravimetric analysis can be in solid or liquid form with the mass normally less than 5g.

In the earlier section, the result of TGA (figure 2.2) has already utilized to show the purity of the carbon nanotube purchased from Shenzhen Nanotech Port Company. In order to study the enhancement of thermal stability of the composites due to the addition of carbon nanotube, the similar procedure of operating the Setaram Labsys TG-DTA/DSC system was employed. Besides, the samples were heated from 100^{o}C to 700^{o}C at a rate of 10^{o}C/min with the flow of air at approximately 40cc/min

2.2.7 Scanning Electron Microscope

The scanning electron microscope (SEM) is a type of electron microscope that images the sample surface by scanning it with a high-energy beam of electrons in a raster scan pattern. The electrons interact with the atoms that make up the sample producing signals that contain information about the sample's surface topography, composition and other properties such as electrical conductivity.

The types of signals produced by an SEM include secondary electrons, back scattered electrons (BSE), characteristic x-rays, light (cathodoluminescence), specimen current and transmitted electrons. These types of signal all require specialized detectors for their detection that are not usually all present on a single machine. The signals result from interactions of the electron beam with atoms at or near the surface of the sample. In the most common or standard detection mode, secondary electron imaging (SEI), the SEM can produce very high-resolution images of a sample surface, revealing details about 1 to 5 nm in size. Due to the way these images are created, SEM micrographs have a very large depth of field yielding a characteristic three-dimensional appearance useful for understanding the surface structure of a sample. Furthermore, SEM is able to provide a wide range of magnifications is possible, from about x 25 (about equivalent to that of a powerful hand-lens) to about x 250,000, about 250 times the magnification limit of the best light microscopes.

Back-scattered electrons (BSE) are beam electrons that are reflected from the sample by elastic scattering. BSE are often used in analytical SEM along with the spectra made from the characteristic X-rays. Because the intensity of the BSE signal is strongly related to the atomic number (Z) of the specimen, BSE images can provide information about the distribution of different elements in the sample. For the same reason BSE imaging can image

colloidal gold immuno-labels of 5 or 10 nm diameters, which would otherwise be difficult or impossible to detect in secondary electron images in non conductive specimens. Characteristic X-rays are emitted when the electron beam removes an inner shell electron from the sample, causing a higher energy electron to fill the shell and release energy. These characteristic X-rays are used to identify the composition and measure the abundance of elements in the sample.

In this research work, the scanning electron microscope was used to examine the failure mechanism of the composites after mechanical testing i.e. tensile test, flexural test and impact test. Moreover, it also applied to inspect the dispersion of carbon nanotubes inside the composite. The images obtained from SEM would be useful to explain the properties improvement of composite due to the reinforcement of carbon nanotubes, and also the influence on interfacial interaction between the carbon nanotube and polymer matrix caused by functionalization. The samples examinations were performed at room temperature 22^{o}C and mean relative humidity 57%, and with the scanning electron microscopes, Leica Stereoscan 440 scanning electron microscope and JEOL Model JSM-6490 scanning electron microscope, which were operated at the accelerating voltage 20kV, throughout the study (Figure 2.15). All the samples under inspection were prepared directly from those specimens right after the mechanical testing. And the samples were clean with alcohol and coated with a conductive layer i.e. gold by a sputter coater for the conduction of electrons during the SEM process (Figure 2.16).

(a) **(b)**

Figure 2.15 (a) Leica Stereoscan 440 scanning electron microscope and (b) JEOL Model JSM-6490 scanning electron microscope samples

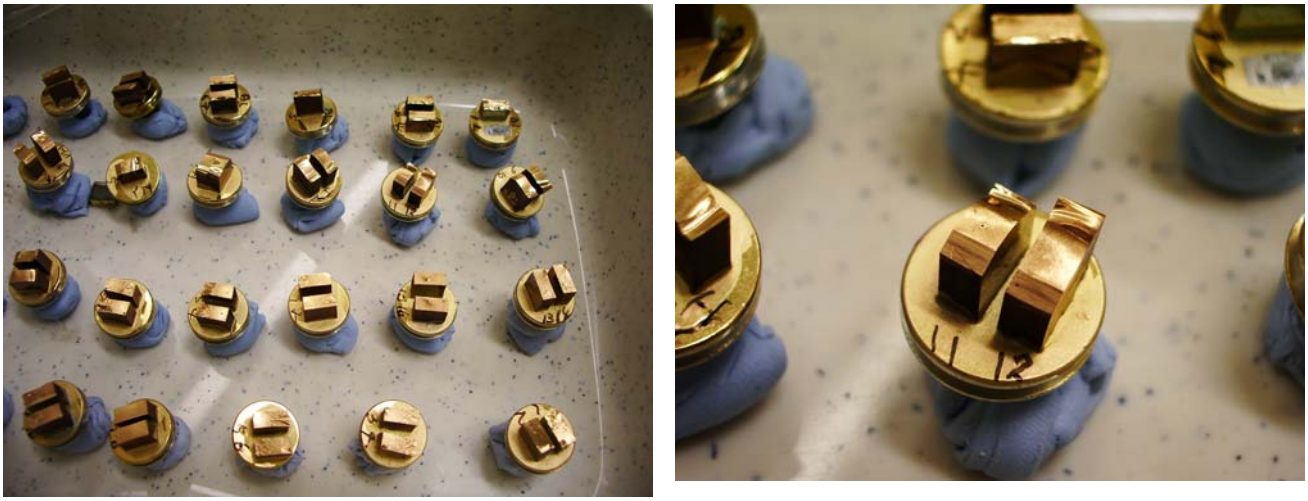

Figure 2.16 Samples prepared for the SEM process.

CHAPTER 3

RESULTS ANALYSIS AND DISCUSSIONS

This chapter aims to show the results obtained from various experiments as mentioned in Chapter 2. These experiments were designed to investigate the properties, such as elastic modulus, flexural modulus, and thermal stability, improvement due to the addition of SWNTs and FSWNTs into the epoxy matrix, and to compare the enhancement caused by FSWNTs over the SWNTs as reinforcement. In general, the experiments could be divided into two categories: (i) Mechanical Property Tests i.e. Tensile Property Test, Flexural Property Test, Impact Test and Microhardness Test, and (ii) Thermal Property Tests i.e. DMA and TGA. Besides, SEM was introduced to examine the facture surface and nanotubes distribution insides the composites. Apart from this, detail analysis and discussion would be present on each experiment based on the results achieved.

3.1 MECHANICAL PROPERTY TESTS

3.1.1 Analysis of Tensile Properties

In the tensile property test, the tensile modulus (modulus of elasticity) and ultimate strength of the nanocomposites have been examined. Figure 3.1 illustrates the tensile behaviors of the nanotube based composites from the tensile property tests. For SWNT/Epoxy composites (figure 3.1(a)), all the composites with different contents of SWNTs show a ductile plastic behavior in terms of the stress and strain. These stress-strain curves exhibit elongation manners after reaching the peak loading. As compares with the result of epoxy, it is found that the addition of SWNTs into the epoxy didn't influence the trend of stress-strain behavior of the materials; however, the extent of elongation has been improved. This extension enhancement was varied from 4.25% produced by 1wt% SWNT/Epoxy composites to 55.75% provided by 3wt% SWNT/Epoxy composites.

In addition, the ultimate strength of the composites was determined to be increased by reinforcing the SWNTs into the neat epoxy. From the experiment, the ultimate strength of epoxy alone was measured to be 50.08MPa. This maximum strength value was found to enhance by 0.48% to 50.2MPa when 1wt% of SWNTs was employed into the composite. With further addition of SWNTs, the ultimate strength was augmented more significant. For composites containing 2wt% to 3wt% of SWNTs, the strength value was gained by 5.73% to 6.87%. However, such improvement was slow down when 4wt% of SWNTs was applied into the composite and the strength value at this nanotube content was measured as 53.5MPa. Though 6.83% of improvement was achieved over the neat epoxy, the ultimate strength was found to decrease to 53.50MPa from 53.52MPa for composites having 3wt% of SWNTs. Nevertheless, this property was raised again as 5wt% of SWNTs was used as filler and the

ultimate strength was obtained to be 54.94MPa with 9.7% improvement above that of epoxy matrix.

On the other hand, contrasts to the SWNT/Epoxy composites, FSWNT/Epoxy composites show totally different behaviors in stress-strain relationship. Figure 3.1(b) shows the stress-strain curves of FSWNT/Epoxy composites. Through the results, it is noticed that all the composites, with different nanotubes contents, demonstrated a typical deformation of brittle plastic in terms of the stress and strain. By comparing with the result of epoxy, the elongation of FSWNT/Epoxy composites after reaching the ultimate strength was obviously shortened. The deformation decrement was varied from 33.06% of 4wt% FSWNT/Epoxy composites to 38.06% of 3wt% FSWNT/Epoxy composites. Apart from this, same as in SWNT/Epoxy composites, the ultimate strength was enhanced due to the addition of FSWNTs. By introducing 1wt% of FSWNTs as filler, the strength value was gained from 50.08MPa of neat epoxy to 51.75MPa of the nanocomposite and given an improvement by 3.33%. When more FSWNTs were introduced into the composites, the enhancement in the strength property was more remarkable, especially as compared to that of SWNT/Epoxy composites. The ultimate strength of FSWNT/Epoxy composites was found to increase as the weight content of nanotubes in the system increased. The augmentation reached the maximum and provided the improvement of 16.91% over the neat epoxy when 5wt% of FSWNTs was used in the composites system.

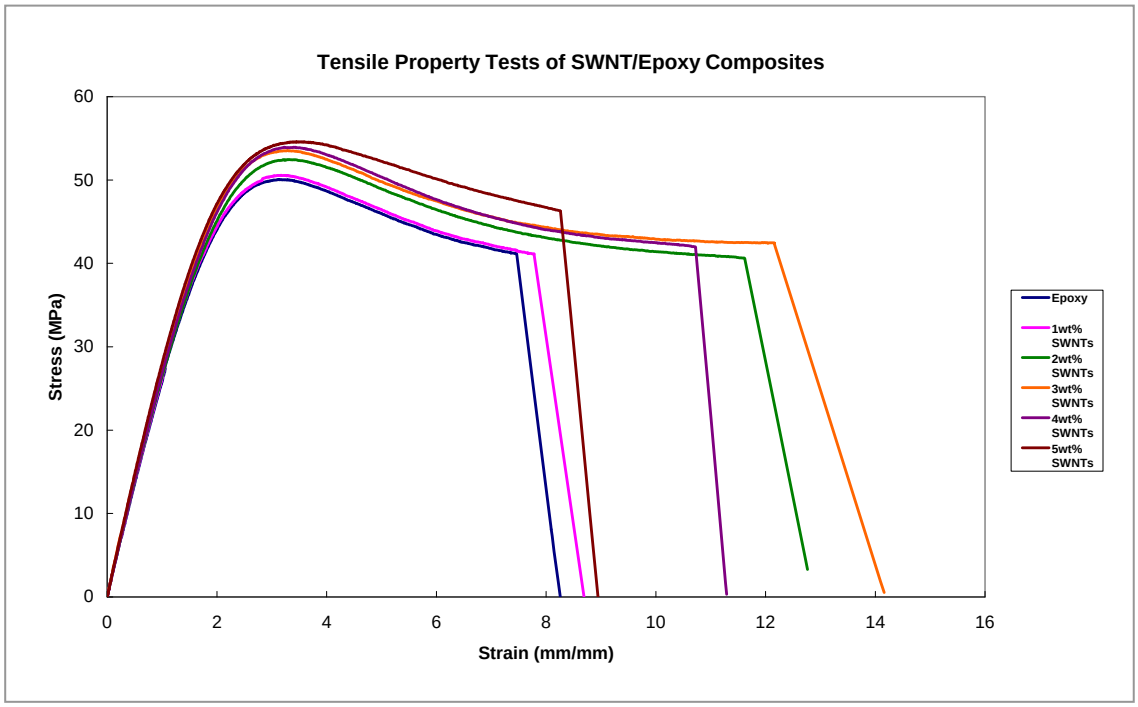

(a)

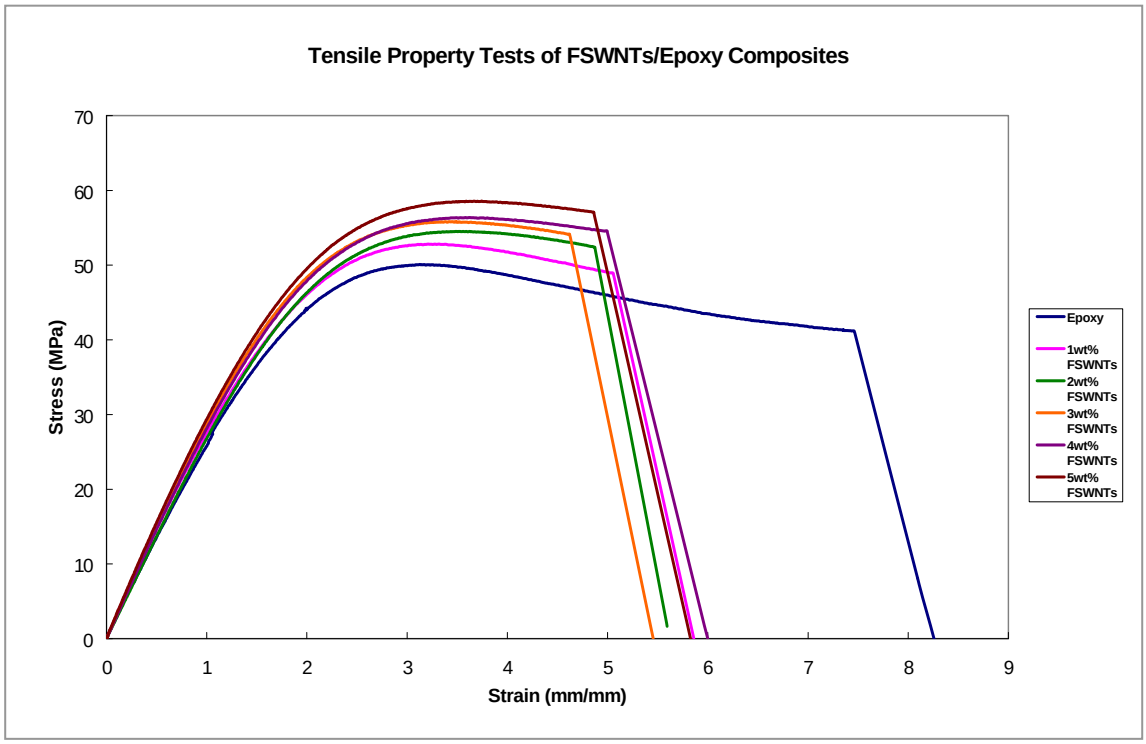

(b)

Figure 3.1 The tensile property test results of (a) SWNT/Epoxy Composites and (b) FSWNT/Epoxy Composites.

Apart from ultimate strength, the tensile modulus of the epoxy was also found to have noticeable increment with the reinforcement of nanotubes. Figure 3.2 shows the results of tensile modulus of the nanocomposite systems as the function of nanotubes content. Through the results, it is revealed that both SWNTs and FSWNTs have significant impact on the tensile modulus of composites. In the tensile property test, the tensile modulus of epoxy was measured to be 2.66GPa. With the addition of 1wt% of SWNTs into the epoxy matrix, it is found that the modulus was enhanced to 2.72GPa with an improvement of 2.26% over the neat epoxy. Further filling of SWNTs into the composites has facilitated the augmentation of the tensile modulus. For composite containing 2wt% of SWNTs, its tensile modulus was increased to 2.76MPa with improvement of 0.04MPa over 1wt% SWNT/Epoxy composite. However, such improvement in modulus was found to be tremulous as illustrated in the figure. When 3wt% of SWNTs was applied, the tensile modulus was enhanced in a faster rate and jumped to a value of 2.85MPa. Nevertheless, this increasing rate was slow down as 4wt% of SWNTs was employed and this composite system provided a tensile modulus of 2.88MPa. For the composites embedded with 5wt% of SWNTs, on the other hand, the tensile modulus is found to improve in a higher rate again and gave a modulus value of 2.98MPa with 12.03% enhancement over the neat epoxy.

Similar to SWNT/Epoxy composites, FSWNT/Epoxy composites present improved tensile moduli with the addition of FSWNTs. However, these values of FSWNT/Epoxy composites were increased in a much faster and steady manner when compare to that of SWNT/Epoxy composites. For composite having 1wt% of FSWNTs, the tensile modulus was increased to 2.75MPa from 2.66MPa of neat epoxy and showed an improvement of 3.38%. By increasing the input of reinforcement, the FSWNT/Epoxy composites were found to provide a much higher tensile modulus than SWNT/Epoxy composites at the same nanotubes

content. The modulus value of 2wt% FSWNT/Epoxy composite was obtained as 2.89MPa which is 1.05 times that of 2wt% SWNT/Epoxy composite. Further addition of FSWNTs (i.e. 3, 4, 5wt %) into the composites was also found to produce the tensile modulus (i.e. 2.97, 3.04, 3.16MPa) which was approximately 1.05 times of that of SWNT/Epoxy composites at the same nanotubes content. Table 3.1 is the summary of the tensile properties of the nanotube based composites measured from the tensile property tests.

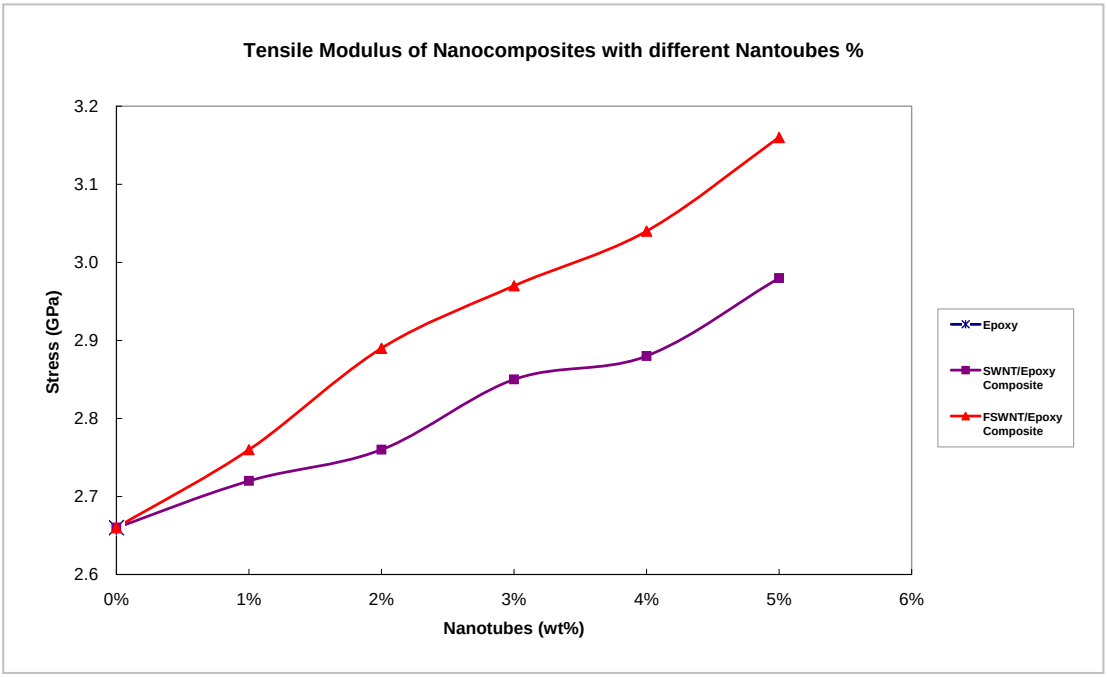

Figure 3.2 The Tensile Modulus of the nanocomposites as the function of nanotubes content.

Table 3.1 The summary of the Tensile Properties obtained from tensile property tests.

Materials	Nanotube Content (wt%)	Tensile Modulus (GPa)	% Improvement	Ultimate Strength (MPa)	% Improvement
Epoxy	0%	2.66 ± 0.07	-	50.08 ± 0.82	-
SWNT/Epoxy Composite	1%	2.72 ± 0.11	2.26%	50.32 ± 1.12	0.48%
	2%	2.76 ± 0.09	3.76%	52.95 ± 1.00	5.73%
	3%	2.85 ± 0.13	7.14%	53.52 ± 0.97	6.87%
	4%	2.88 ± 0.10	8.27%	53.50 ± 1.28	6.83%
	5%	2.98 ± 0.14	12.03%	54.94 ± 1.18	9.70%
FSWNT/Epoxy Composite	1%	2.75 ± 0.08	3.38%	51.75 ± 1.11	3.33%
	2%	2.89 ± 0.10	8.65%	52.80 ± 0.98	5.43%
	3%	2.97 ± 0.08	11.65%	55.80 ± 0.96	11.42%
	4%	3.04 ± 0.11	14.29%	56.36 ± 0.10	12.54%
	5%	3.16 ± 0.09	18.80%	58.55 ± 1.01	16.91%

The results of the tensile property test demonstrated that both SWNTs and FSWNTs exhibited significant impact on the load transfer efficiency of the composites. By the reinforcement of nanotubes, the tensile modulus and ultimate strength of the composites were improved. Moreover, these tensile properties were increased as the function of nanotube content. As 5wt% of nanotubes was applied, both tensile modulus and ultimate strength of the composites systems achieved the maximum. Though both tensile properties of the materials showed observable enhancement due to the addition of nanotubes, its effect on ultimate strength was comparatively moderate. On the other hand, through the comparison of the results, it is evaluated that the employment of FSWNTs into the composites system would provide a more favorable improvement in tensile properties. Also, these properties were increased in a much faster and steady approach than that of the SWNT/Epoxy system.

These results lend credence to the postulate that functionalization of the single-walled carbon nanotube by nitric acid and sulphuric acid may aid in securing the nanotube-matrix interface allowing for greater load transfer from the matrix to the nanotubes. The aggravation in interfacial interaction between matrix and nanotubes provides an excellent ability to resist from fracture and thus increase the tensile properties of the composites.

This interfacial interaction between the nanotubes and epoxy matrix could also investigate through the utilization of SEM. Figure 3.3 shows SEM images of the fracture surfaces of the Neat Epoxy, SWNT/Epoxy composites and FSWNT/Epoxy composites systems. Figure 3(a) illustrates the failure surface of the neat epoxy after the tensile property test. Through the micrograph, it is noticed that the failure of neat epoxy exhibited a brittle manner which was indicated by the ridge like patterns formed on the fracture surface. With the filling of nanotubes into the epoxy, the roughness of the fracture surface was found to increase according to the nanotube content. Figure 3(b) (i)-(v) and 3(c) (i)-(v) shows the fracture surfaces of the SWNT/Epoxy composites and FSWNT/Epoxy composites with different nanotubes weight percentages. The images of SEM demonstrated that the fracture of both nanotube based composites present a brittle behavior through the debris formed on the surfaces. As the content of nanotubes increased, the amount of debris created on the fracture surface augmented and formed in a smaller scale. However, the variation between the two nanotube based composite systems became obvious at the nanotube content of 3-5wt%.

By comparing the figure 3(b) (iii)-(v) to the figure 3(c) (iii)-(v), it is found that the fracture surfaces of SWNT/Epoxy composites contained both ridge like patterns together with debris, which is indicated by the red arrows in those figures. However, on the other hand, FSWNT/Epoxy composites showed different behaviors than SWNT/Epoxy composites.

When the amount of FSWNTs increased (i.e. 3-5 wt%), more debris were formed and with a dense but uniformed pattern (figure 3(c) (iii)-(v)). The surface roughness was found to enhance gently with the addition of FSWNTs. The fracture behaviors of the composites systems were suggested to relate to the interfacial interaction between the nanotubes and epoxy, and also the dispersion of nanotubes inside the epoxy matrix. As the interaction between the nanotubes and epoxy was getting stronger, the ability of the material to resist from tensile fracture became stronger. Thus, when failure occurred, debris was formed on fracture surfaces. Also, as the content of nanotubes increased, the resistance to failure was enhanced; therefore, the density of debris was increased on the surface. Furthermore, the dense and uniformed pattern of debris on the fracture surfaces of FSWNT Epoxy composites indicated that the FSWNTs were distributed uniformly inside the composite while the ridge like pattern with debris showed on the fracture surfaces of SWNT/Epoxy composites demonstrated the poor dispersion of SWNTs inside the epoxy. These results, in turn, implied that the functionalization of SWNTs can improved the dispersion of nanotubes inside the epoxy and also can provide a better interaction with the epoxy matrix.

The above conclusions were further proved by the SEM micrographs with higher magnifications as shown in figure 3.4. Figure 3.4 (a)-(b) present closer images of the fracture surface of SWNT/Epoxy composites through the SEM. Through the micrographs, it is noticed that the SWNTs clusters were formed insides the composites. These agglomerates showed poor wetting of epoxy and were parallel to the fracture surface, which would severely affected the load transfer between the epoxy and nanotubes, and therefore, lower the tensile properties of the composites. Besides, the size and number of these aggregates were found to enlarge with increased SWNTs applied into the composites. Contrast to the SWNT/Epoxy composite, the nanotubes reinforced in FSWNT/Epoxy composites provided a uniform

dispersion in the composite as indicated in figure 3.4 (c)-(d). The FSWNTs showed a good wetting of epoxy and most of them were perpendicular to the fracture surface, which would enhance the efficiency of load transfer inside the FSWNT/Epoxy composites and hence gave better mechanical properties than SWNT/Epoxy composites. This finding provided evidence for the strong interaction (bonding) created between the functionalized SWNTs and epoxy matrix, and could be adopted as the reason for the higher achievement in tensile properties and over than that of SWNT/Epoxy composites.

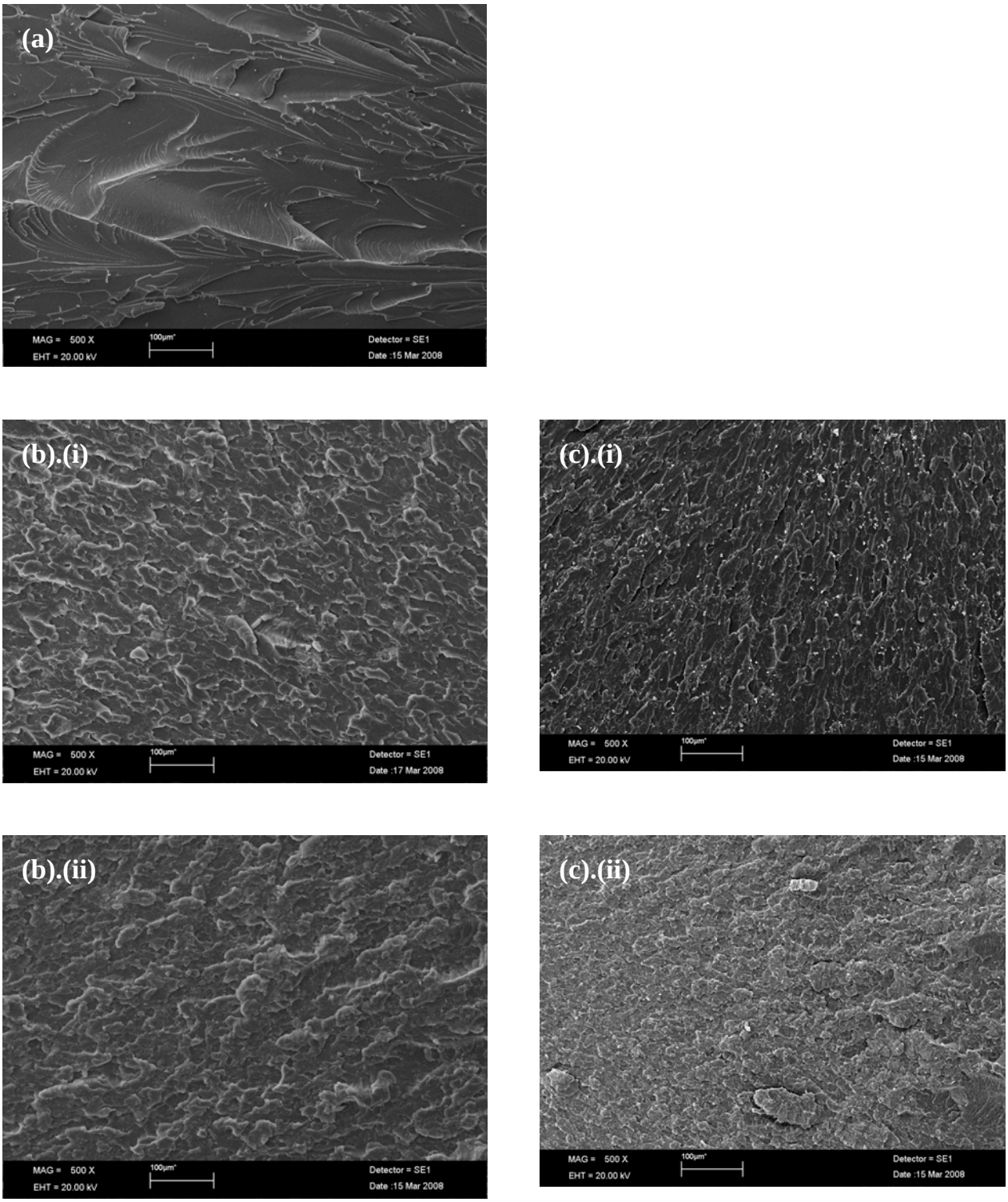

Figure 3.3 The fracture surface of specimens after the tensile property test – (a) Neat Epoxy, (b) (i)-(v) SWNT/Epoxy Composites i.e. 1wt% - 5wt%, and (c) (i)-(v) FSWNT/Epoxy Composites i.e. 1wt% - 5wt%.

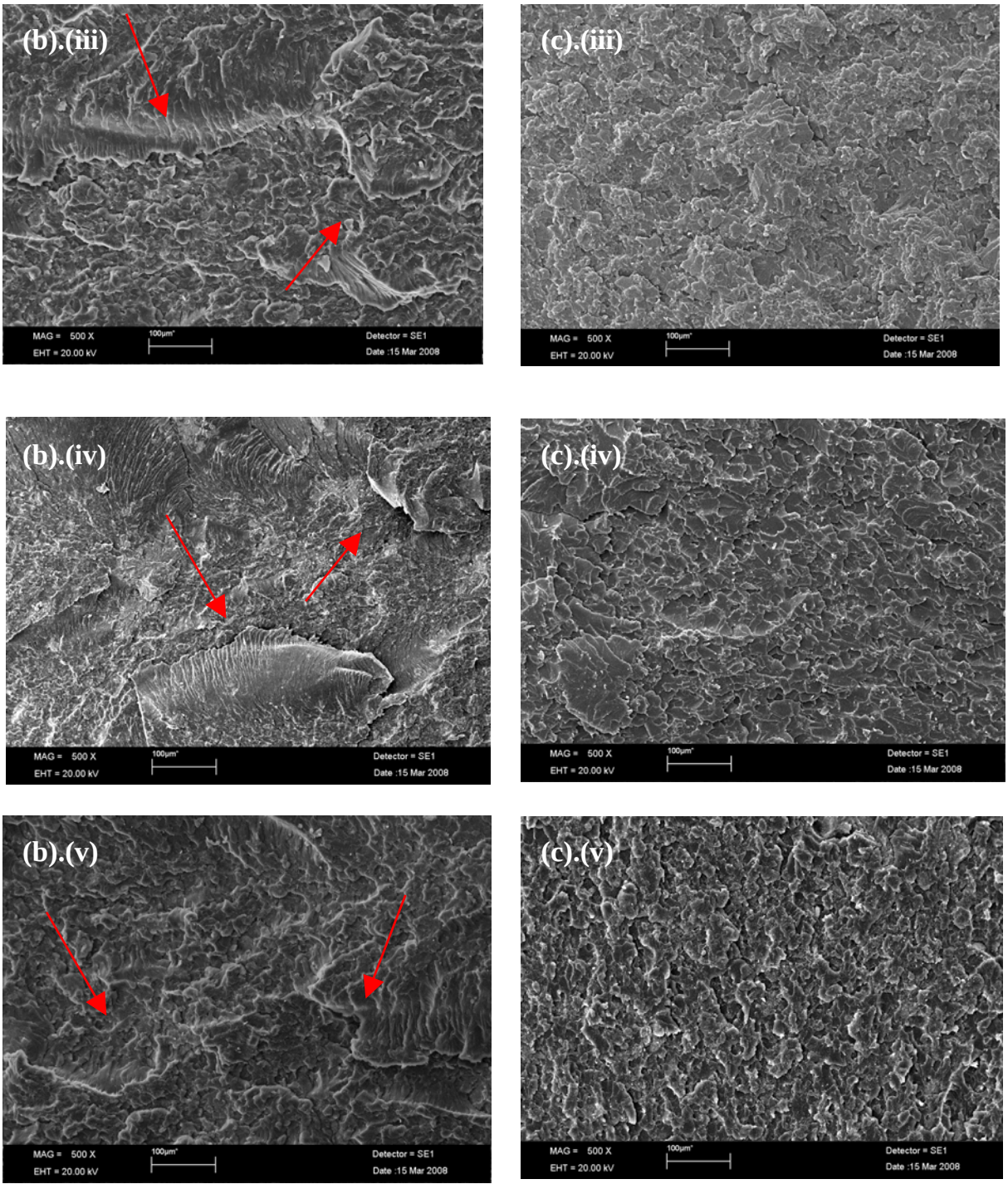

Figure Continued

Figure 3.3 The fracture surface of specimens after the tensile property test – (a) Neat Epoxy, (b) (i)-(v) SWNT/Epoxy Composites i.e. 1wt% - 5wt%, and (c) (i)-(v) FSWNT/Epoxy Composites i.e. 1wt% - 5wt%.

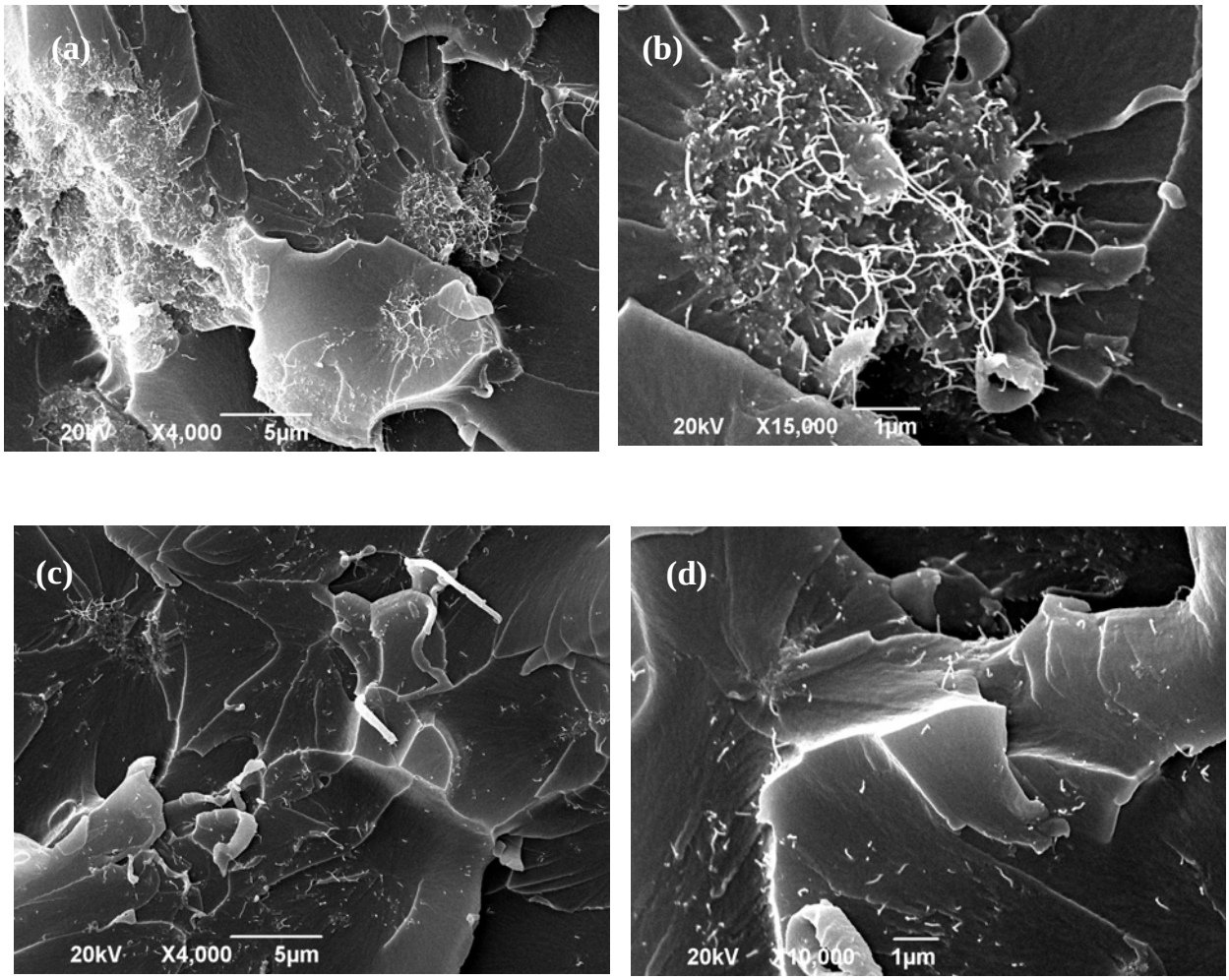

Figure 3.4 The dispersion of nanotubes inside the composite system. (a)-(b) SWNT/Epoxy Composites and (c)-(d) FSWNT/Epoxy Composites.

3.1.2 Analysis of Flexural Property

The flexural property test employed in this study was the 3-Point Bending test. Through this test, the effects from SWNTs and FSWNTs on the flexural modulus of the composites systems were investigated. However, the ultimate flexural stress were not able to conclude as the composites specimens did not fail within 5% strain limited as required by the test method of standard ASTM D790. Figure 3.5 shows the results of the 3-Point bending test in term of load-deflection curves. Through the figure 3.5(a) and (b), it is noticed that both SWNT/Epoxy composites and FSWNT/Epoxy composites provided better resistance to deflection as compared to neat epoxy. Moreover, these two composites systems exhibited similar increasing profile in load-deflection curve. In order to study the composite systems more comprehensively, the flexural moduli were calculated for each system with different nanotubes contents. This flexural property can be obtained by calculating the slope of the initial straight line portion of the load-deflection curve and substitute in equation 2.6 as mentioned in chapter 2. Figure 3.6 illustrates the flexural modulus of the nanotube based composites with different nanotubes contents. From the figure, it is revealed that the flexural modulus of both SWNT/Epoxy composites and FSWNT/Epoxy composites increased gradually with the nanotubes contents and provided the maximum value when the weight percentage of nanotubes reached 5wt%. This improvement in flexural property of composites due to the reinforcement was found to be outstanding.

In the flexural property test, the neat epoxy was found to provide a flexural modulus of 2.445GPa. By adding 1wt% of SWNTs into the epoxy matrix, it is found that the flexural modulus of the composites was improved by 2.32% from 2.445GPa of neat epoxy to 2.501GPa. Further filling of SWNTs would provide further enhancement of the flexural property of composites, however, such increment was found with certain fluctuations. For

composites containing 2wt% of SWNTs, the flexural modulus was increased to a value 2.532GPa and a 3.57% improvement was obtained over the neat epoxy. Although enhancement was achieved with increased nanotubes content, the rate of increment was slow down as shown in the figure. When 3wt% of SWNTs was applied, the rate of enhancement was raised again and gave a flexural modulus of 2.639GPa with an improvement of 7.94%. Similar phenomenon was found at SWNTs content of 4 and 5wt%. For composites embedded with 4wt% of SWNTs, similar to that with 2wt% SWNTs, the rate of increment was comparatively moderate when compared to that with 3wt% SWNTs. The flexural modulus was measured to be 2.693GPa and provided 10.15% improvement over the epoxy alone. And for the composites with 5wt% of SWNTs, similar to that with 3wt% SWNTs, the rate of improvement was increased again and gave the maximum value of flexural modulus which was 2.802GPa and have an enhancement by 14.61%.

Opposing to SWNT/Epoxy composites, the flexural modulus of FSWNT/Epoxy composites was increased more steadily with the nanotubes contents. For the 1wt% FSWNT/Epoxy composites, its flexural modulus was enhanced by 3.60% from 2.445GPa of the neat epoxy to 2.533GPa. When 2wt% of FSWNTs was employed into the composites, its flexural property was gained to 2.6GPa, and a 6.36% in improvement was obtained over the neat epoxy. Similarly, 6.36%-14.49% improvement was attained for composites containing 3wt% to 5wt%. By comparing the results with SWNT/Epoxy composites, it is shown that the rate of improvement in flexural modulus of FSWNT/Epoxy composites was more dramatic. Besides, the flexural modulus of FSWNT/Epoxy composites at different nanotubes contents (i.e. 1, 2, 3, 4, 5wt%) was found to superior to that of SWNT/Epoxy composites having the same nanotubes weight percentages by 1.28%, 2.7%, 1%, 3.9% and 1.7%.

The above results of 3-Point Bending test were summarized in table 3.2. Through the table of results, it is cleared that both SWNT/Epoxy composites and FSWNT/Epoxy composites provided attractive improvement in flexural modulus over the neat epoxy. As the application of nanotubes increased, the flexural property was also increased and gave a maximum value when 5wt% of nanotubes was used. When comparing the two types of composites systems, it is found that the introduction of FSWNTs into the composites was more favourable for property enhancement. Hence, apart from the tensile properties, functionalization of SWNTs was also provided a better improvement in flexural property. Figure 3.7 shows the fracture surface of the neat epoxy and also that of the two composites systems.

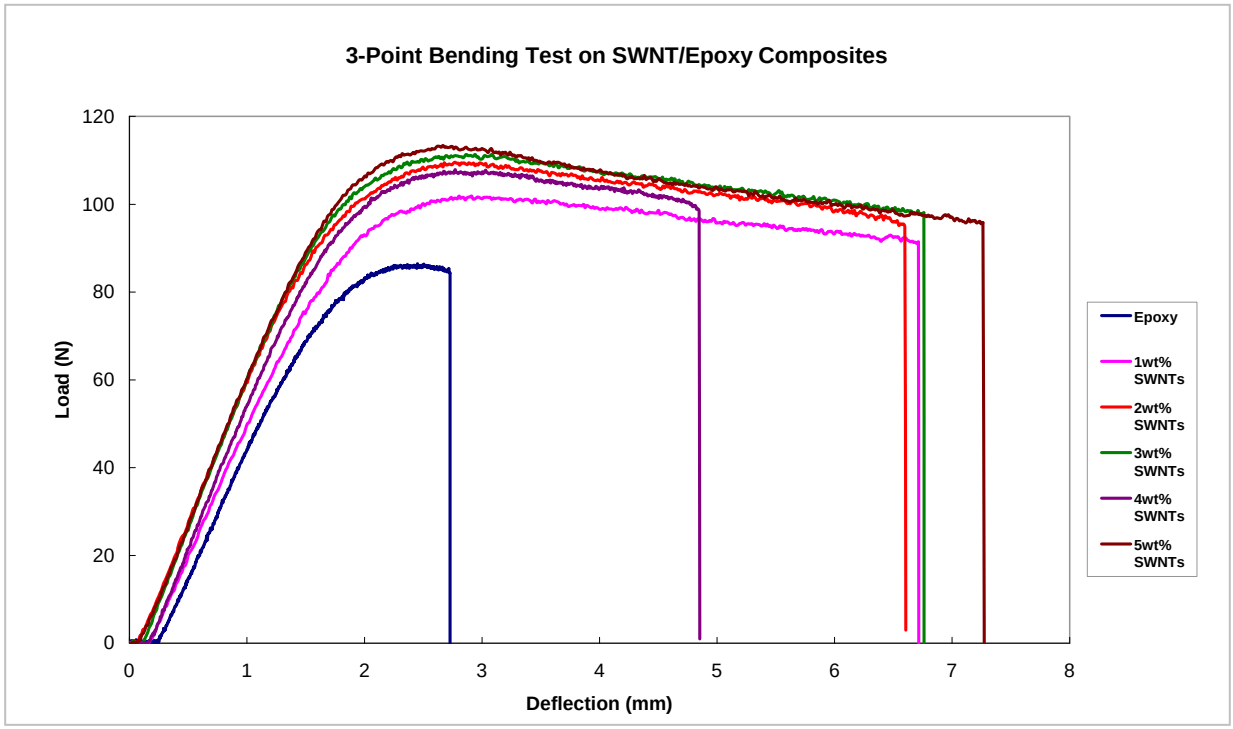

(a)

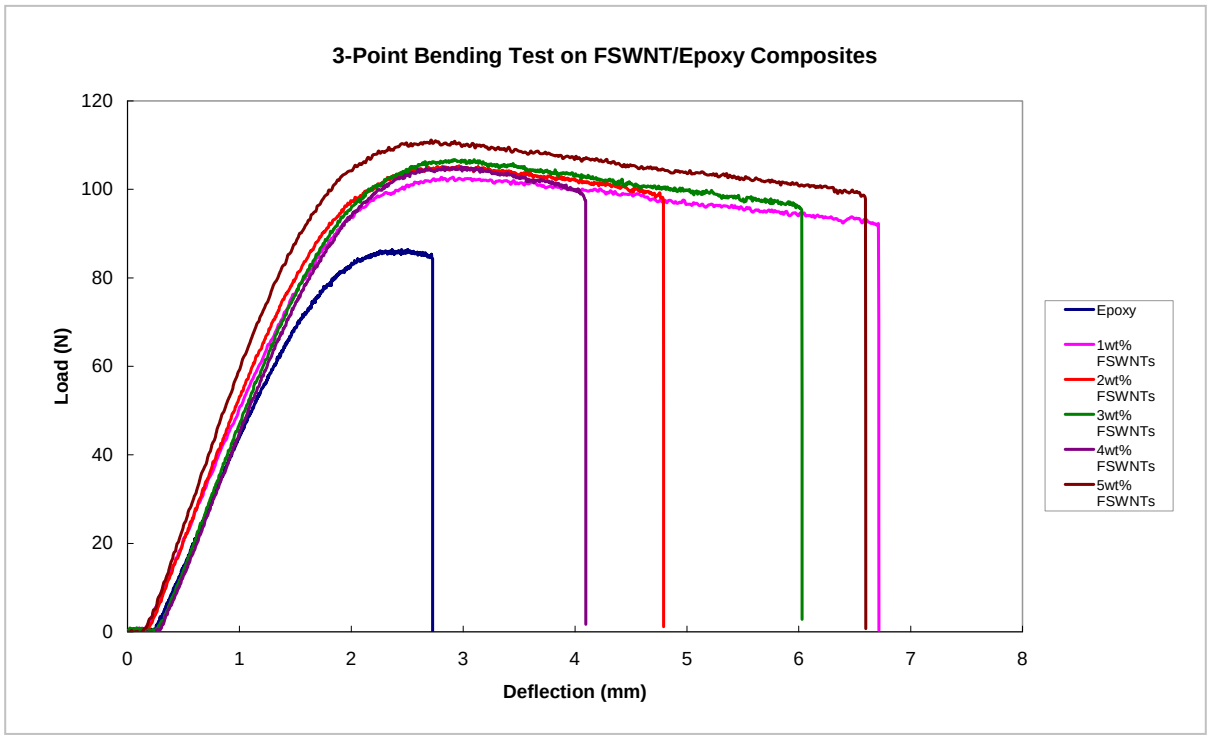

(b)

Figure 3.5 The 3-Point Bending Test results of (a) SWNT/Epoxy Composites and (b) FSWNT/Epoxy Composites.

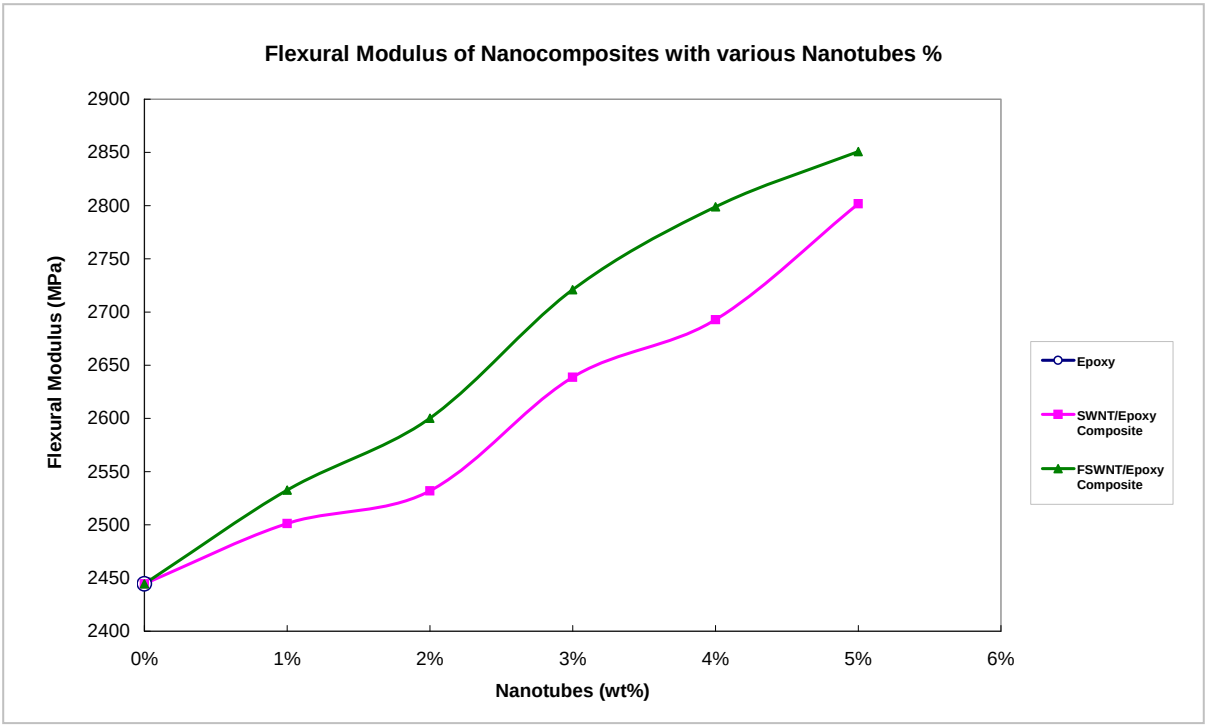

Figure 3.6 The Flexural Modulus of the nanocomposites as the function of nanotubes content.

Table 3.2 The summary of the Flexural Modulus obtained from 3-Point Bending Tests.

Materials	Nanotube Content (wt%)	Flexural Modulus (GPa)	% Improvement
Epoxy	0%	2.445 ± 0.085	-
SWNT/Epoxy Composite	1%	2.501 ± 0.163	2.32%
	2%	2.532 ± 0.205	3.57%
	3%	2.639 ± 0.192	7.94%
	4%	2.693 ± 0.177	10.15%
	5%	2.802 ± 0.200	14.61%
FSWNT/Epoxy Composite	1%	2.533 ± 0.110	3.60%
	2%	2.600 ± 0.067	6.36%
	3%	2.721 ± 0.048	11.30%
	4%	2.799 ± 0.071	14.49%
	5%	2.851 ± 0.102	16.61%

Figure 3.7(a) shows the fracture surface of neat epoxy. A step was found at the bottom of the specimen because, during the flexural property test, the material was under compression along the top of the specimen while under tension along the bottom of the specimen, such coupling effect caused the material to produce sagging deformation and finally break in the step manner. Figure 3.7 (b) (i)-(v) and (c) (i)-(v) shows the fracture surfaces of SWNT/Epoxy composites and FSWNT/Epoxy composites with different nanotubes contents. Same as in tensile specimen, debris were found on the fracture surface of the nanotube based composites.

When compared to the fracture surface of neat epoxy (figure 3.7(a)), it is noticed that the step created by the coupling effect in the composite systems was not as obvious as in neat epoxy, and a lot of river line patterns were found on that area. It is believed that the area with river line patterns worked as a transition region where the compression and tension effect took place. The reinforcement of nanotubes improved the property of material to resist from the coupling effect caused by the sagging deformation, thus prevented the material from failure and forming a step structure as in neat epoxy. Although both SWNT/Epoxy composites and FSWNT/Epoxy composites demonstrated similar patterns in their fracture surface, a crack was observed near the transition region in all the SWNT/Epoxy composite systems (i.e. 1-5wt%). By comparing the results with neat epoxy, it is known that no crack was formed in the pure matrix. Also, through the outcomes of FSWNT/Epoxy composites, it is revealed that the addition of FSWNTs with good dispersion (as pointed out in tensile property test section) didn't initial any crack during the 3-Point bending test. Thus, the results obtained from SWNT/Epoxy composites may account for the agglomerates created from the SWNTs. As shown in tensile section, the agglomerates were poor in wetting which would

lower the load transferability of the reinforcement. Hence cracks may easily initiate in the region where agglomerates were assembled.

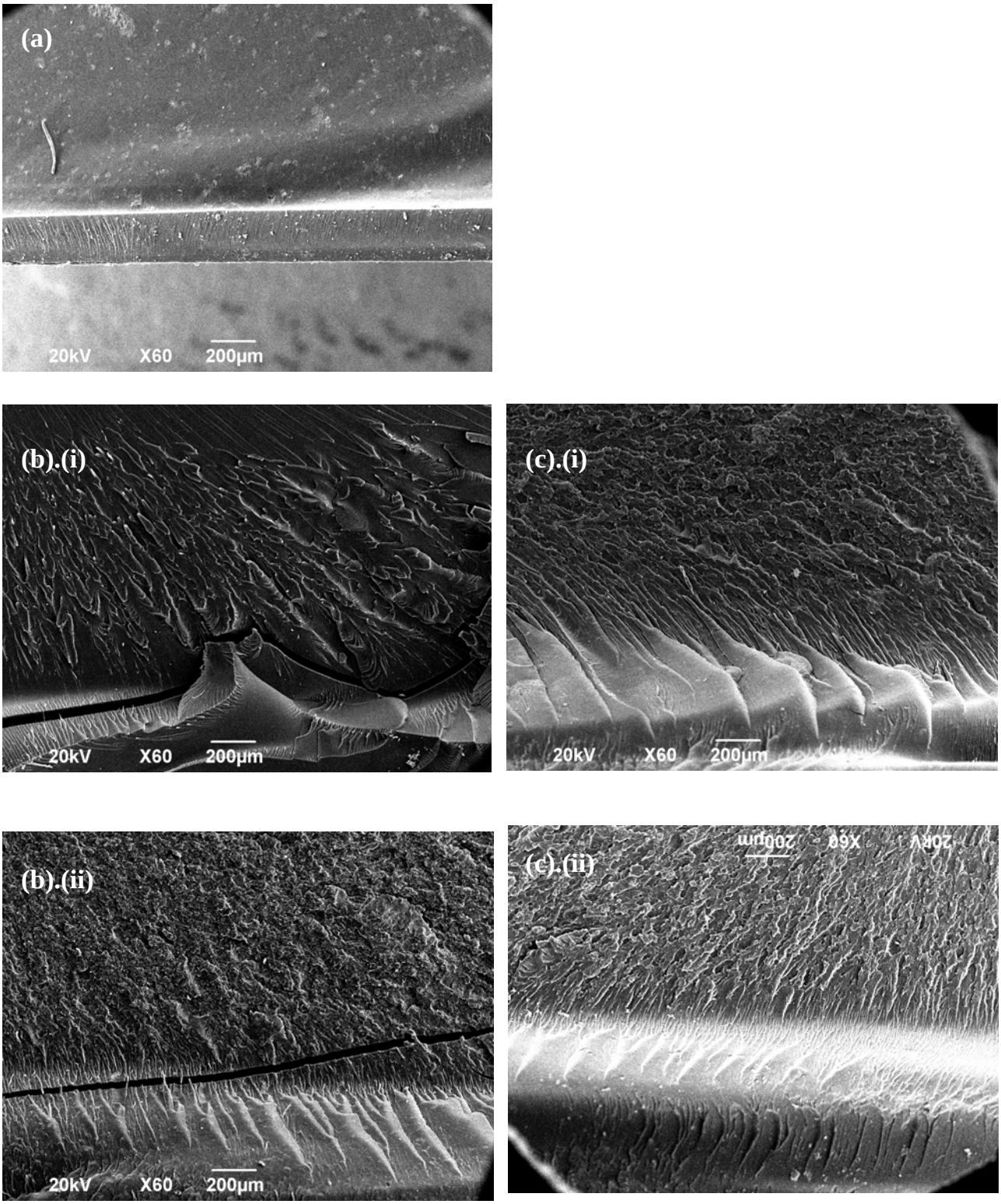

Figure 3.7 The fracture surface of specimens after the 3-Point Bending Test – (a) Neat Epoxy, (b) (i)-(v) SWNT/Epoxy Composites i.e. 1wt% - 5wt%, and (c) (i)-(v) FSWNT/Epoxy Composites i.e. 1wt% - 5wt%.

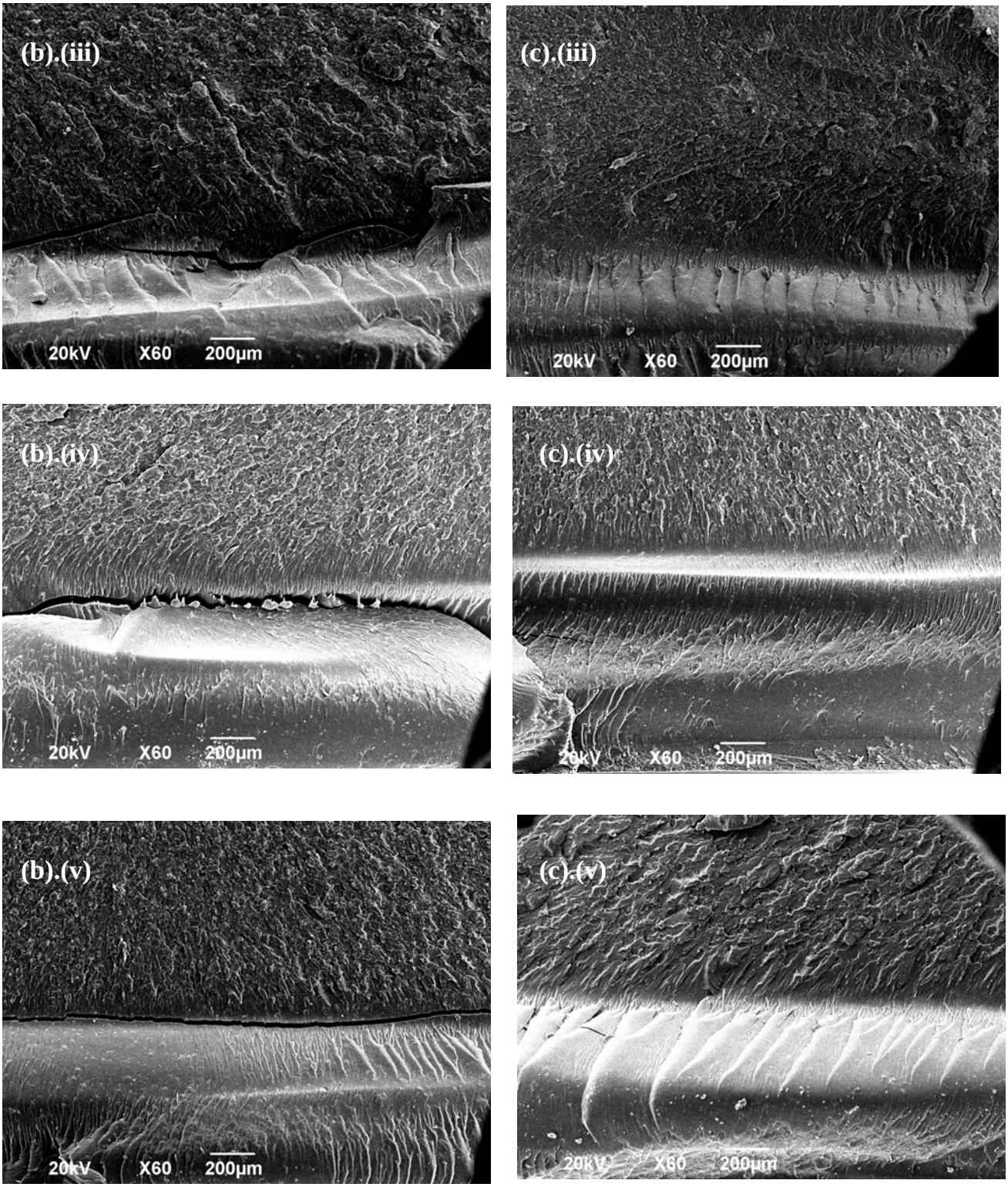

Figure Continued

Figure 3.7 The fracture surface of specimens after the 3-Point Bending Test – (a) Neat Epoxy, (b) (i)-(v) SWNT/Epoxy Composites i.e. 1wt% - 5wt%, and (c) (i)-(v) FSWNT/Epoxy Composites i.e. 1wt% - 5wt%.

3.1.3 Analysis of Impact Property

In the izod impact test, all types of composites specimens failed in a "complete break" mode (figure 3.8) and exhibited a brittle behaviour as there was no drawing or necking down in the broken area. The effects of both purified SWNT and functionalized SWNT on the composites in the mean of notched izod impact strength are shown in figure 3.9. Figure 3.9 is the impact strength of the composites as the function of nanotubes content. The calculated values revealed in the figure have been adjusted with the toss correction as mentioned in chapter 2 because the measured values of fracture energy were less than 27 J/m for all specimens during the experiment. Through the impact test results, the neat epoxy was found to have an impact value of 1486.72 J/m^2 and both the SWNT/Epoxy and FSWNT/Epoxy composites showed a remarkable alteration in the impact properties over the neat epoxy alone. For the SWNT/Epoxy composites, the impact strength increased gradually with the increasing content of SWNTs until it reached the maximum value at 3wt% of SWNTs. The impact strength was enhanced by 24.28% from 1486.72 J/m^2 of the neat epoxy to 1846.92 J/m^2 for composites containing 3wt% of SWNTs. Similarly, 4.39% to 9.99% improvement was obtained for composites containing 1wt% to 2wt% of SWNTs. Although the addition of SWNTs showed an attractive enhancement on the impact property of composites, the impact strength value was found to decrease as further filling of SWNTs into the epoxy matrix. The impact strength was lowered to 1618.79 J/m^2 from the maximum value 1846.92 J/m^2 for composite having 4wt% of SWNTs, however, the impact property of this composite still able to provide 8.88% improvement over the neat epoxy. The composites embedded with 5wt% of SWNTs, on the other hand, were found to experience a dramatic decrease in impact strength which was 1171.15 J/m^2. This impact value was much lower than that of the neat epoxy, which showed a property deterioration of -21.23% of the material.

While comparing the two curves in figure 3.9, the FSWNT/Epoxy composites were revealed to present a more favorable augmentation in impact property when compared to that of SWNT/Epoxy composites containing the same weight percentage of nanotubes. And the impact strength was found to increase at a faster rate in the FSWNT/Epoxy composites. For composites having 1wt% of FSWNTs, the impact value was increased to 1687.41 J/m^2 from 1486.72 J/m^2 of neat epoxy and showed an improvement of 13.50%. Similar enhancement was found in further addition of FSWNTs. When 2wt% of FSWNTs was applied in the composite, its impact strength was gained to a value of 1792.32 J/m^2, and a 20.56% in improvement was obtained over the neat epoxy. A spectacular impact value was achieved when the composites were embedded with 3wt% of FSWNTs. At this content, the impact strength of composites reached the maximum value of 2247.52 J/m^2 and showed an enhancement of 51.17%. However, such trend in increasing was not able to hold with further filling of FSWNTs into the composites. The impact strength was decreased to 1960.67 J/m^2 from the highest value 2247.52 J/m^2 of composite having 4wt% of FSWNTs. Although there was a diminution in impact value, the composite was yet provided a 31.88% improvement over the neat epoxy. For the composites having 5wt% FSWNTs, similar to the result of 5wt% SWNT/Epoxy composites, were having a decrease in impact strength and gave a value of 1760.83 J/m^2. However, conversely, these composites acquired an increment in impact strength of 18.44% when compared to that of neat epoxy.

The results of izod impact test indicate a significant influence induced by using the SWNTs and FSWNTs as reinforcement in epoxy. Both SWNT/Epoxy and FSWNT/Epoxy composites exhibited an improvement in impact strength when 1wt%-5wt% of nanotubes (except the 5wt% SWNT/Epoxy composites) were reinforced into the composites. By comparing the results of these two types of composites, it is revealed that the introduction of

FSWNTs into the epoxy as reinforcement would provide a more attractive enhancement than using the purified SWNTs. Apart from this, the impact value was found to change in a faster manner, especially at the 3wt% of FSWNTs. At this content, the impact strength of FSWNT/Epoxy composites was superior to that of SWNT/Epoxy composites, having the same weight percentage of nanotubes, by 21.69%. Other FSWNT/Epoxy composites with various weight contents (i.e. 1, 2, 4, 5 wt%) also gave a favourable improvement (i.e. 8.72, 9.60, 21.12, 50.35%) over the SWNT/Epoxy composites with the same nanotubes weight percentages. Netherless, different from SWNT/Epoxy composites, the impact property of FSWNT/Epoxy composites were declined in a lower rate from the nanotubes content 4wt% to 5wt%, and the impact value of these composites still able to achieve an improvement over the epoxy alone. In addition, it is found that the impact strength would reach its maximum when the nanotube weight content was 3wt% for both kinds of nanotubes composites. This suggested that the weight percentage of 3 was the optimal nanotube content that would provide the best impact strength for the nanotube epoxy composites.

Table 3.3 is the summary of the results obtained from Izod Impact Tests. It is shown that the variations in those results obtained from SWNT/Epoxy composites were much larger than that in FSWNT/Epoxy composites. While the range of variation was kept within $\pm$ 6.30 for all weight percentages of FSWNT/Epoxy composites, the SWNT/Epoxy composites showed a diverse variation from a minimum $\pm$ 10.23 for 5wt% of SWNTs to a maximum of $\pm$ 19.45 for 3wt% of SWNTs.

(a) **(b)**

Figure 3.8 Composite specimens (from left to right: Neat Epoxy, SWNT/Epoxy composite and FSWNT/Epoxy composite) after the Izod Impact Test (a) Side view and (b) Top View

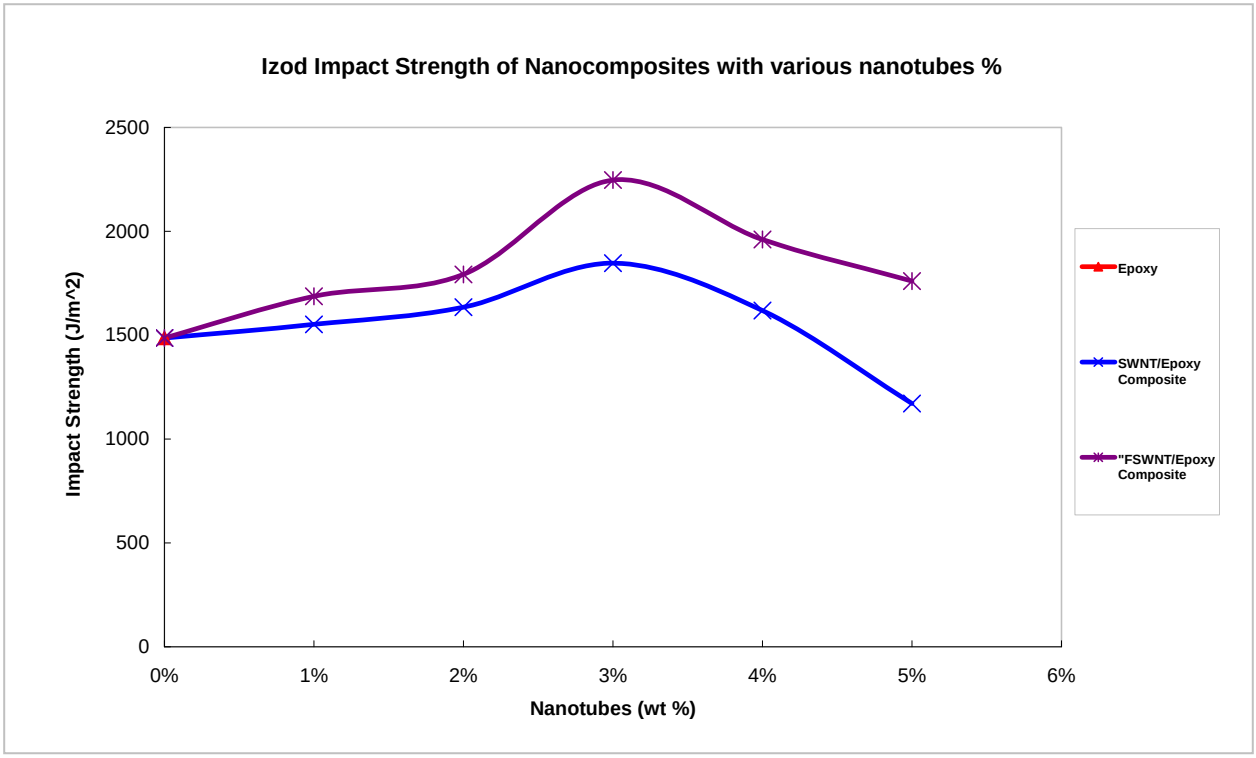

Figure 3.9 The impact strength of the nanocomposites as the function of nanotubes content.

Table 3.3 The summary of the impact results obtained from Izod Impact Tests.

Materials	Nanotube Content (wt%)	Impact Strength (J/m^2)	% Improvement
Epoxy	0%	1486.72 ± 3.05	-
SWNT/Epoxy Composite	1%	1552.01 ± 12.63	4.39%
	2%	1635.23 ± 15.05	9.99%
	3%	1846.92 ± 19.45	24.28%
	4%	1618.79 ± 14.01	8.88%
	5%	1171.15 ± 10.23	-21.23%
FSWNT/Epoxy Composite	1%	1687.41 ± 3.61	13.50%
	2%	1792.32 ± 5.44	20.56%
	3%	2247.52 ± 5.74	51.17%
	4%	1960.67 ± 5.05	31.88%
	5%	1760.83 ± 6.30	18.44%

The results analysis obtained above were attributed to the fact that nanotubes worked as a good medium for load transfer. Through the application of nanotubes, the toughness and load transferability of materials were enhanced; however, the percentage of nanotubes applied would severely affect the results. From the izod impact test, it is shown that the application of both purified SWNT and functionalized SWNT as reinforcement could improve the impact strength of the materials. The best impact property was obtained when 3wt% of nanotubes was used. The FSWNTs provide the better results over the SWNTs when employed as the reinforcement in epoxy. It is because the interfacial interaction between matrix and nanotubes were improved as bonding was formed between the functional groups on nanotubes surface and the epoxy. As more bonding were formed, a dense cross-link structure would be created thus providing an excellent ability to resist from fracture and also improving better medium

for load transfer. Additionally, the dispersion of FSWNTs in the epoxy was improved as less nanotube clusters were formed inside the composites. However, further increase in the nanotube content would lower the impact strength of the composites since, as more nanotubes were input into the material, the chance of crack initiation would easily be raised during the load transfer.

In this study, the impact property was lowered when the nanotubes content was more than 3wt%. The degradation in properties indicates the nanotubes was turned into the dominant medium instead of reinforcement, thus weaken the load transferability. Moreover, the overall performance of SWNT/Epoxy composites was apparently fluctuated when compared to that of FSWNT/Epoxy composites, the reason of this may account to the agglomerates formed inside the composites. As more SWNTs were reinforced into the composites, more nanotubes were able to cluster together, thus causing difficulties in controlling the property. And because of this, there was a serious deterioration of impact value when 5wt% of SWNTs was embedded in the SWNT/Epoxy composites.

In order to examine the failure mechanism of the nanotube/epoxy composites due to impact test, SEM was utilized to study their fracture surfaces. Neat epoxy, 3wt% SWNT/Epoxy composites and 3wt% FSWNT/Epoxy composites were investigated under the microscopy. Figure 3.10 shows the SEM images with low magnification of the composite specimens. Through the micrographs, it is noticed that the neat epoxy exhibited a smooth brittle fracture surface after the impact test while the nanotube/epoxy composites showed a rougher surface comparatively. It is suggested that as nanotubes were filled into the epoxy, bonding were formed between them. Such bonding would enhance toughness of the composites and thus resist them from breakage.

Figure 3.11 and 3.12 give the images with higher magnification at the cleavage of composites specimens due to the impact force. By comparing figure 3.11(a) and 3.12(a), it is observed that the fracture surface of SWNT/Epoxy composite contained the river lines which were more obvious and coarse. However, for those appeared in the fracture surface of FSWNT/Epoxy composite were much fine in shape. When examined these broken lines through the close-up micrographs as shown in figure 3.11 (b) and 3.12 (b), the embedded nanotubes in the composites were clearly shown. In figure 3.11 (b), the SWNTs were dispersed around the broken lines randomly and, at the same times, they tended to cluster together and formed the nanotubes networks. These networks show a poor wetting of epoxy and were parallel to the fracture surface, which were unflavored to the load transfer between the epoxy and nanotubes. And therefore, the impact strength of the composites was lower. Since it is not possible to control the number and location of the formed nanotube agglomerates, hence the measured impact values show apparent fluctuation.

Besides, it also revealed that as more SWNTs were added into the composites, the impact property was decreased since more agglomerates may form during the composites fabrication. Opposing to the SWNT/Epoxy composite, the nanotubes reinforced in FSWNT/Epoxy composite were much better in dispersion around the hackle region, and there was no nanotubes networks are found as shown in figure 3.12 (b). The nanotubes shows a good wetting of epoxy and most of them were perpendicular to the fracture surface, thus provided a prefect condition for maximizing the load transfer inside the composite and hence a greater impact strength was obtained. These SEM images were adaptable as an indirected explanation to the results obtained from the izod impact test

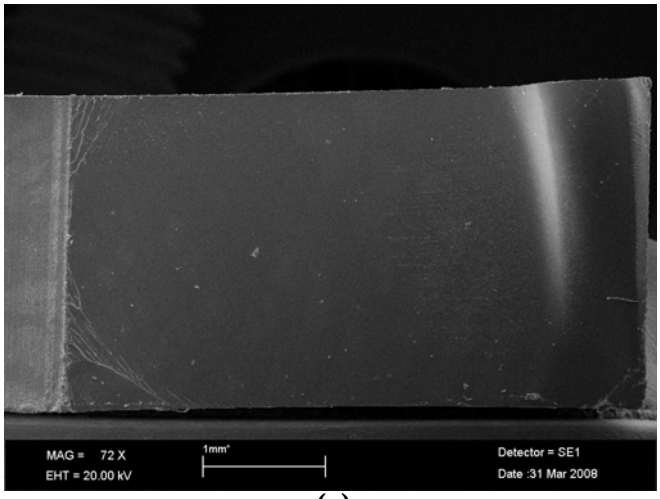

(a)

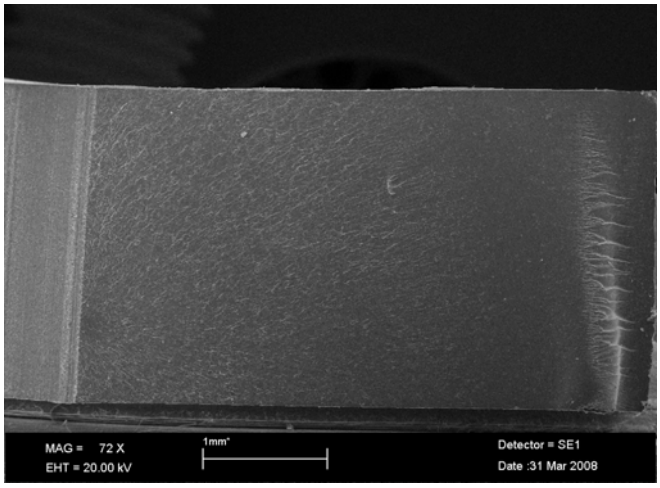

(b)

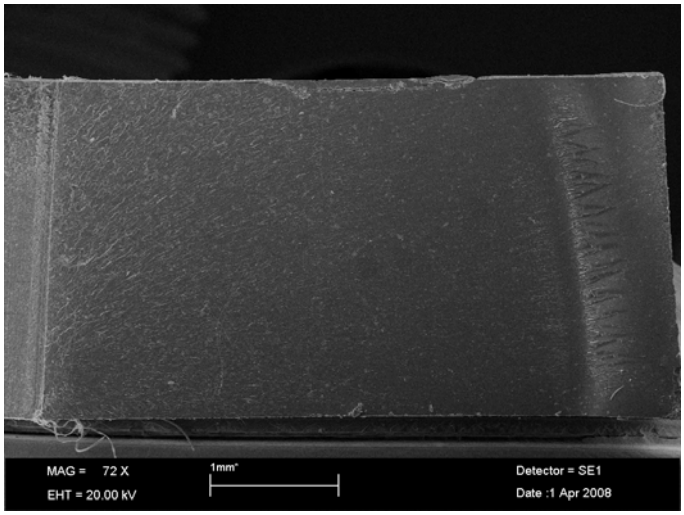

(c)

Figure 3.10 The SEM images of fracture surfaces of the specimens after the Izod Impact Test (a) Neat Epoxy, (b) 3wt% SWNT/Epoxy Composite and (c) 3wt% FSWNT/Epoxy Composite.

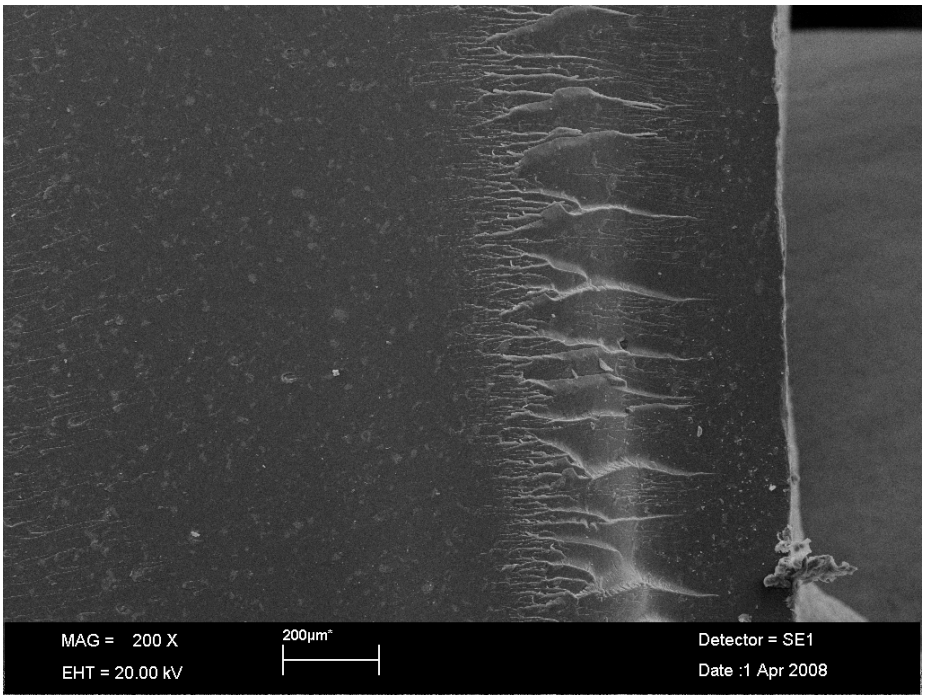

(a)

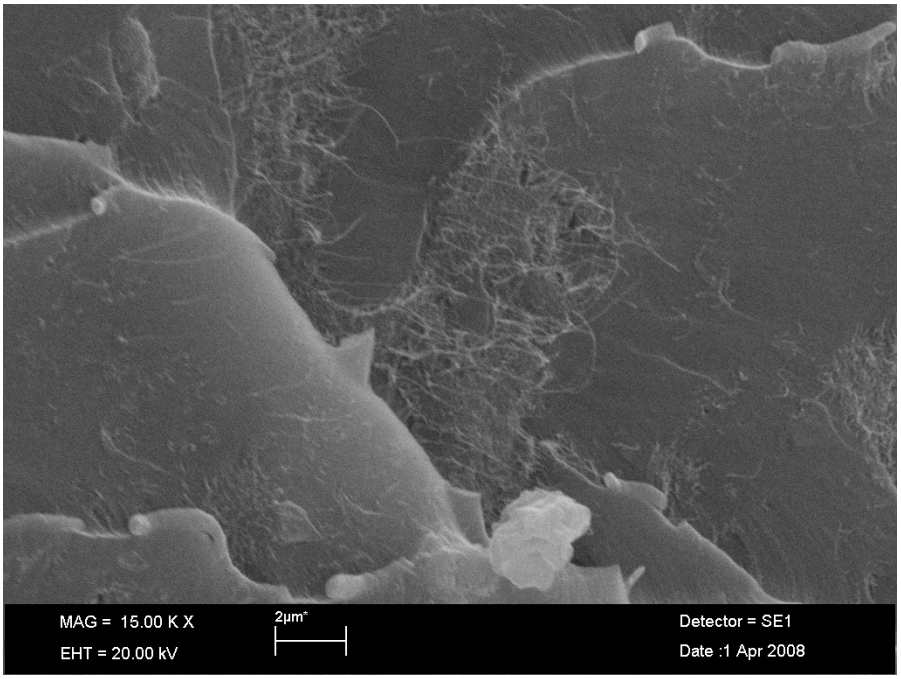

(b)

Figure 3.11 The higher magnificent SEM images of fracture surfaces of the specimens - 3wt% SWNT/Epoxy Composite

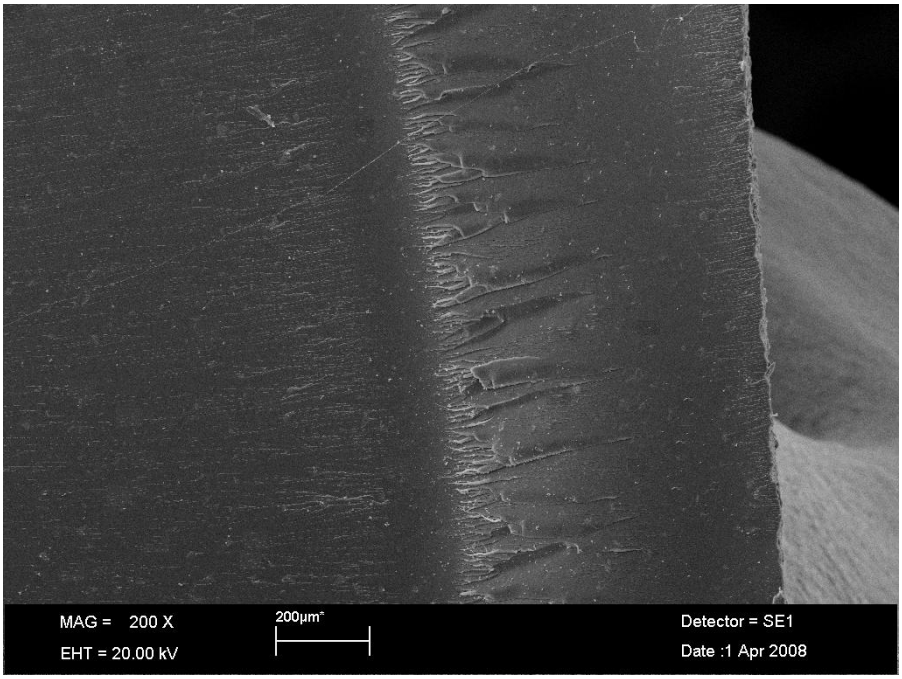

(a)

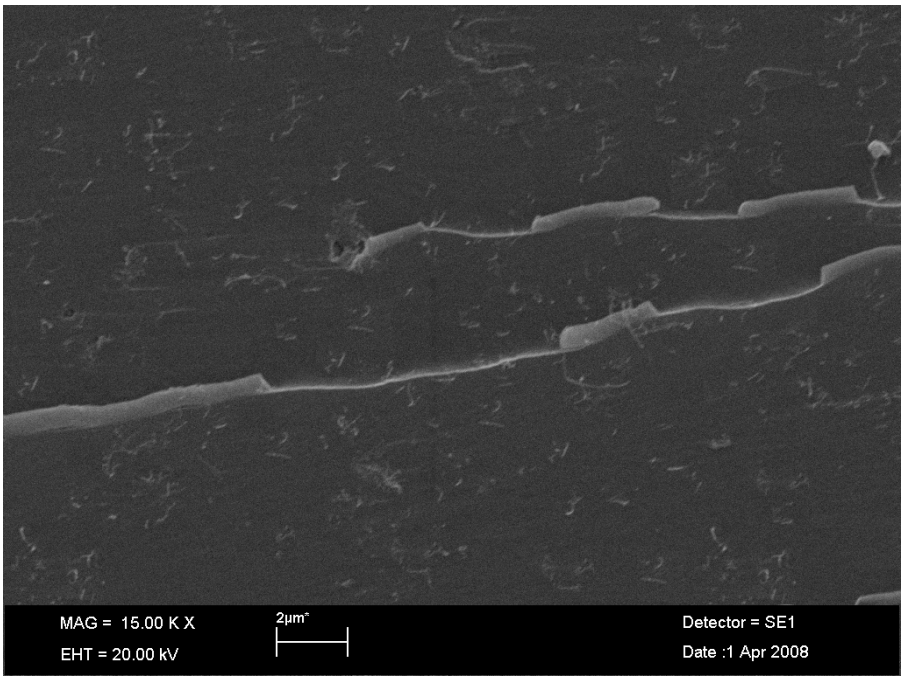

(b)

Figure 3.12 The higher magnificent SEM images of fracture surfaces of the specimens - 3wt% FSWNT/Epoxy Composite

3.1.4 Analysis of Hardness Property

In the microhardness test, all composites specimens were investigated using the Vicker's type of diamond in a microhardness tester. The results from the microhardness tests have present a facilitation of hardness value by adding the nanotubes into the epoxy matrix. Figure 3.13 shows the Vicker's hardness of the composites as the function of weight percentage of nanotubes. According to the results, the hardness value of the neat epoxy was measured to be 14.375 Hv. Besides, the reinforcements of both SWNTs and FSWNTs in the epoxy matrix were found to enhance the hardness property of the neat epoxy. For the SWNT/Epoxy composites, the improvement of hardness value was noticeable as the addition of SWNTs increased. The Vicker's hardness was enhanced by 9.88% from 14.375 Hv of neat epoxy to 15.795 Hv for composites with 1wt% of SWNTs. With further augment of nanotubes content, the improvement in hardness property was more obvious, especially when 5wt% of SWNTs was introduced into the composite. At the content, the Vicker's hardness was found to be 18.08 Hv which provided the improvement by nearly 26% over the neat epoxy. Although the addition of nanotube from 2wt%-4wt% also gave aggravation in the hardness value, the rate of improvement was rather moderate when compare to that of nanotubes content at 1wt% and 5wt%. The Vicker's hardness in this range of nanotubes content was obtained to be within 16.3-17 Hv and the percentage in improvement was laid between 13.6% and 17.8% over the neat epoxy.

By comparing the results in figure 3.13, it is found that the FSWNT/Epoxy composites show gradually improvement in hardness value, however, with a slower rate, when compared to SWNT/Epoxy composites containing the same nanotubes content. For composites having 1wt% of FSWNTs, the Vicker's hardness was enhanced to 14.75 Hv from 14.375 Hv of neat epoxy and showed an improvement of 2.61%. Similar enhancement was

found in further filling of FSWNTs. When 2wt% of FSWNTs was employed in the composite, its hardness value was gained to 15.075 Hv with a 3.85% improvement. As more nanotubes were added, 3wt%-5wt%, the hardness property was altered gradually from 15.925 to 16.78 Hv with the percentage improvement various from 10.78 – 16.73%.

The results from microhardness test designated the improvement of hardness property by reinforcing the SWNTs and FSWNTs into epoxy. Both SWNT/Epoxy and FSWNT/Epoxy composites showed an enhancement in Vicker's hardness when 1wt%-5wt% of nanotubes were added into the composites. By comparing the results of both types of composites, it is revealed that the reinforcement of FSWNTs into the epoxy would provide less attractive results than applying the SWNTs as filler. The hardness values of FSWNT/Epoxy composites were found to be lower than that of SWNT/Epoxy composites when having the same nanotubes content. Different from the results obtained in previous sections, the results suggested SWNTs were better as reinforcement than FSWNTs and its composites provided a delighted improvement in the property of composite. The percentage improvements of SWNT/Epoxy composites over the FSWNT/Epoxy composites at the same nanotubes content i.e.1, 2, 3, 4, 5 wt% were found to be 7.085%, 8.345%, 3.108%, 4.506% and 7.747%. Besides, from table 3.4, it is shown that the standard deviations in the results of SWNT/Epoxy composites were comparatively higher that that of FSWNT/Epoxy composites by approximately $\pm$ 0.1. However, such variations were relatively consistent for both types of composites, thus provided a reliable support of the data obtained. Although the SWNT/Epoxy composites gave better outcomes in the microhardness test, the increase in hardness value was not as steady as in FSWNT/Epoxy composites.

The results analysis of the microhardness test has given important information on the enhancement of hardness property due to the reinforcement of SWNTs and FSWNTs. Through the introduction of nanotubes, the resistance of materials against deformation due to the applied load was improved. Though the analysis shown that SWNT/Epoxy composites provide better hardness property over the FSWNT/Epoxy composites, such conclusion may be induced due to the agglomerates formed inside the composites. As pointed out by prior sections, the SWNTs tended to assemble and form nanotubes networks inside the composites. As the network of nanotubes grew larger, the composites embedded with such nanotubes clusters would have greater ability to resist from deformation. Since agglomerates may create in any locations inside the composites, thus causing variation in measured values. As shown in the data of SWNT/Epoxy composites, at nanotubes content of 2wt%-4wt%, the Vicker's hardness were close in value i.e. 16.333 Hv for 2wt% of SWNTs, 16.42 Hv for 3wt% of SWNTs and 16.930 Hv for 4wt% of SWNTs. Furthermore, when the nanotubes content rose to 5wt%, the hardness value was jumped to 18.08 Hv. The incoherent in property improvement due to the addition of SWNTs present the possibility of the formation of agglomerates inside the composites. Contrasting to SWNT/Epoxy composites, the results obtained from FSWNT/Epoxy composites show a steadily increase of hardness values together with the nanotubes content. And as referred to the SEM micrographs in earlier sections, the FSWNTs showed a better dispersion and adhesion inside the composites. Hence, the Vicker's hardness provided by these composites would be more homogenous and reliable. Nevertheless, such conclusion should be further studied to investigate the reasons of causing the enhancement of hardness property by reinforcing the SWNTs.

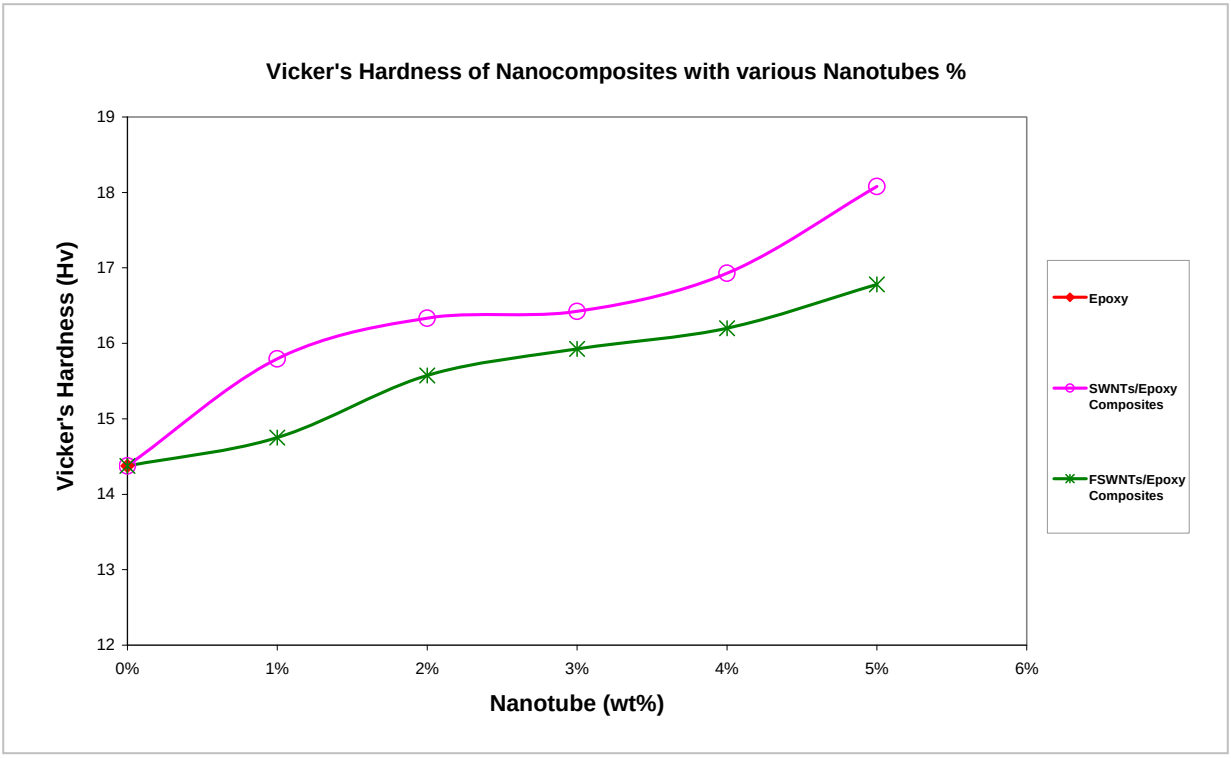

Figure 3.13 The Vicker's Hardness of the nanocomposites as the function of nanotubes content.

Table 3.4 The summary of the Vicker's Hardness obtained from Microhardness Tests.

Materials	Nanotube Content (wt%)	Vicker's Hardness (Hv)	% Improvement
Epoxy	0%	14.375 ± 0.152	-
SWNT/Epoxy Composite	1%	15.795 ± 0.308	9.88%
	2%	16.333 ± 0.214	13.62%
	3%	16.420 ± 0.192	14.23%
	4%	16.930 ± 0.204	17.77%
	5%	18.08 ± 0.307	25.77%
FSWNT/Epoxy Composite	1%	14.75 ± 0.166	2.61%
	2%	15.075 ± 0.173	8.35%
	3%	15.925 ± 0.119	10.78%
	4%	16.200 ± 0.135	12.70%
	5%	16.780 ± 0.119	16.73%

3.2 THERMAL PROPERTY TESTS

3.2.1 Investigation of Dynamics Mechanical Analysis

Rheological investigation of nanotube based composites, as a complement of mechanical tests; give a better understanding of the influence of carbon nanotube reinforcements on the viscoelastic properties of polymeric composites. In order to examine the viscoelastic behaviors of composites due to the filling of SWNTs and FSWNTs, DMA was adopted to study the properties of composites including glass transition temperature, storage modulus and viscosity.

Among all, the most straightforward manner to evaluate changes in viscoelastic behavior is to measure the glass transition temperature of the composites. Figure 3.14 shows the loss factors of the composites systems obtained from DMA. As introduced in section 2.2.5, the loss factor is the ratio of loss modulus to storage modulus. The temperature at which the maximum of this ratio occurs can be taken as the glass transition temperature of the material. Through the results, it is noticed that both composites systems exhibited a decrease in glass transition temperature, T_g, due to the introduction of carbon nanotubes. Moreover, the declination in glass transition temperature was accelerated as the reinforcement of nanotubes increased.

Figure 3.14(a) and (b) illustrate the tendency of decrease in glass transition temperature in the composites systems. For the SWNT/Epoxy composites, the loss factor profiles showed a rumpled pattern when compared to that of FSWNT/Epoxy composites. Although the reduction of glass transition temperature was inversely proportional to the nanotubes content, the peak value of the curves were in an uneven distribution manner. On

the other hand, for FSWNT/Epoxy composites, similar to SWNT/Epoxy composites, the glass transition temperature was inversely proportional to the nanotubes content; however, the loss factor profiles show a more even distribution. The glass transition temperature of the composites systems are summarized in table 3.5. The results demonstrated that both composites systems, with nanotube content 1-5wt%, have a glass transition temperature lower than neat epoxy. Also, the weakening in glass transition temperature of FSWNT/Epoxy composites was more apparent than SWNT/Epoxy composites, especially with 5wt% of SWNTs as reinforcement.

Table 3.5 The summary of glass transition temperature and storage modulus of the nanocomposites

Materials	Nanotube Content (wt%)	Glass Transition Temperature, T_g (^oC)	Storage Modulus E' at 30^oC (GPa)	Storage Modulus E' at 110^oC (GPa)
Epoxy	0%	69.462	29.901	0.264
SWNT/Epoxy Composite	1%	69.315	27.385	0.353
	2%	68.446	25.269	0.357
	3%	67.596	24.620	0.312
	4%	67.34	23.166	0.326
	5%	66.617	22.285	0.325
FSWNT/Epoxy Composite	1%	69.147	32.102	0.370
	2%	67.998	37.396	0.361
	3%	67.510	39.797	0.348
	4%	66.721	40.685	0.355
	5%	64.455	45.502	0.407

Apart from glass transition temperature, storage moduli of the composites systems were also measured. Figure 3.15 shows the storage modulus of composites systems as a

function of temperature. From the results, it is observed that, below the T_g, the SWNT/Epoxy composites have storage modulus lower than the neat epoxy. The storage modulus was decreased as the nanotubes content increased. However, the phenomenon was versed when temperature was higher than T_g value of the systems. As the temperature was above T_g, the storage modulus of the SWNT/Epoxy composites was greater than that of neat epoxy. Unfortunately, the increase in storage modulus of the SWNT/Epoxy composites was rather fluctuated and was not proportional to the amount of nanotubes applied.

Opposing to SWNT/Epoxy composites, the FSWNT/Epoxy composites shows an enhancement of storage modulus when compared to the response of the neat epoxy, at both low and high temperatures. When the temperature was below T_g, the storage modulus was increased and proportional to the weight of FSWNTs input. However, when the temperature was higher than T_g, the increase of storage modulus was also experienced fluctuations but with a much smaller variation when compared to that of SWNT/Epoxy composites. Table 3.5 summarized the results of storage modulus of the composites system at temperatures of 30^{o}C and 110^{o}C which was below and above their T_g values. Through the evaluation of the two composites systems, it is found that the enhancement of storage modulus of the composites due to the reinforcement of FSWNTs was much superior to that of SWNTs no matter what temperature condition was applied to the materials.

In addition, the viscosity of the composites systems was obtained according to the equation 2.13. Figure 3.16 demonstrates the relation of the complex viscosity of composites systems to the nanotubes contents at room temperature. It is found that the viscosity of both SWNT/Epoxy composites and FSWNT/Epoxy composites increased with the content of reinforced nanotubes and was raised steadily at room temperature. The neat epoxy was

calculated to provide a viscosity of 3.075GPa.s. For composites containing 1% of SWNTs, it viscosity was enhanced to 3.361GPa.s which was 1.09 times that of neat epoxy. Similarly, for composites having different SWNTs contents from 2wt% to 5wt%, the viscosity was gained by 1.26 times to 1.59 times that of neat epoxy respectively. On the other hand, for FSWNT/Epoxy composites, the augmentation in viscosity was even more obvious than SWNT/Epoxy composite. The viscosity was determined to be 3.556GPa.s and was 1.17times over the neat epoxy when 1wt% of FSWNTs was employed in the composites. Further addition of FSWNTs into the epoxy matrix gave a much higher viscosity than using the same weight content of SWNTs comparatively. The aggravation in viscosity of the composites with FSWNTs contents varied from 2wt%-5wt% was found to provide a value ranged from 4.076GPa.s to 5.494GPa.s, which was 1.17 times to 1.79 times of that of epoxy alone.

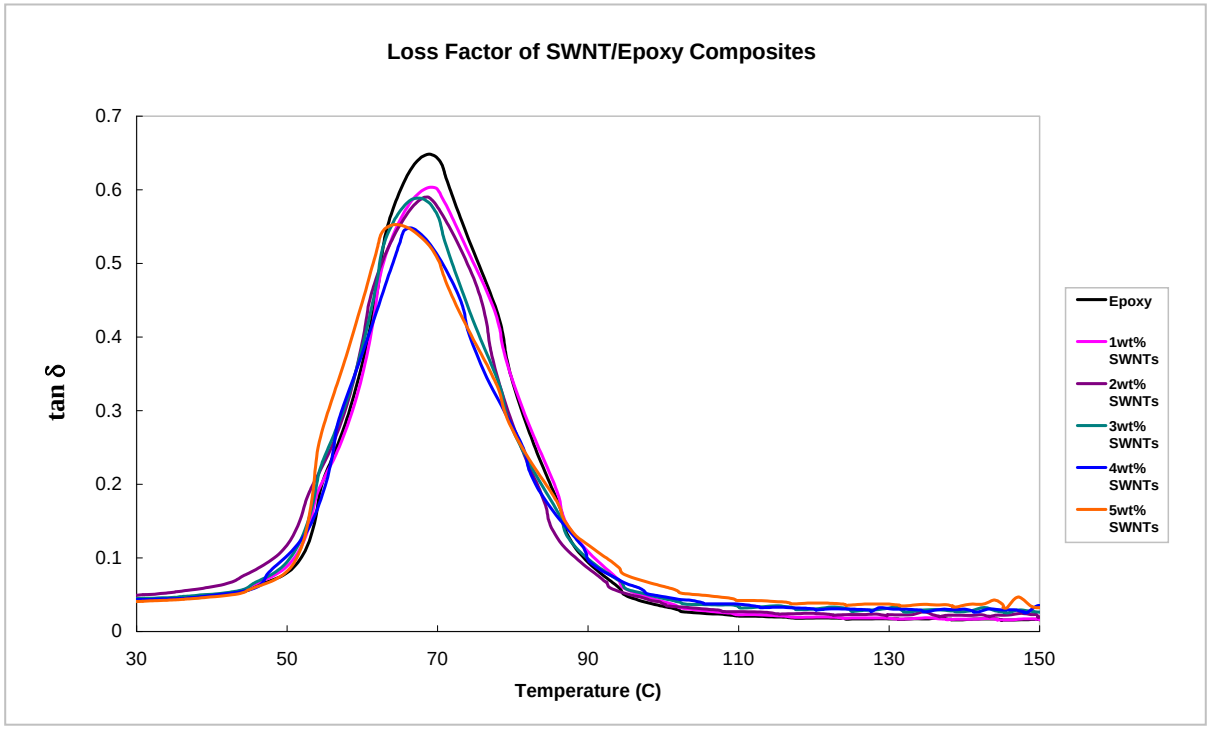

(a)

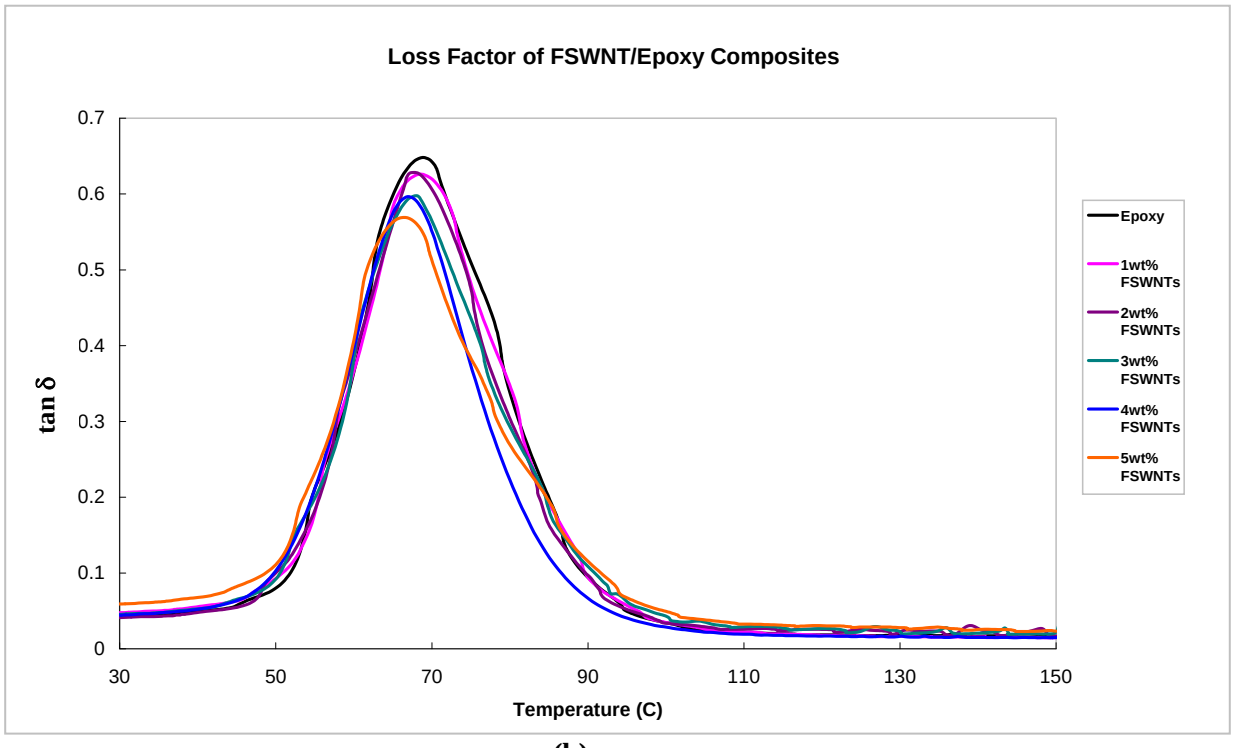

(b)

Figure 3.14 Loss Factor of the composites systems as a function of temperature (a) SWNT/Epoxy Composites with different nanotubes wt% and (b) FSWNT/Epoxy Composites with different nanotubes wt%

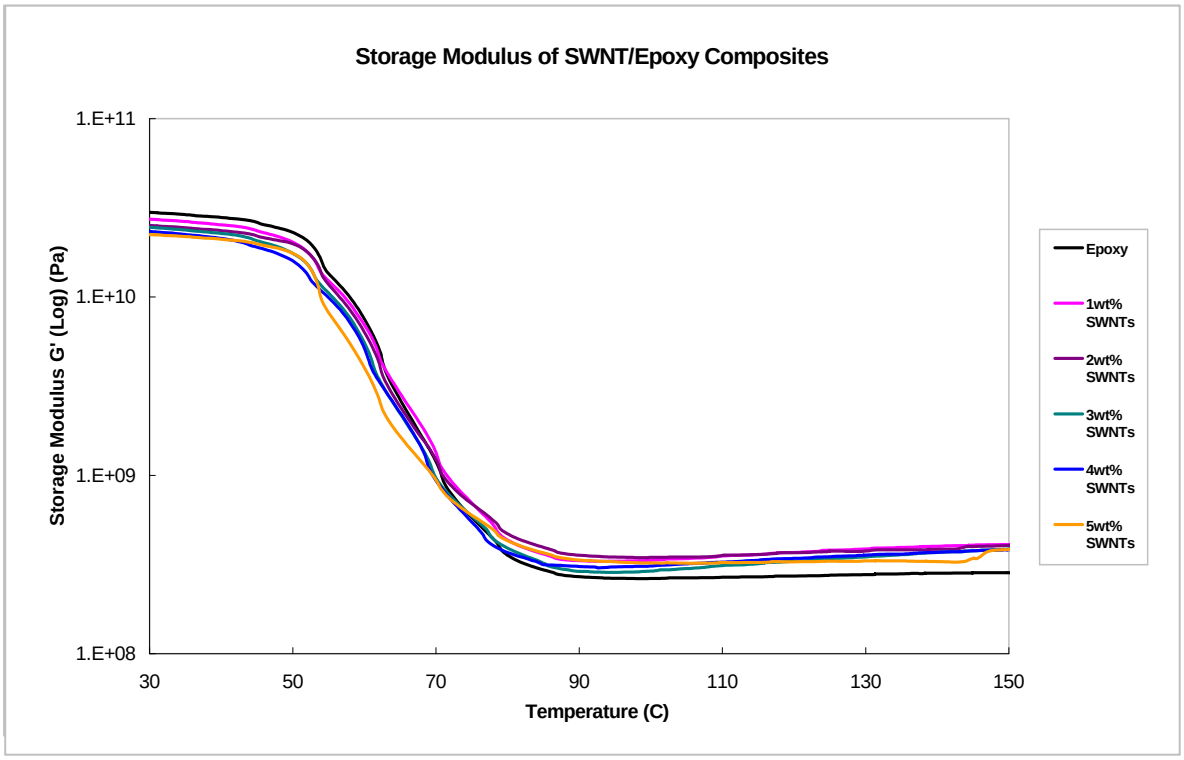

(a)

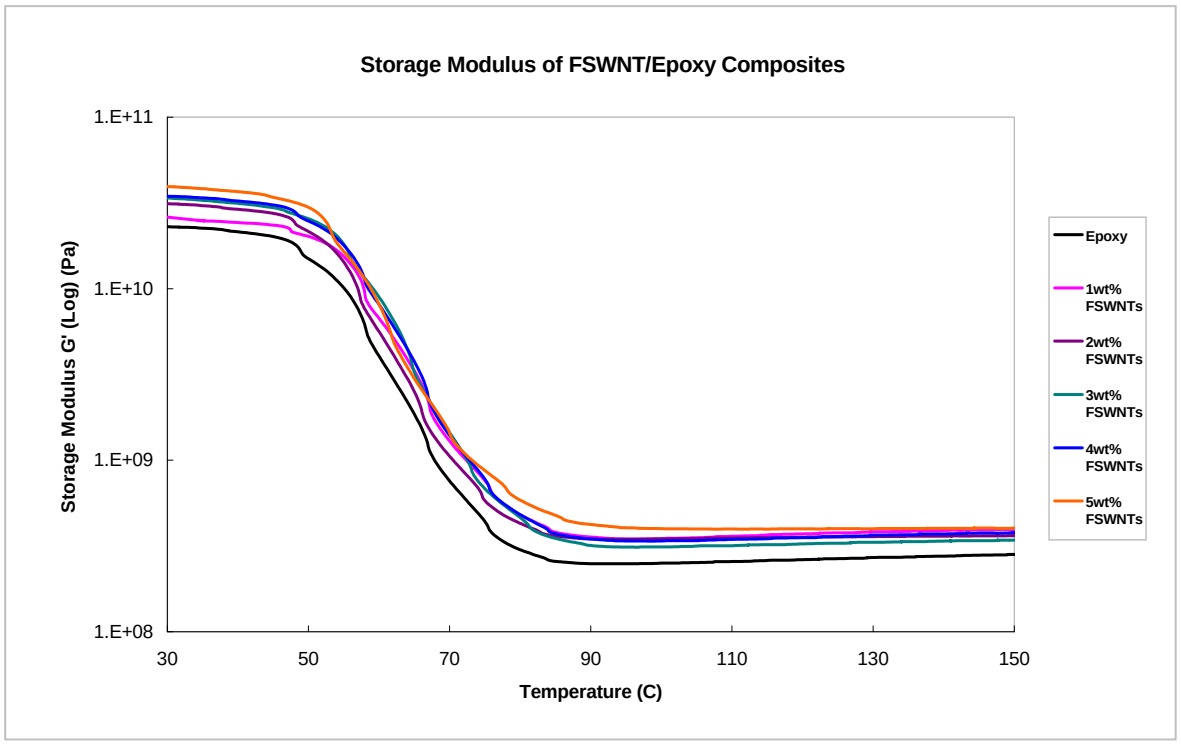

(b)

Figure 3.15 Storage Modulus of the composites systems as a function of temperature (a) SWNT/Epoxy Composites with different nanotubes wt% and (b) (a) FSWNT/Epoxy Composites with different nanotubes wt%

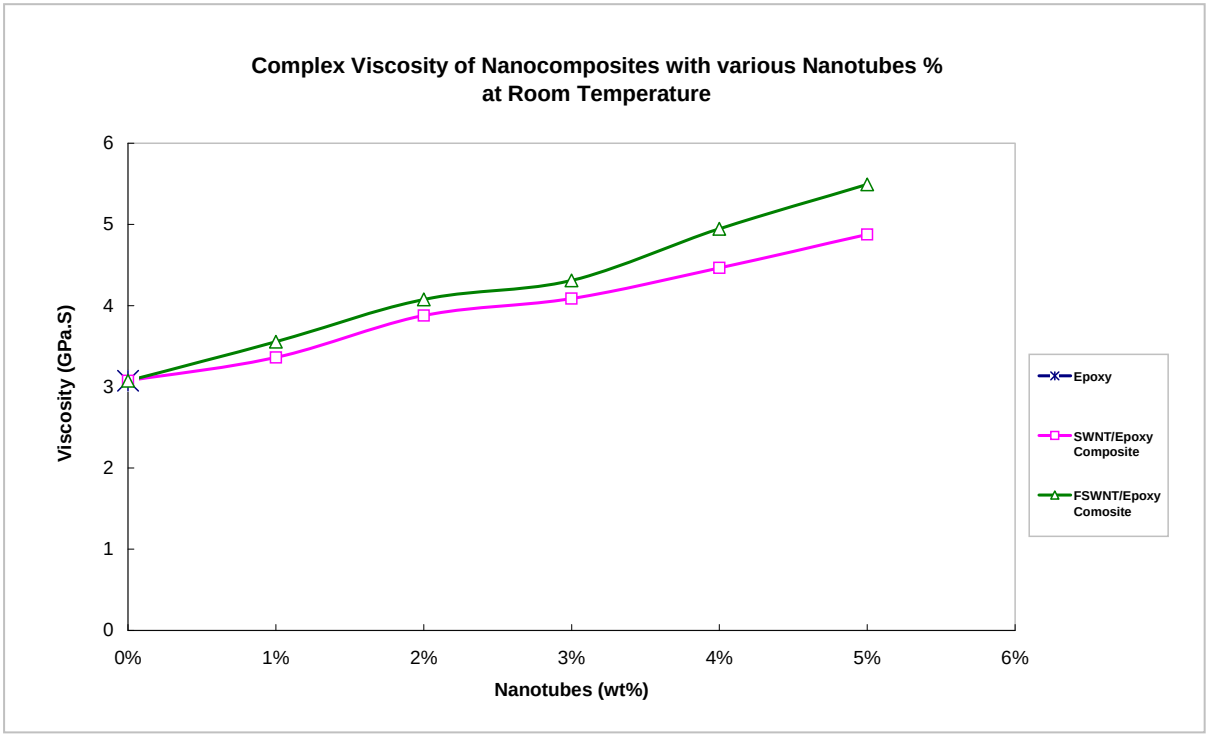

Figure 3.16 Complex Viscosity of the nanocomposites as the function of nanotubes content.

Table 3.6 The summary of complex viscosity of the nanocomposites.

Materials	Nanotubes Content (wt%)	Complex Viscosity (GPa.s)	Enhancement in Property (Multiplication)
Epoxy	0%	3.075	-
SWNT/Epoxy Composite	1%	3.361	1.09
	2%	3.878	1.26
	3%	4.085	1.33
	4%	4.463	1.45
	5%	4.875	1.59
FSWNT/Epoxy Composite	1%	3.556	1.17
	2%	4.076	1.33
	3%	4.310	1.4
	4%	4.945	1.61
	5%	5.494	1.79

The results obtained from DMA demonstrated the reinforcement of SWNTs and FSWNTs would cause enhancement in viscoelastic properties of composites. Also, the influence on these properties due to the functionalized nanotubes was more apparent than the purified nanotube. During the analysis, the intensity of loss factor peak was shifted to lower temperature with increasing nanotubes content in both SWNT/Epoxy and FSWNT/Epoxy composites. Such reduction in values of loss factor is expected to be caused by the adsorption of curing agent HY 956 by the nanotubes. The alteration of curing stoichiometric ratio would weaken the glass transition temperature and also the crosslink density of cured epoxy system. For FSWNT/Epoxy composites, apart from the adsorption of curing agent, the functional groups of epoxy prepolymer may also adsorb into the functionalized SWNTs because of strong interfacial bond, which may lead to further non-stoichiometric balance between epoxy polymer and curing agent, thus causing the inhibition of cross-linking reaction between them. Thus, the FSWNT/Epoxy composites show a significant decrease in T_g value when compare to SWNT/Epoxy composites.

Furthermore, the storage modulus measured from DMA also shows the impact owing to the reinforcement of nanotubes. The storage modulus is indicative of the elastic modulus of composites. In this study, the modulus decreased gradually as temperature increased, due to increased molecular chain movement and flexibility, until the glass transition region reached. However, the type of reinforced nanotubes was revealed to provide either enhanced or adverse effect on the modulus of neat epoxy. When the temperature was below T_g, the modulus of neat epoxy was enhanced as the content of FSWNTs increased. The improved modulus of composites is predicted to be caused by the strong interaction between FSWNTs and epoxy matrix, which induced the stiffening effect inside the composites. The stiffening effect was more significant as the weight fraction of FSWNTs in composites increased.

Although the modulus of FSWNT/Epoxy composites exhibited variation when the temperature was above T_g, these values were still shown apparent enhancement over the neat epoxy.

In contrast to the FSWNT/Epoxy composites, the reinforcement of SWNTs was found to deteriorate the storage modulus as the temperature was lower than the T_g. Besides, the modulus of composites was found to decline with the increased content of SWNTs. Such results are found to be different from that of FSWNT/Epoxy composites, and are proposed to be caused by the agglomerates formed inside the composites. The formation of SWNTs agglomerates would lessen the molecular chain creation between the epoxy and individual nanotube, and also inside the epoxy, thus lower the restriction in molecular chain mobility. However, as the temperature was increased above T_g, the nanotubes clusters in the composites were able to disperse and produce cross-linking with the epoxy matrix. Hence, the SWNT/Epoxy composites provided an improved storage modulus over the epoxy alone. However, such improvement was not as much as in FSWNT/Epoxy composites due to the weak interfacial interaction between the nanotube and epoxy matrix comparatively.

The overall influence on the viscoelastic properties of the composites system due to the addition of nanotubes can be studied through the viscosity evaluated from DMA results. Both composites systems showed higher viscosity than neat epoxy, and viscosity increased as enlarging the nanotube content in composites at room temperature. It is revealed that the SWNTs would provide the cross linking effect which restricted the molecular mobility in the composites systems. However, as indicated by the low storage modulus of SWNT/Epoxy composites, the improved viscosity of the composites was believed to be caused by the large energy lost due to the friction of polymer chain movement. As more SWNTs were introduced

into the composites, the energy lost caused by the chain movement became more serious. On the other hand, as in the case of storage modulus, the improved interfacial interaction between functionalized nanotubes and epoxy matrix would limit the molecular chain movement, hence giving high viscosity values in FSWNT/Epoxy composites rather than SWNT/Epoxy composites.

3.2.2 Investigation of Thermogravimetric Analysis

The introduction of thermogravimetric analysis (TGA) in this study is aimed to investigate the influence on thermal stability of epoxy due to the reinforcement of SWNTs and FSWNTs. Carbon nanotubes have been already reported as materials with extremely high thermal conductivity [173,174]. The addition of nanotubes into polymer matrix was proposed to enhance the thermal stability of the material once the interfacial interaction between nanotubes and polymer matrix has been improved. Besides, according to Chen et al. [175], the uniformity of dispersion of nanotubes would produce a significant impact on the thermal stability of materials. It is reported that the uniform dispersion of nanotubes would raise the overall thermal conductivity of the composite; hence increase its thermal stability. Since the thermal stability of the materials can be reflected by its thermal decomposition temperature, therefore, through the thermal decomposition temperature measured from TGA, one could obtain useful information on the behaviour of interfacial interaction and dispersion between different types of nanotubes and epoxy matrix.

The results obtained from TGA are shown in figure 3.1.7. The TG-DTG curves of pure epoxy, 1wt% SWNT/Epoxy and 1wt% FSWNT/Epoxy composites are presents separately in figure 3.17 (a)-(c). In the TGA, the TG curve shows the change in profile of mass (W) of the specimens during the temperature (T) variation. On the other hand, the DTG is the first derivative (dW/dT) of the TGA scans. Through the figure 3.17 (a)-(c), it is found that all curves exhibited similar weight loss profile. For pure epoxy, as shows in figure 3.17 (a), the TG-DTG curves show a three step consuming process. The first consumption occurred between the temperature 100^{o}C and 300^{o}C. This first drop in the curve was accounted to the volatilization of water that was accumulated during the composite fabrication process. The second drop in the TG curve is observed in the temperature of 320^{o}C

to 400^{o}C and most of the pure epoxy is consumed in this temperature range. For those remaining was consumed and indicated as the third drop in TG curve which lied in the temperature zone 500^{o}C - 600^{o}C. In order to evaluate the thermal decomposition temperature of the epoxy, which required most of thermal energy to break the bonding inside the epoxy, the DTG is applied to find out the temperature at which the derivative of the TG curve would reach the minimum. From the result of the DTG curve, it is revealed that the epoxy would decompose at the temperature 350.2^{o}C.

By studying the TG-DTG curves in figure 3.17 (b) and (c), it is present that the thermal decomposition temperature of the SWNT/Epoxy composite was 349.73^{o}C and was closed to thermal value of epoxy. The thermal decomposition temperature didn't increase with the addition of high conductivities SWNTs implying that the dispersion of nanotubes in the epoxy was poor and the interfacial interaction between them was weak. However, on the other hand, the thermal decomposition temperature of FSWNT/Epoxy composite was found to have the value of 353.68^{o}C, which was higher than that of the neat epoxy. The raise of this thermal value was attributed to the increased thermal energy required to break the additional bonds which was formed between the functionalized nanotubes and the polymer matrix. Also, such enhancement can also contribute to the improvement in dispersion of SWNTs due to functionalization. These results provide essential information on the improvement of nanotubes caused by functionalization.

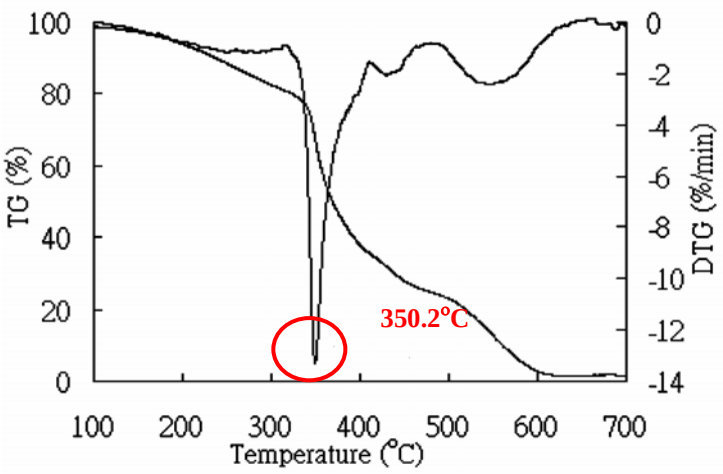

(a)

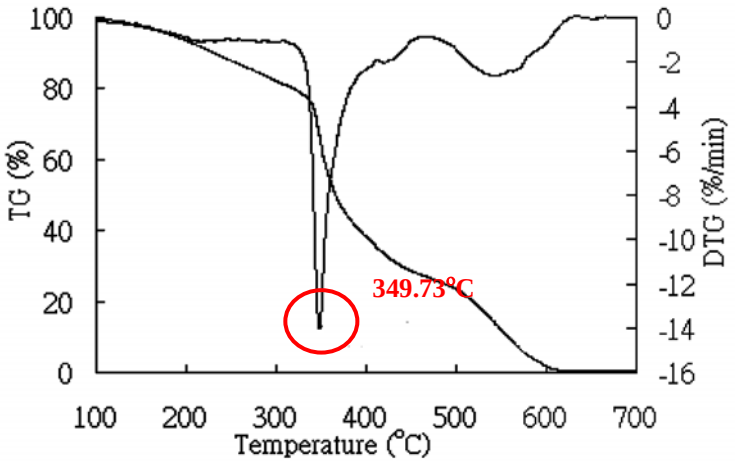

(b)

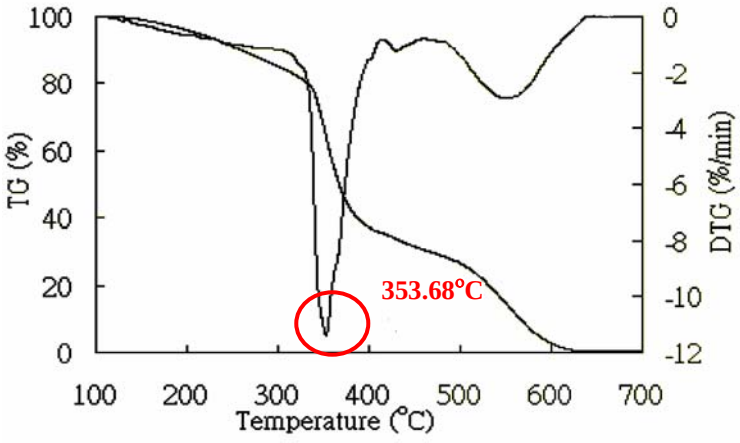

(c)

Figure 3.17 TG-DTG curves achieved from TGA. (a) Neat Epoxy, (b) SWNT/Epoxy composite and (c) FSWNT/Epoxy composite

3.3 CONCLUSIONS

The reinforcement of single-walled nanotubes into the epoxy was found to induce remarkable impacts on the properties of neat epoxy. Besides, the functionalization on nanotubes was revealed to provide much attractive results which were superior to the purified nanotubes as filler in composites. Mechanical properties, such as elastic modulus, flexural modulus, impact strength, hardness, of the composites were found to enhance due to the addition of nanotubes. However, such enhancements were varied according to the amount of nanotubes applied. According to the outcomes from tensile property test and flexural property test, it is present that the modulus increased steadily with the nanotube content applied into the composites system and would be maximized when 5wt% of nanotubes was used. Moreover, in the study of impact strength, the maximum value was obtained as 3wt% of nanotubes was employed. Further filling of nanotubes was found to lower the impact property of the composites. On the other hand, through the results of microhardness test, it is noticed that the introduction of SWNTs would provide a better hardness value than that of FSWNTs. And the hardness reached the peak value when 5wt% of nanotubes was employed. The differences in consequences due to the reinforcements were attributed to the improved interfacial interaction, between the nanotubes and epoxy matrix, and the nanotubes dispersion, inside the composites, which caused by functionalization of nanotubes. The SEM analysis indicated the effect of functionalization and provided an evidence for such enhancement.

Apart from mechanical properties, thermal analysis, i.e. DMA and TGA, were also carried out to investigate the effect on the epoxy properties due to the addition of SWNTs and FSWNTs. The results showed that interaction between purified SWNTs and epoxy matrix was comparatively poor while strong cross-linking was formed between the FSWNTs and

neat epoxy, thus provided a good explanation for the delighted properties obtained by FSWNT/Epoxy composites.

CHAPTER 4

MOLECULAR MODELING OF CARBON NANOTUBE

4.1 INTRODUCTION

The reinforcement of carbon nanotubes into the polymer matrix was shown to provide attractive enhancements in the material properties of composites. Apart from the dispersion of nanotubes, such improvements were examined to be highly relied on the interfacial interaction between nanotubes and polymer. The formation of strong interaction has already been proved to be an essential factor for high load transferability in the composites. In general, there are two main mechanisms of load transfer from a matrix to filler; the first type is the micromechanical interlocking between fiber and matrix while the second mechanism is the chemical bonding between them. According to the experiments, it was revealed that materials properties of FSWNT/Epoxy composites were shown to be superior to those of SWNT/Epoxy composites and neat epoxy. Besides, chemical bindings were established within the FSWNT/Epoxy composites due to chemical functionalization. Although FSWNT/Epoxy composites gave the most delighted results in experiments, the SWNT/Epoxy composites were also demonstrated apparent enhancements over the neat epoxy. Without significant chemical bonding with epoxy matrix, the improvement in properties of SWNT/Epoxy composites may account for the micromechanical interlocking formed inside the structures. However, due to the atomically smooth surface of nanotubes, the formation of

physical interlocking would be difficult unless there is changes in shape of nanotubes occur during the composites fabrication.

In this chapter, focus will be put on the influences on nanotube structure caused by the temperature variation. During the composites fabrication, nanotubes were processed under different temperature conditions i.e. solution mixing process, curing process. Under such circumferences, the nanotubes may allow to deviate from its cylindrical shape due to the energy gain from the thermal environment. In order to examine the effect induced by the alteration in temperature, molecular simulations were used to investigate the structural variation of the carbon nanotube. These simulations provide the theoretical insight into the topic, and a thorough understanding of these structural variations shed light on the process development and property characterization of nanotube based composites.

4.2 MODELING METHODS IN MOLECULAR SIMULATION

Molecular simulations have been proved to be an extremely useful technique to investigate the nature of materials before engaging in real experiments or processing. These modeling techniques provide guidance for advanced materials development by offering a thorough understanding of molecular behaviors. There are several simulation techniques which are currently in use to study the properties of carbon nanotubes and their related materials, including Ab Initio Simulations, Molecular Dynamics, Monte Carlo Simulations and Molecular Mechanics. The brief descriptions of each method are indicated as follows:

(a) Ab Initio Simulations [176-179]

Ab initio, also named as first principles, simulations solve the quantum mechanical equations governing the behavior of a system. These simulation methods give more accurate results than classic molecular simulations, however, they are computationally intensive and time consuming for structures composed of few thousand of atoms.

(b) Molecular Dynamics [180-184]

Molecular dynamics simulations deal with the time-dependent process of moving molecules. Through the calculation of intermolecular forces on particles, the trajectory of moving molecules can be predicted. Analyzing the route using the technique of statistical mechanics, a detailed description on the bulk behavior of materials can be obtained. Such simulations normally involve the application of potential models to characterize the nature of interaction between the atoms which are under studied. In general, these models are formulated and parameterized by existing experimental data. This method provides efficient modeling of the structures with less computational time, however, its accuracy will be relied on the parameters available to the system.

(c) Monte Carlo Simulations [185-188]

Monte Carlo simulations are similar to molecular dynamics, in which, the trajectory of moving molecules is generated to evaluate the behaviors of the material. These simulation methods are mostly applied to investigate the thermodynamics properties of the system and cannot be used to simulate the time-dependent properties of the materials.

(d) Molecular Mechanics [189-192]

Molecular Mechanics, different from the simulations above, is introduced to solve for equilibrium. During simulation, the potential energy of the structures is minimized with respect to the atom positions, and a new set of atom position is generated when the system reaches its equilibrium state. The thermal conditions, i.e. temperature and pressure, cannot be controlled or monitored in this simulation method.

In order to evaluate the structural variation of carbon nanotube due to the temperature influence, two modeling techniques, i.e. Molecular Mechanics and Molecular Dynamics, were employed in this study. The molecular mechanics was first applied to equilibrate the system, so to achieve the most stable structure of the carbon nanotube before carry out the thermal analysis. This carbon nanotube was then employed to examine its thermal behavior through molecular dynamics. The molecular dynamics was used in this work as it can handle a large molecular system with computational efficiency and acceptable accuracy.

4.3 POTENTIAL ENERGY MODEL

In molecular mechanics, atoms are treated as masses or spheres bonded to each other with springs. The molecular system is modeled via classical mechanics and a set of approximations is employed to represent the molecular system under examination. The set of approximations is an analytical expression, also known as force field, which provides the potential energy of a molecular system in terms of the atomic coordinates. These potential energy functions, their derivatives and parameterization govern the equilibrium in molecular mechanics.

In general, the total potential energy of a molecular system is the sum of individual components of the potential, such as bond, angle, and torsion potentials. According to the interaction range between atoms, these potential energy functions can be divided into two categories – bonding interaction and non-bonding interaction. The bonding interaction is referred to the interaction formed by chemical bonding and bonding geometry while the non-bonding interaction implied the attraction other than chemical bonding. Typically, the general forms of potential energy functions utilize in the molecular mechanics are indicated as follows:

4.3.1 Bonding Potential

(a) Bond Stretching

The bond stretching potential describes the chemical bond formed between two atoms. This term is associated with the deformation of a bond from its standard equilibrium length.

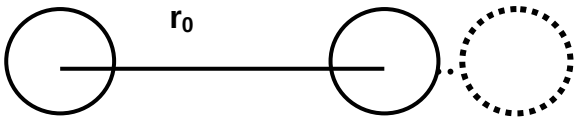

For small displacement from equilibrium, a harmonic function is employed

$$E_{bond} = \sum_{bonds} K_r (r - r_o)^2 \qquad (4.1)$$

in this equation, K_r and r_0 are force field parameters for a specific pair of atoms connected by a certain spring. Moreover, K_r is the force constant of the spring, r_0 and r are the values indicated the equilibrium and displaced distances of the atoms in the bond.

(b) Angle Bending

The angle bending potential is applied to indicate the energy change due to the deformation of angle from its normal value.

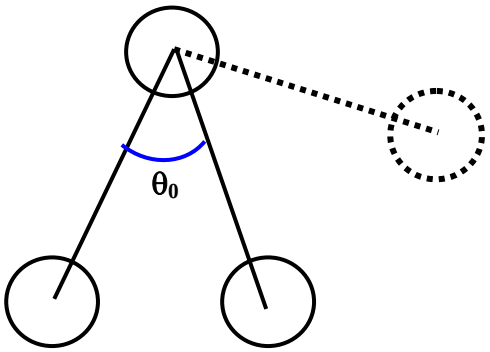

For small displacement from equilibrium, similar to bond stretching, a harmonic functions is utilized,

$$E_{bond\ angle} = \sum_{angles} K_{\theta}(\theta - \theta_o)^2 \qquad (4.2)$$

in the equation, K_0 and are θ the force field parameters in the systems. Besides, K_0 is the bending force constant, θ_0 and θ are the values implied the equilibrium and bended angles between the atoms in the bond.

(c) Dihedrals

The dihedral potential, also known as torsional potential, account for the energy barrier to rotation caused by the chemical bonds. This term associated with the tendency of dihedral angles to have n-fold of symmetry and have minimum energy for different conformations.

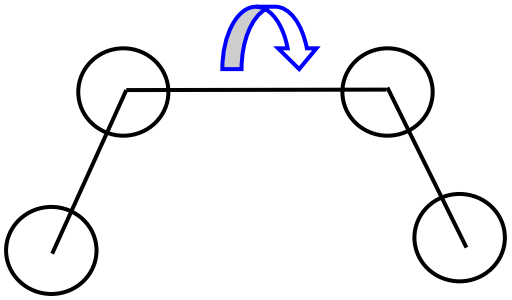

In molecular mechanics, the dihedral potential is often implemented as a truncated Fourier series,

$$E_{diherals} = \sum_{diherals} \frac{V_n}{2}\left[1+\cos(n\phi-\phi_0)\right] \tag{4.3}$$

the parameter V_n represent the dihedral force constant, n is the periodicity of the Fourier term, ϕ_0 is the phase angle, and ϕ is the dihedral angle. Through different combination of parameters n and ϕ_0, the potential function can characterize the energy state of diverse conformations of the studied system. By including sum of terms of the above kind, dihedral angle interaction of arbitrary complexity can be described.

4.3.2 Non-Bonding Potential

(a) Van der Waals Potential

The van der Waals force is the weakest intermolecular forces exist between atoms. The term describes the repulsive forces keeping two non bonded atoms apart at close range and attractive force drawing them together at long range.

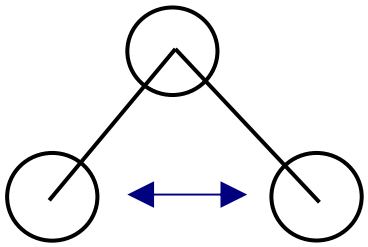

A 6-12 function, also known as Lennard-Jones function, is used to simulated van der Waals interaction in the force field,

$$E_{vanderWaals} = \sum_{ij \in vdW} \left[\frac{A_{ij}}{R_{ij}^{12}} - \frac{B_{ij}}{R_{ij}^{6}} \right] \tag{4.4}$$

In the equation, R_{ij} is the nonbonded distance between two atoms; A_{ij} and B_{ij} are van der Waals parameters for the interacting pair of atoms. The R^{-6} terms implied the attractive London dispersion interaction between two atoms, and R^{-12} term describes the repulsive interaction caused by Pauli exclusion.

(b) Hydrogen Bonding Potential

The hydrogen bonding describes the attractive force between one electronegative atom and a hydrogen atom which covalently bonded to another electronegative atom. The hydrogen bonding potential in molecular mechanics does not contribute apparently to the hydrogen bonding attraction between two atoms; instead, it is implemented to fine-tune the distances between these atoms. The expression of hydrogen bonding potential is shown as follows:

$$E_{Hbonds} = \sum_{ij \in H-bond} \left[\frac{C_{ij}}{R_{ij}^{12}} - \frac{D_{ij}}{R_{ij}^{10}} \right] \tag{4.5}$$

Similar to van der Waals potential, R_{ij} is the nonbonded distance between two atoms while C_{ij} and D_{ij} are the coefficient for appropriate donor-acceptor pairs in the bonding.

(c) Electrostatic Potential

The electrostatic potential represents the attraction caused by charge pairs in the system. Different from van deer Waals force, electrostatic force will still effective even the charges are far away from each other. The expression of electrostatic potential is indicated as follows:

$$E_{EEL} = \sum_{ij \in electrostatic} \left[\frac{q_i q_j}{\varepsilon R_{ij}} \right] \tag{4.6}$$

In this model, ε is the effective dielectric constant, q_i and q_j is the point charge carried by two atoms (i and j), and R_{ij} is the distance between the atoms.

4.4 MOLECULAR DYNAMICS SIMULATION

The aim of molecular dynamics is to predict the changes in a molecule as a function of time after an energy input is added to a molecule at equilibrium. Any changes in a system from one chemical state to another, the transformation of molecules between their various possible states are described by kinetics. As the chemical states are relied on the changes in atomic position, r_i, over time (i.e. velocity), thus the kinetics of the system can be acquired once the parameters are obtained.

Newton's equation, $F_i = m\,a$, is used in the molecular dynamics to simulate atomic motion. The rate and direction of motion are governed by the forces that the atoms of the system exert on each other as described by Newton's equation. In practice, the atoms are assigned initial velocities that conform to the total kinetic energy of the system, which in turn, is dictated by the desired simulation temperature. This is carried out by slowly heating the system and then allowing the energy to equilibrate among the constituent atoms. The basic ingredients of molecular dynamics are the calculation of the force on each atom, and from that information, the position of each atom can be evaluated.

The force on an atom can be calculated from the change in energy between its current position and the displacement it's made. This can be recognized as the derivative of the energy with respect to the change in the atom's position $F_i = -\frac{dE}{dr_i}$. The energy term in the equation can be calculated using molecular mechanics methods as mentioned in previous section. Though molecular mechanics are limited to applications that do not involve drastic changes in electronic structure such as bond making/breaking, it is appropriate in this study as the interest in this work is in the motion of atoms rather than electrons. Since atoms are much heavier than electrons, hence it is possible to treat their motion classically.

In addition, according to the Newton's equation, the atomic accelerations are computed from the forces and masses. Besides, the velocities are next calculated from the accelerations based on the relation $a_i = \frac{dv_i}{dt}$ and the position of the atoms can be calculated from the velocity $v_i = \frac{dr_i}{dt}$.

Once the velocity of the atoms is evaluated, the kinetic energy of the systems can be defined in term of the velocity $K = \frac{1}{2}\sum_{i=1}^{N} m_i v_i^2$. The total energy of the system can then be obtained through the summation of the kinetic and potential energies $H(r, p) = K(p) + E(r)$, where r = the set of Cartesian coordinates and p = momenta of the atoms.

4.5 MODELING OF CARBON NANOTUBE

4.5.1 Generation of Carbon Nanotube

In order to generate the nanotube system for study, a new type of visual computational software, HyperChem, was utilized in this work. HyperChem is a molecular modeling program equipped with different modeling methods such as molecular mechanics, molecular dynamics and monte carlo simulation, and also force field parameters required in each simulation technique. Besides, with the build-in element database, HyperChem allows the user to construct the molecular systems visually in the software platform. Moreover, different script commands are allowed to be written into the software to customize the simulation process of the system.

The nanotube models which generated in the simulation include the (10, 10) armchair and (17, 0) zig-zag single-walled carbon nanotubes. These two nanotube types are employed as they are the main focus of the research studies in the last decade. Also, armchair and zig-zag nanotubes represent the two extremes in the nanotube category, thus any variations in the structure of these nanotubes would expect to be more significant. As the interest in this work is to gain insight to the temperature influence on the nanotube structure, thus,

neglecting the size of the nanotube, the selection of these nanotubes is considered to be acceptable.

Once the carbon nanotubes were generated, geometry optimization was carried out on the constructed systems through molecular mechanics method. During molecular mechanics modeling, the deviation of nanotube structures from their cylindrical shapes was rectified, and the systems were turned into their most stable, equilibrium state which is essential for the thermal analysis follows.

4.5.2 Implementation of Molecular Mechanics

In this study, the force field MM+ was selected for the molecular mechanics modeling of carbon nanotube. This force field is developed for organic molecules and is unique among the force fields in the way it treats bonds and angles. Both the bond and angle terms can contain higher order terms than the standard quadratic. Besides, these bond and angle potentials express a harmonic motion better than a harmonic potential.

The MM+ force field is an extension of MM2 which was developed by Allinger and co-workers [193-195]. It uses the latest MM2 (1991) parameters and atom types (provided directly by Dr. Allinger) with the functional forms modified to facilitate the simulation process which could not manage by using the MM2 force field. The potential energy functions provide by the MM+ force field are shown as below:

(a) Bong Stretching Potential

$$E_{bond} = 143.88 \sum_{bonds} \frac{1}{2} K_r (r - r_o)^2 [1 + CS(r - r_o)] \quad (4.7)$$

The cubic stretch term is a factor CS times the quadratic stretch term. This constant CS can be set to an arbitrary value and the default value for MM+ is CS =-2.0.

(b) Bond Dipoles Potential

MM+ calculations do not usually have an electrostatic charge-charge interaction nor define a set of atomic charges for atoms. Instead, the electrostatic contribution comes from defining a set of bond dipole moments associated with polar bonds. The center of the dipole is defined to be the midpoint of the bond and two dipoles μ_i and μ_j, separated by R_{ij} , as shown below:

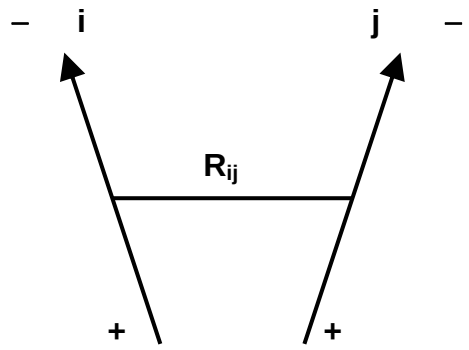

The MM+ dipole interaction energy is :

$$E_{dipole} = 14.39418\, \varepsilon \sum_{ij \in polar\ bonds} \mu_i \mu_j \left[\frac{\cos \chi - 3 \cos \alpha_i \cos \alpha_j}{R_{ij}^3} \right] \quad (4.8)$$

where ε is the dielectric constant and has a value of 1.5 which is the same as in the MM2 force field. The angle χ is the angle between the two dipole vectors, and α_i and α_j are the angles that the two dipole vectors make with the $\mathbf{R}_{ij}$ vector.

(c) Angle Bending Potential

The quadratic angle bending term in MM+ is identical to that of equation (4.2) defined before, apart from a factor 1/2. Three θ_0 values are given for each MM+ bond, θ^A, θ^B and θ^C. If θ^B is available, then it is used in preference to the normal θ^A, for angles where the central atom has one hydrogen atom directly attached to it. If θ^C is available then it is used in preference to the normal θ^A for angles where the central atom has two hydrogen atoms directly attached to it. If no hydrogen atoms are attached to the central atom or if θ^A or θ^B values are not available (when they are relevant), the normal θ^A is used. MM+ also includes a sextic angle bending term. The final form for the angle bending energy is:

$$E_{bond\ angle} = 0.043828 \sum_{angles} \frac{1}{2} K_\theta (\theta - \theta_o)^2 \left[1 + SF(\theta - \theta_o)^4\right] \qquad (4.9)$$

The sextic bending term is a scale factor SF times the quadratic bending term. This constant SF can be set to an arbitrary value and the default value for MM+ is SF = 7.0 x 10^{-8}, however, the value may vary when the atoms are in a three- or four-membered ring.

(d) Bond Stretch and Angle Bending Cross Potential

Apart from the standard potential functions introduced in earlier section, MM+ includes coupling between bond stretching and angle bending. If the angle is defined to include atoms

i, j, and k, where k is the central atom, then MM+ couples stretching of the ik and jk bonds with the angle:

$$E_{stretch-bend} = 2.51118 \sum_{angles} K_{sb} (\theta - \theta_o)_{ikj} \left[(r - r_o)_{ik} + (r - r_o)_{jk} \right] \qquad (4.10)$$

If atom i or atom j is a hydrogen, the deformation ($r-r_0$) is considered to be zero. Thus, no stretch-bend interaction is defined for XH_2 groups. If R is an atom other hydrogen, the values of the stretch-bend force constants would alter according to the position of the atom located,

i.e. $K_{sb} = 0.120$ for XR_2 (X = atom in 1st long row)

$K_{sb} = 0.090$ for XRH or $K_{sb} = 0.250$ for XR_2 (X = atom in 2nd long row)

$K_{sb} = -0.400$ for XRH

(e) Out-of-Plane Bending Potential

Besides the Bond Stretch and Angle Bending Cross Potential, MM+ force field also includes another bending potential, know as Out-of-Plane Bending Potential. An atom that has sp^2 hybridization tends to be coplanar with its attached atoms. This effect is accounted for by improper torsions in other force fields and by out-of-plane-bending interactions in MM+. The following situation indicating an atom that is sp^3 hybridized. While bonded to 3 atoms in the same plane,

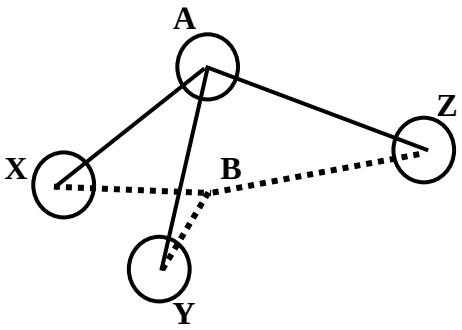

B is the projection of A onto the XYZ plane. When the central atom (A) of these angles is sp^2 hybridized, the angle bending calculations are modified to use the in-plane angles XBZ, XBY and ZBY in equation (4.8) with the standard force constants defined in force field rather than the standard angles XAZ, XAY, and ZAY. In addition, out-of-plane components are computed as well, for the out-of-plane angles AXB, AZB, and AYB. These last three calculations use equation (4.8) as well, but with θ_0 equal to 0 and special out-of-plane bending constants, K_θ, defined in the force field.

(f) Dihedrals Potential

The dihedral angle or torsional energy interaction in MM+ is of the general form of equation 4.3 but explicitly includes n=1, 2, and 3 with a phase angle ϕ_0=0:

$$E_{diherals} = \sum_{diherals} \frac{V_1}{2}(1+\cos\phi)+\frac{V_2}{2}(1-\cos 2\phi)+\frac{V_3}{2}(1+\cos 3\phi) \qquad (4.11)$$

The values of V_1, V_2, and V_3, in kcal/mol, are obtained from MM2 parameters library and the MM+ force field uses special values for the torsional force constants when the atoms are in a four-member ring.

(g) Van der Waals Potential

The MM+ van der Waals interactions do not use a Lennard-Jones potential but combine an exponential repulsion with an attractive $1/R^6$ dispersion interaction. The basic parameters are a van der Waals radius r_i^* for each atom type and a hardness parameter ε_i which determines the tendency for the atoms to attract together. The parameters for a pair are obtained from individual atom parameters as follows:

$$r_{ij}^* = r_i^* + r_j^* \tag{4.12}$$

$$\varepsilon_{ij} = \sqrt{\varepsilon_i \varepsilon_j} \tag{4.13}$$

The van der Waals interaction is then calculated as:

$$E_{van\,der\,waals} = \sum_{ij \in vdW} \varepsilon_{ij} \left(2.9x10^5 \exp(-12.5\rho_{ij}) - 2.25\rho_{ij}^{-6}\right) \tag{4.14}$$

where

$$\rho_{ij} = \frac{R_{ij}}{r_{ij}^*} \tag{4.15}$$

At short distances ($r_{ij} \leq 3.311$) the above expression is replaced by:

$$E_{van\,der\,waals} = 336.176 \sum_{ij \in vdW} \varepsilon_{ij}\, \rho_{ij}^{-2} \tag{4.16}$$

For CH interactions the normal ε and r* values are replaced by special CH values:

$$\varepsilon_{CH} = 0.046 \quad \text{and} \quad r_{CH}^* = 3.340$$

For XH bonds, where X is any heavy atom, the hydrogen electron density is not thought to be centered at the position of the hydrogen nucleus but displaced along the bond somewhat, towards X. The MM+ force field reduces the XH bond length by a factor of 0.915 strictly for the purposes of calculating van der Waals interactions with hydrogen atoms.

The summation of all the potential functions above would give the total potential energy of the system. Geometry Optimization was carried out based on this total potential energy of the system. This process aimed to find the coordinates of a molecular structure that represent a potential energy minimum. For a potential energy E and Cartesian coordinates r_i, the optimized coordinates satisfy the equation,

$$\frac{\partial E}{\partial r_i} = 0 \tag{4.17}$$

Different types of algorithms such as Steepest Descent method, Conjugate Gradient method, and Black Diagonal method can be used to solve the above equation. In this work, conjugate gradient method (Polak-Ribiere method) was utilized for this purpose. This method uses both current gradient and the previous search direction to drive the minimization, thus provides an efficient converges rate when compares to other methods.

4.5.3 Implementation of Molecular Dynamics Simulation

The process of geometry optimization leaded nanotube systems reaching their stable and equilibrium position. In the study, the (10, 10) armchair nanotube model has a diameter of 13.570Å and length of 162.419Å; also 2700 atoms were applied in this system. On the other hand, for (17, 0) zig-zag nanotube model, the structural diameter has a value of 13.318Å and the length was 162.774Å. Total number of 2652 atoms was employed in the

system. The two kinds of models were generated to have similar dimension with an aspect ratio of 1:12, so to avoid the any deviation in structural variation due to the difference in size.

The thermal analysis on the optimized models was simulated via molecular dynamics. In the simulation, non periodic boundary condition in all three directions is adopted and the nanotubes models were tested under four different temperatures i.e. 300K, 500K, 700K, and 900K. This was carried out by slowly heating the system, which was initially at absolute zero 0K, and then allowing the energy equilibrate among the constituent atoms. The heating was performed by scaling up the velocities of all the atoms in the last configuration of a given molecular dynamics run to generate the initial condition for the next run corresponding to a higher energy. The classical Newton's equations of motion, as mentioned in section 4.3, were applied to investigate the systems performance. A time step of 0.01fs was employed for the molecular dynamics simulation and an overall simulation time 30ps was set to guarantee a good thermalization of the energy among all the degree of freedom. Figure 4.1 illustrates the simulation procedures as a flowchart.

In HyperChem, the temperature is monitored via the relationship with the average kinetic energy $K_{avg} = \frac{1}{2N}\sum_{A} m_A(v_{xA}^2 + v_{yA}^2 + v_{zA}^2) = \frac{3}{2}kT$, where N is the no of atoms in the system, m_A is the mass if the A^{th} atom, v_{xA} is the x-component of the velocity of the A^{th} atom, k is the Boltzmann constant and T is the temperature. Moreover, the Newton's equations of motion utilized in this study were integrated numerically using the Leap-frog Algorithm.

The leap-frog algorithm uses the simplest central difference formula for a derivative

$$\frac{df}{dt} = \frac{f(t+\Delta t) - f(t-\Delta t)}{2\Delta t} \tag{4.18}$$

as the basis for a simple iterative scheme to integrate Newton's equations of motion. If $v_{-1/2}$ is a first guess at a velocity (for the time t_0 -1/2Δt) and $\mathbf{x}_0$ is a position at time t_0, then by computing first a new velocity and coordinate, and repeat these processes, the following integration would be obtained,

$$v_{1/2} = v_{-1/2} + a_0 \Delta t \tag{4.19}$$

$$x_2 = x_0 + v_{1/2} \Delta t \tag{4.20}$$

$$v_{3/2} = v_{1/2} + a_1 \Delta t \tag{4.21}$$

$$x_2 = x_1 + v_{3/2} \Delta t \tag{4.22}$$

The new coordinates (**x**) and accelerations (**a**) are computed at integral times and the velocities (**v**) at half integral times. The time step Δt entered by the user is the time between evaluations of **a**, i.e., $\Delta t = t_1 - t_0$. The temperatures reported at integral times are the averages of the values on either side, determined from $\mathbf{v}_{i+1/2}$ and $\mathbf{v}_{i-1/2}$.

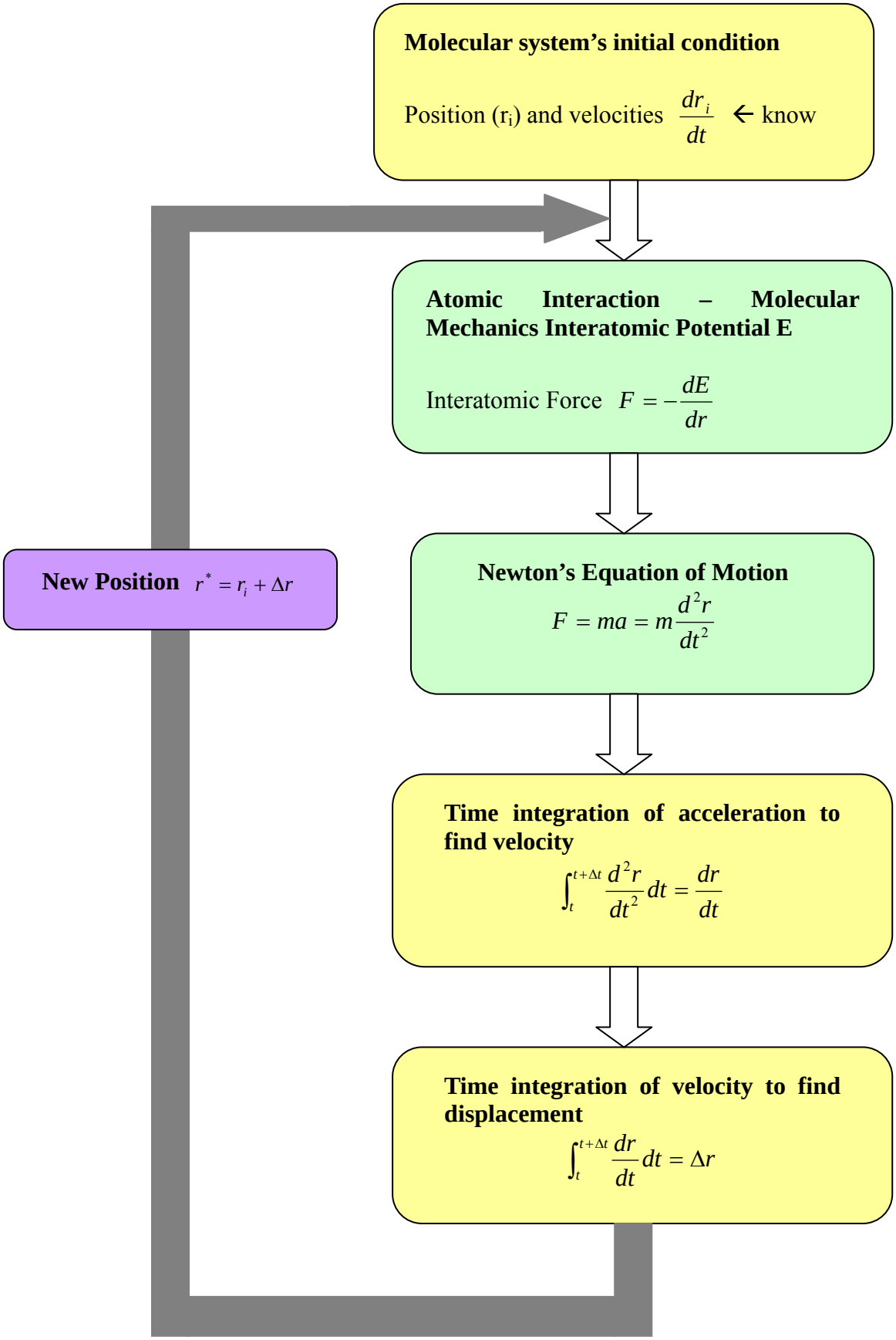

Figure 4.1 Flowchart of Molecular dynamics simulation

4.6 EVALUATION OF SIMULATION RESULTS

4.6.1 Temperature Variation

In order to verify whether the nanotubes systems have reached the desired temperatures (300K, 500K, 700K, and 900K) during molecular dynamics simulation, the variation of temperature over the simulation time period has been examined and shown in Figure 4.2. It can be clearly seen from the graph that the temperature reaches the desired value at time period of 10ps for both armchair and zig-zag type of nanotube. And after which there was an oscillation around the average value. It can be observed that the fluctuations increased with increasing temperature. This in turn implies for higher temperatures difference between the average temperature and the higher desired temperature. Through examining the pattern of the temperature profile, the oscillatory behavior seems to be replicated at various temperatures. This indicates that the basic numerical scheme in the algorithm is essentially identical and system temperature is linearly scaled with the desired temperature.

Although the fluctuation behaviors are similar in both types of nanotubes systems, it is noticed that the temperature oscillation at 900K was comparatively diverse. For the simulation temperature 300K to 700K, the fluctuations in both nanotube systems were moderated and similar. However, when the modeling temperature rose to 900K, it is revealed that the variation in temperature was much vigorous in the armchair nanotube system while that in zig-zag nanotube model remained gentle. Such results indicated that simulation algorithm worked well in modeling the zig-zag nanotube system in all temperature condition that under studied. On the other hand, for the armchair nanotube system, the numerical simulation would become relatively unsteady when the temperature reached 900K, however,

for temperature 700K and less, the simulation algorithm could give more reliable results as in the zig-zag nanotube model.

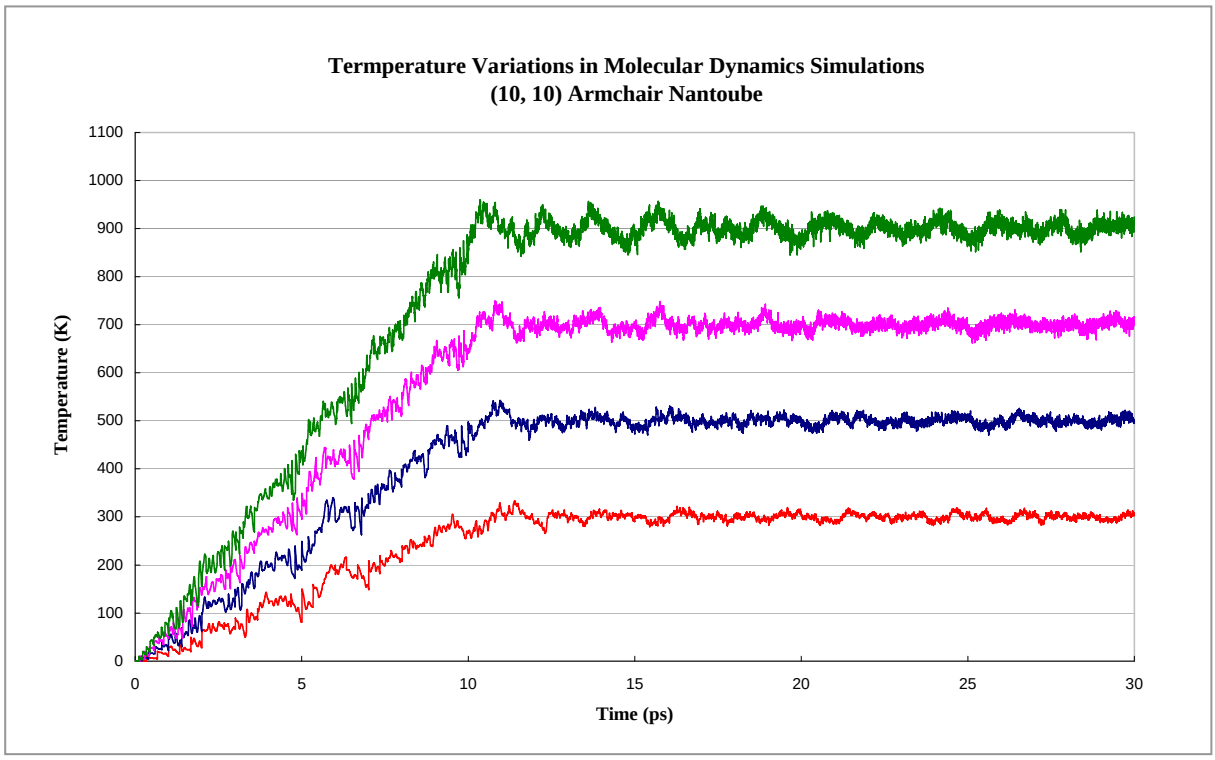

(a)

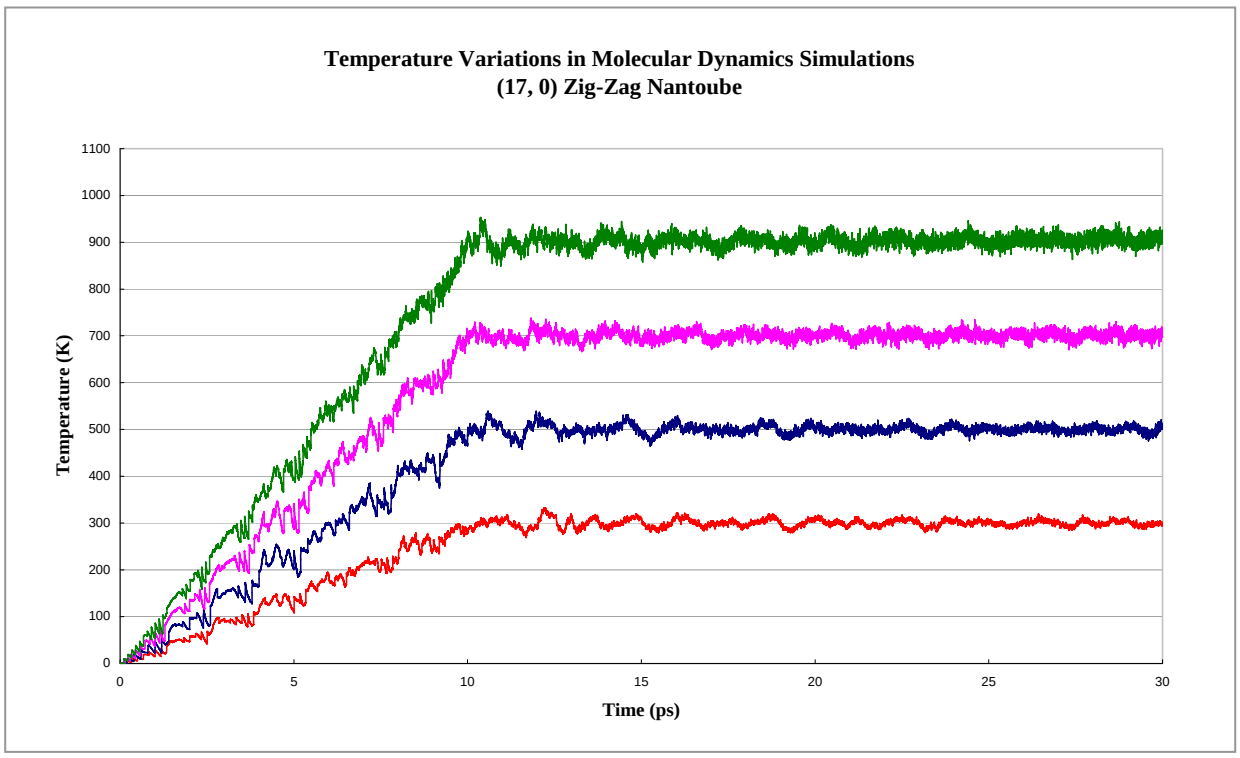

(b)

Figure 4.2 Temperature variations in the nanotubes systems during molecular dynamics simulation.

4.6.2 Equilibrium State

The necessary and sufficient condition for an isolated system to reach equilibrium is that entropy of the system reaches a maximum. However, entropy cannot be directly measured and we hence need to measure a number of thermodynamic variables indirectly to ascertain that the system has the equilibrium state. The choice of the variables and the magnitude of acceptable values for each of them make the determination of equilibrium become very challenging. In general attaining thermodynamic equilibrium means achieving thermal, mechanical and chemical equilibrium. Thermal equilibrium is state of the system at which there are no forces exist that drive heat transfer. Mechanical equilibrium is the state at which the net force causing change in the shape of size of the system is zero. Chemical equilibrium is the state at which there are no forces driving chemical reactions, phase transitions, and diffusion in mass transfer.

Identifying equilibrium in molecular dynamics has to be carried out over a finite duration of time, of interest to the property, rather than at any instant. The conditions necessary for ascertaining achievement of equilibrium in molecular dynamics [196] are,

(i) The total number of atoms N, the total energy E should be a constant independent of time. The fluctuations in the kinetic and the potential energy must be equal in magnitude (absolute values) as the total energy is remains constant.

(ii) The thermodynamic properties i.e. temperature, configurational internal energy should be fluctuating about stable average values.

(iii) Properties' averages should not be largely affected and retain their equilibrium values by small perturbations, for example temperature.

(iv) The time average of any property should be same for different macroscopic parts, provided the number of particles among the parts is kept the same.

In this work, the number of atoms used in both kinds of nanotubes models was retained, i.e. 2700 atom for armchair system and 2652 atoms for zig-zag model throughout the simulation. Besides, the results shown that the temperature in all the cases of simulation was varied around an average value during the simulation as indicated in figure 4.2.

Apart from this, figure 4.3 and 4.4 illustrate the energy variations in armchair and zig-zag nanotube systems during molecular dynamics simulation. From the results, it is noticed that the total potential energy of the systems varied between 4324 to 5763 kcal/mol for armchair nanotube system, and between 7283 to 7895 kcal/mol for zig-zag nanotube model. Both of the systems have fluctuation around the average value and armchair system show a larger deviation than the zig-zag model. The energy fluctuations in the systems reflected the statistical variations in positions of atoms and hence their momenta. Such oscillations are acceptable as the variation was relatively small when comparing with the total potential energy of the systems. Moreover, these values were reached when the simulation time was around 11-12ps which were happened right after the simulated temperature has reached.

Besides, the kinetic energy was a direct consequence of maintaining the temperature and also reached an equilibrium value in the same time step i.e. 11-12ps. And, similar to the

situation of potential energy, the variation of kinetic energy in zig-zag nanotube model was found to be much smaller than that of the armchair system, provided that the effect of velocity scaling in the zig-zag model to reach the desired temperature was much effective than that in the armchair system. On the other hand, the total energy of the two types of systems also showed the similar behavior as in kinetic and potential energy, that is, it reached an equilibrium state when the simulated time arrived at 11ps and this energy also with fluctuation but was around an average value.

The results from the modeling demonstrated that the nanotubes systems were able to reach the equilibrium during the molecular dynamics simulation, and the parameters and algorithms used in the simulation are acceptable.

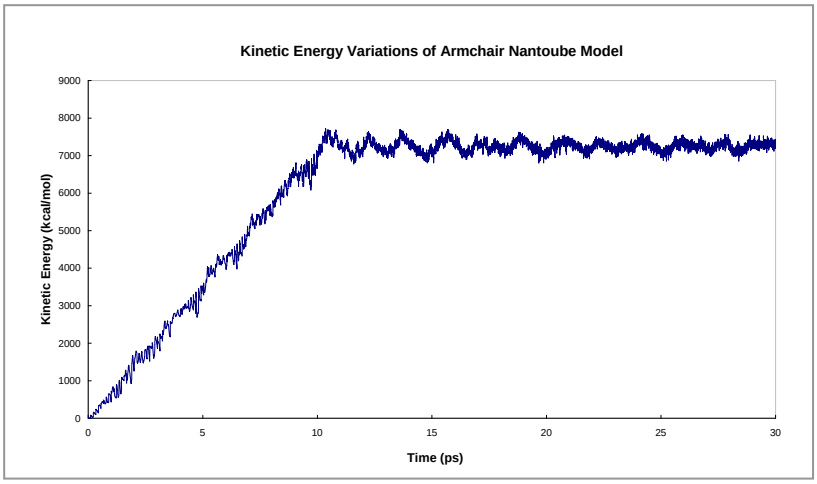

(a)

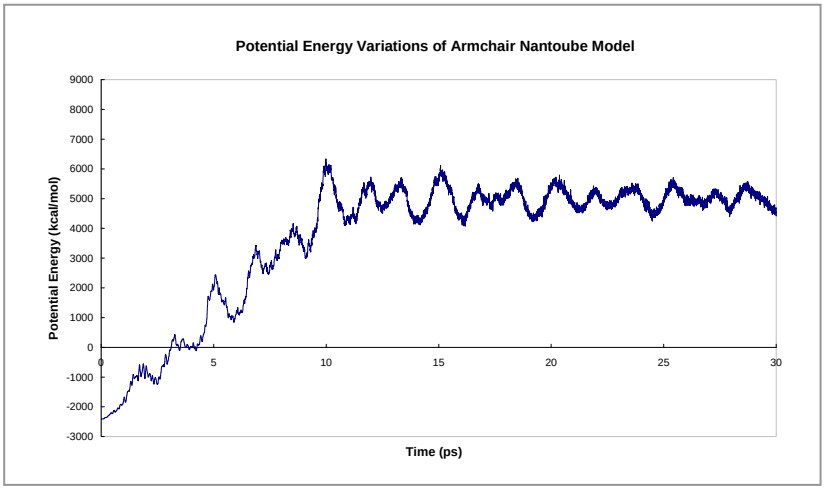

(b)

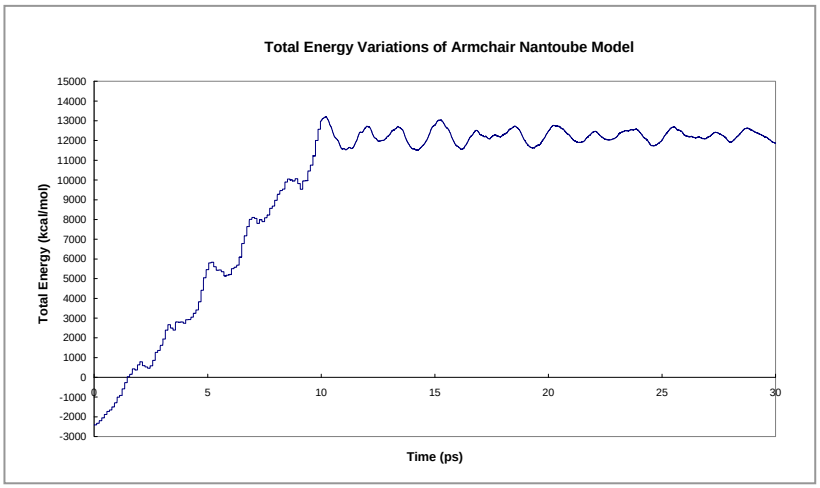

(c)

Figure 4.3 Variations in system energy of armchair nanotube over time (a) Kinetic Energy, (b) Potential Energy, and (c) Total Energy

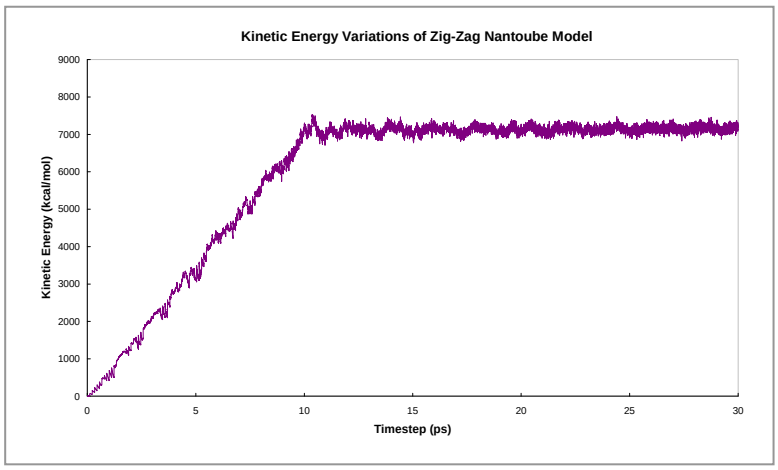

(a)

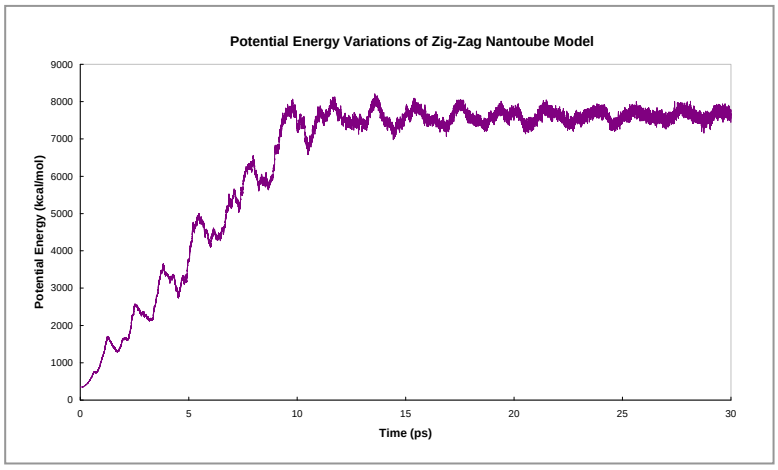

(b)

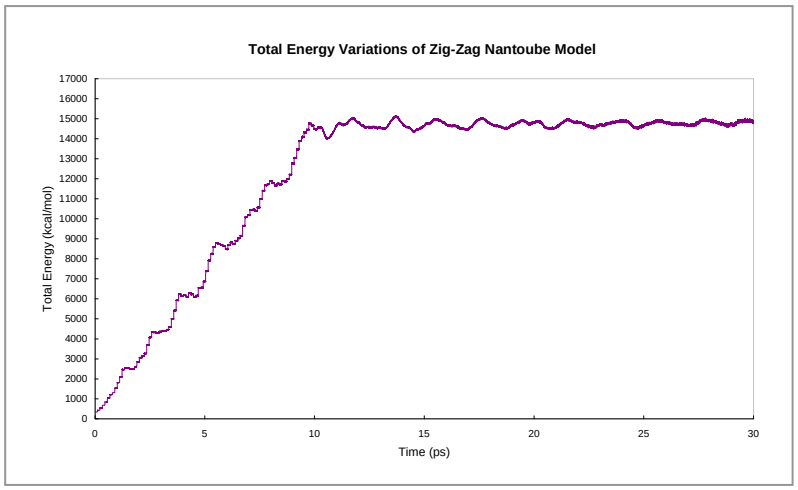

(c)

Figure 4.4 Variations in system energy of zig-zag nanotube over time (a) Kinetic Energy, (b) Potential Energy, and (c) Total Energy

4.6.3 Structural Variation of Carbon Nanotube

The structural deviation of carbon nanotube from its cylindrical shape was found through the molecular dynamics simulation in all modeling conditions. Figure 4.5 shows the cylindrical shapes of the armchair and zig-zag carbon nanotubes before the thermal analysis. The carbon nanotubes were in their most stable and equilibrium situation and were obtained via geometrical optimization.

Results of molecular dynamics simulations are illustrated in Figure 4.5 to 4.9. Twisting of nanotube is observed in the simulations of both armchair and zig-zag systems, and the degree of twisting increased with the temperature. During the simulation processes, elongation of the nanotubes was noticed together with twisting. The elongation occurred not only in the axial direction, but also in the sideway of the nanotubes and combined with the twisting action which shown in figure 4.6 and 4.8. Meanwhile the alteration of bending and twisting behaviors are indicated by the end views of nanotubes in figure 4.7 and 4.9.

When compared the results of armchair nanotube system and zig-zag nanotube model, the temperature variation is found to have a stronger influence on the zig-zag nanotube. During the increase of temperatures, both types of nanotubes changed from their original cylindrical shape at 0 K to an elongated, twisted form at higher temperature. However, the bending effect is overtaking the twisting effect in armchair nanotube and the degree of bending is increased with temperature. For the zig-zag nanotube, the phenomenon of twisting and elongation are also observed; yet, the variation of such behaviors was different from that of armchair nanotube. The twisting behavior is more obvious than the bending effect in zig-zag nanotubes. And the degree of twisting is much larger than that of armchair one. Such results demonstrated that during the simulation, the atoms in nanotube gained enough

energy to move about its original position and thus causing the distortion of the nanotube. However, due to the structural difference between zig-zag and armchair nanotubes, unlike degree of distortion of nanotubes were created.

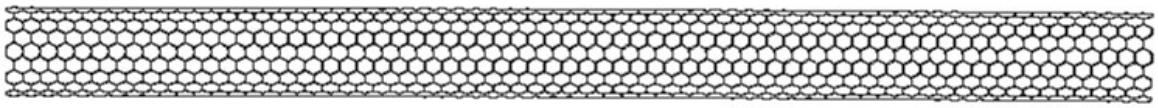

(a)

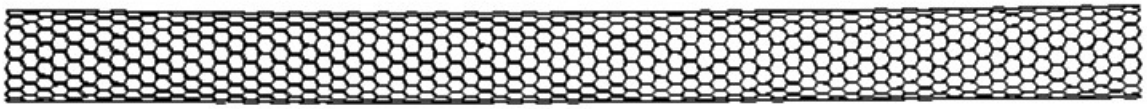

(b)

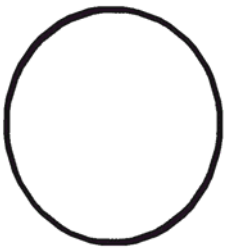

(c)

Figure 4.5 Different views of the modeled structure of the carbon nanotubes after geometrical optimization. (a) Side view of (10, 10) Armchair carbon nanotube, (b) Side view of (17, 0) Zig-Zag carbon nanotube, and (c) End view of carbon nanotube (same for armchair and zig-zag type of carbon nanotube)

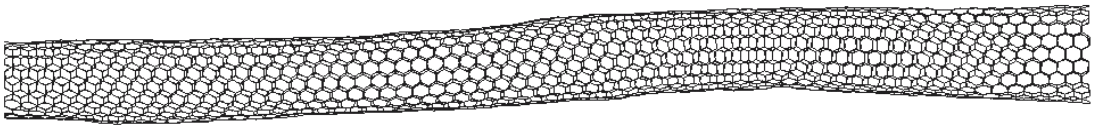

300K

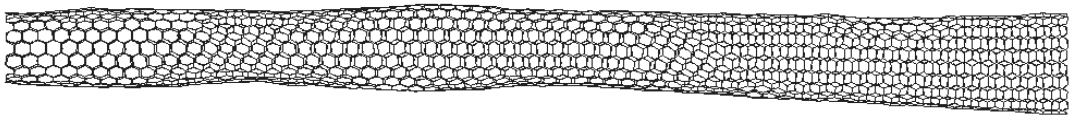

500K

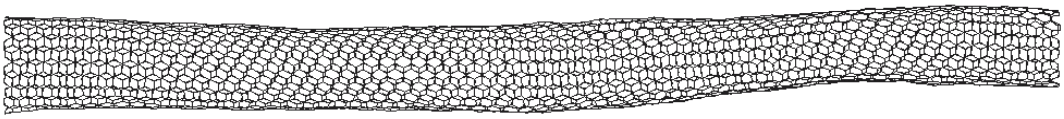

700K

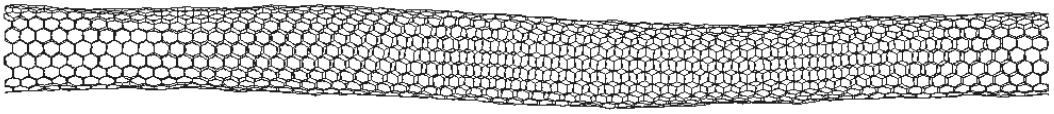

900K

Figure 4.6 Side View of the armchair (10, 10) nanotube at different simulation temperatures.

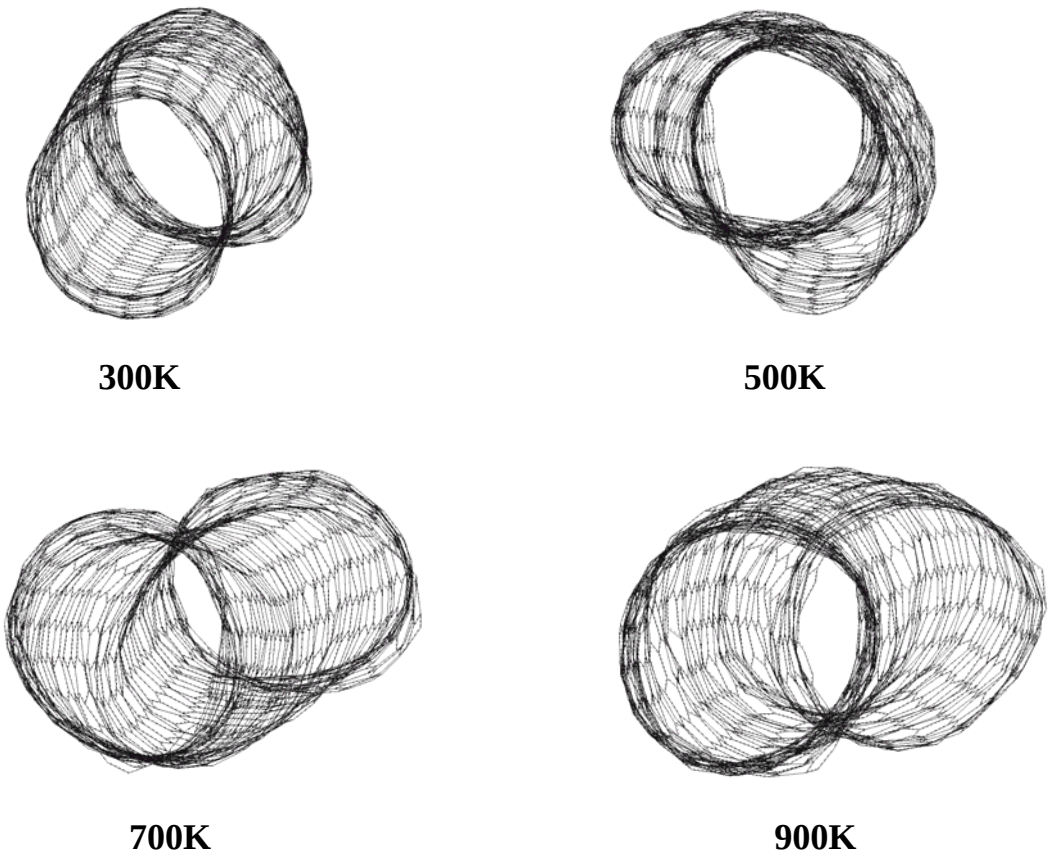

Figure 4.7 End view of the armchair (10,10)) nanotube at different simulation temperatures

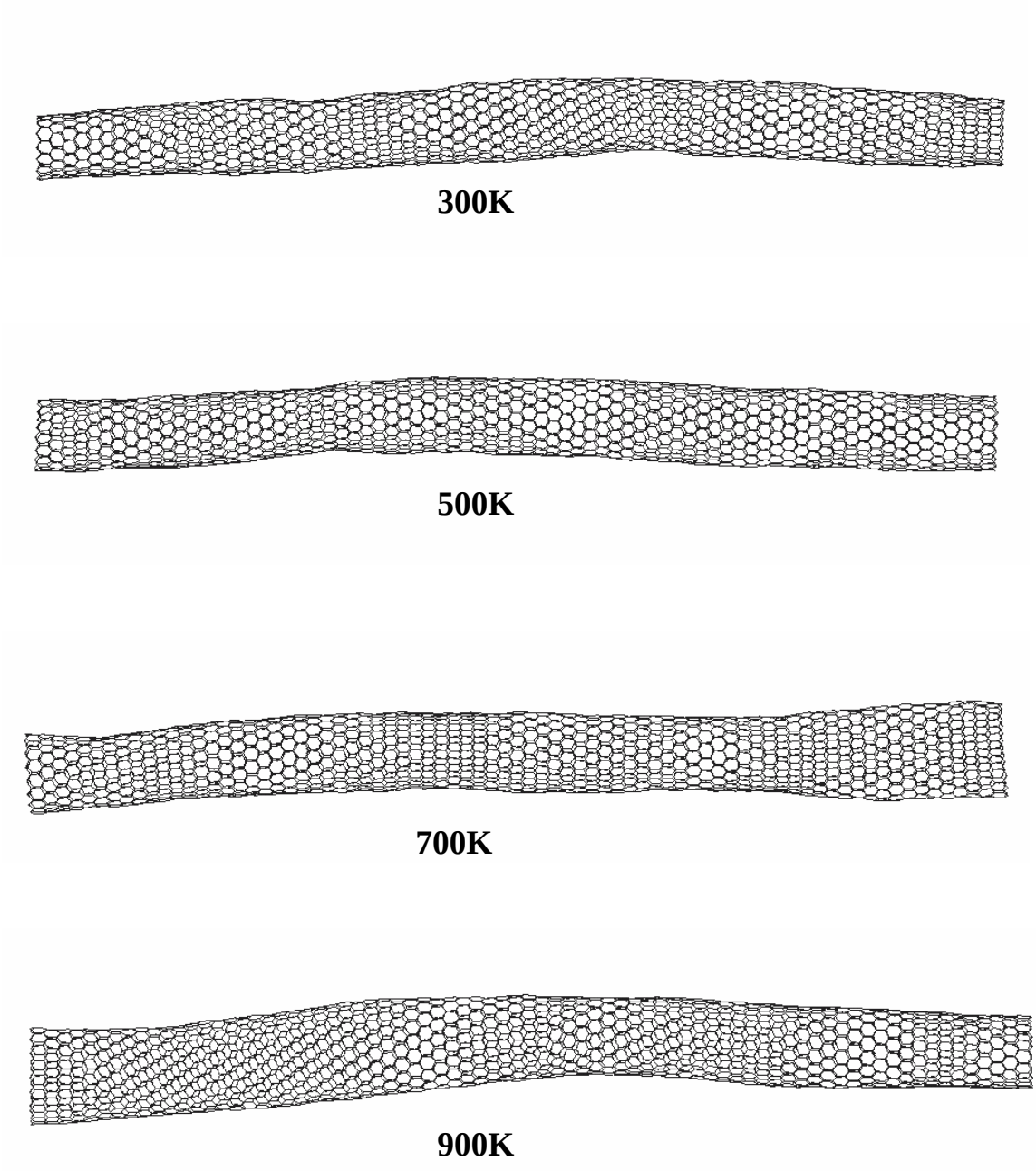

Figure 4.8 Side View of the zig-zag (17, 0)) nanotube at different simulation temperatures

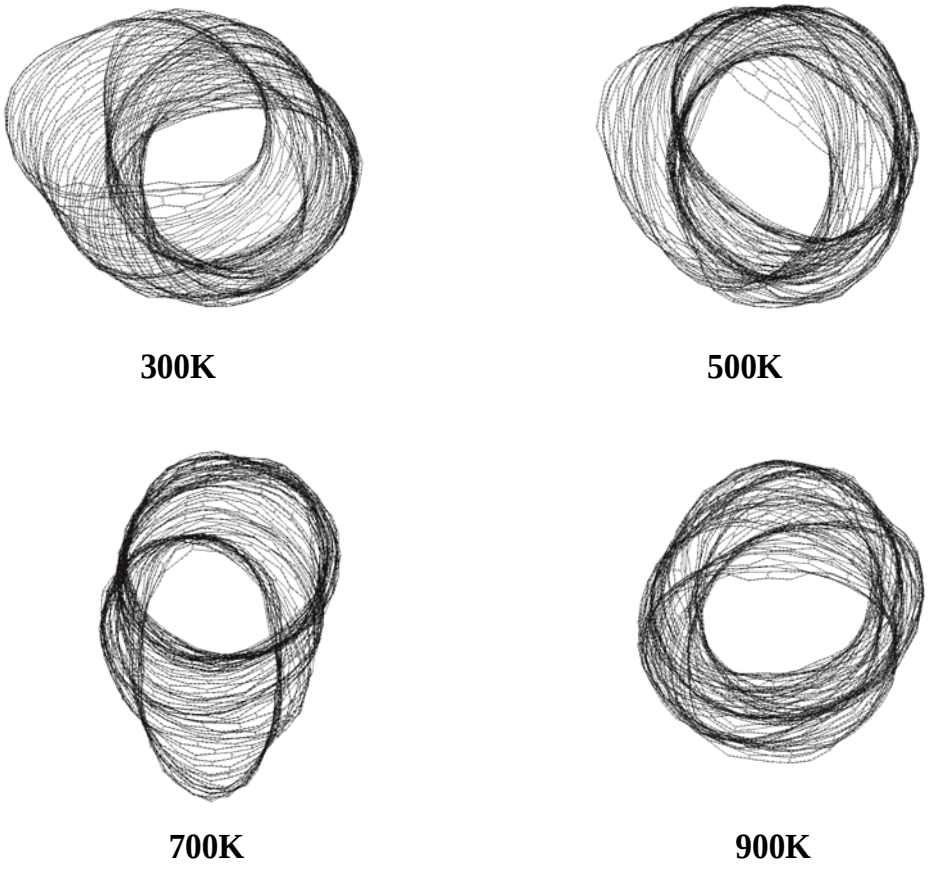

Figure 4.9 End View of the zig-zag (17, 0)) nanotube at different simulation temperatures

Further insights into the structural variation can be investigated through the table 4.1 and 4.2. Table 4.1 illustrates the potential energies of the armchair and zig-zag nanotubes systems obtained from the geometrical optimization. Some of the potential energy terms, e.g. electrostatic potential, out of plane potential, are not included in the table because these functions did not produce any effects in the simulation or their values are equal to zero. From the results, it is found that the dihedral (torsional) energy was the dominant component of the nanotubes' total energy. Neglecting the Van der Waals energy, the dihedral energy was found to be at least 50 times the rest of the energy terms in armchair nanotube model while it was at least 20 times the energy terms in the zig-zag system. Though the Van der Waals energy has significant impact on the total energy of the systems, this non-bonding energy would have the least influence on the formation of the internal structure of the systems. Moreover, by comparing the energy terms in the armchair and zig-zag systems, it is revealed that the dihedral energy in armchair model was twice the value of that in zig-zag one. However, the rest of the energies in the armchair system were lower than that in the zig-zag model. These findings pointed out that the nanotubes' structure was highly relied on their dihedral property. Any external influence on this value would easily sway the cylindrical nanotubes into some other forms.

Table 4.2 shows the energies of the (10, 10) armchair and (17, 0) zig-zag nanotube systems achieved through molecular simulations. From the results, it is noticed that the energies of both nanotubes systems increased with the simulation temperature. Besides, since the mass of atom was the same in both nanotubes systems and the velocity of the atom was monitored through the relation with temperature (mentioned in section 4.5.3), the kinetic energy of the nanotubes models was almost the same. The similarity in the kinetic value implied that the total energy of the systems would be depended strongly on the potential

energy. Referring to the evaluated values, it is known that the potential energy of both types of nanotube systems was enhanced evenly with the simulation temperatures. The potential energy of the armchair nanotube system was gained from it minimum energy state at -2408.1 kcal/mol to the maximum value 4451.655 kcal/mol at 900 K. Meanwhile, the energy value of the zig-zag nanotube model was augmented from its equilibrium state with 350kcal/mol to the state with maximum energy i.e. 7573.343 kcal/mol at 900K. The increment in potential energy in both nanotubes systems was attributed to the change in internal structure of the nanotubes due to the gain in temperature. And such increment was mostly caused by the torsion motion in this study.

Furthermore, figure 4.10 provides a better picture on the variation of the system energy of armchair and zig-zag nanotubes models over different simulation temperatures. Through the figure, it is noticed that all the energy types, i.e. kinetic, potential and total energy, were improved with increased modeled temperature. And the increment of energy was found to be proportional to the modeling temperature in the simulation.

Table 4.1 Evaluated potential energies of the (10, 10) armchair and (17, 0) zig-zag nanotube systems via geometrical optimization.

	Potential Energy (kcal/mol)					
Carbon Nanotube	**Bond Stretching (kcal/mol)**	**Angle Bending (kcal/mol)**	**Dihedral (kcal/mol)**	**Van der Waals (kcal/mol)**	**Bond Stretching And Angle Bending (kcal/mol)**	**Total (kcal/mol)**
(10, 10) Armchair	87.514	86.266	-4659.810	2086.100	-8.172	-2408.102
(17, 0) Zig-Zag	114.916	95.650	-2271.540	2420.340	-9.361	350.005

Table 4.2 Energies of the (10, 10) armchair and (17, 0) zig-zag nanotube systems through molecular simulations.

	(10, 10) Armchair CNT			(17, 0) Zig-Zag CNT		
Simulation Temperature (K)	**Kinetic Energy (kcal/mol)**	**Potential Energy (kcal/mol)**	**Total Energy (kcal/mol)**	**Kinetic Energy (kcal/mol)**	**Potential Energy (kcal/mol)**	**Total Energy (kcal/mol)**
0	0	-2408.100	-2408.1019	0	350.0089	350.0053
300	2480.659	1.081596	2481.741	2341.840	2856.600	5198.440
500	4016.932	1551.943	5568.875	3976.577	4407.258	8383.835
700	5644.748	3082.221	8726.968	5540.195	5998.066	11538.260
900	7403.346	4451.655	11855	7254.192	7573.343	14827.540

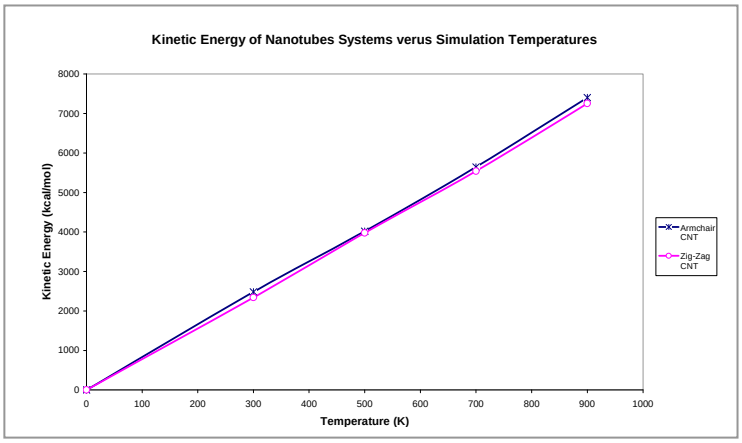

(a)

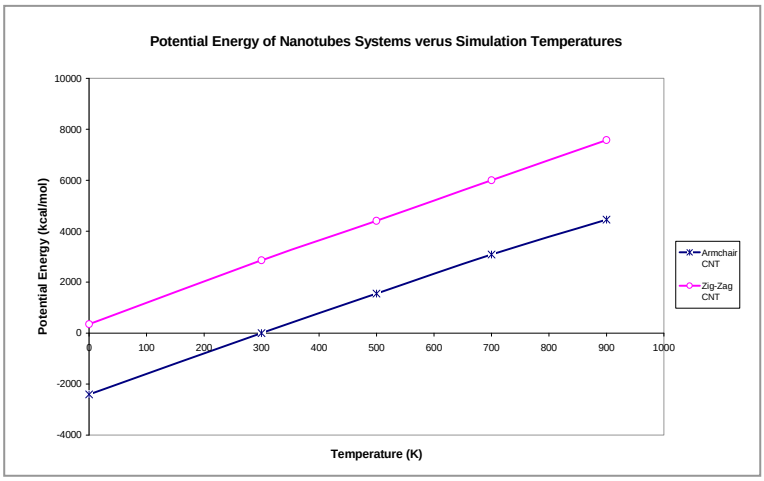

(b)

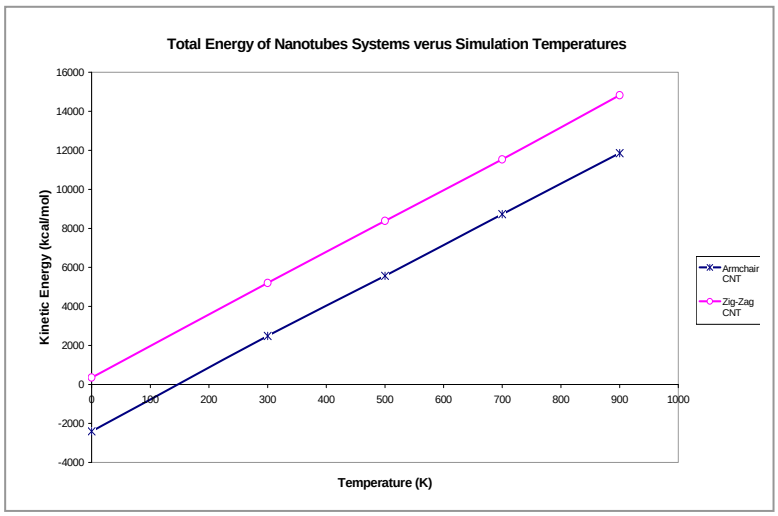

(c)

Figure 4.10 Variations in system energy of armchair and zig-zag nanotube models over different simulation temperatures (a) Kinetic Energy, (b) Potential Energy, and (c) Total Energy

4.7 CONCLUSION

In this chapter, a complete modeling of armchair and zig-zag type of single-walled carbon nanotube was discussed. Major computational methods in molecular simulation were briefly introduced. Molecular dynamics simulation was chosen for nanotubes modeling due to its computational efficiency and accuracy. In molecular dynamics simulations, the potential energy model is essential. In this work, the potential energy model required in the energy calculation was introduced and formulated. Besides, the simulations of the nanotubes systems were carried out through a new modeling program, HyperChem. The results achieved from the molecular dynamics simulation shown that the geometrical properties of the armchair and zig-zag nanotubes were subjected to change with temperature. And the alteration in nanotubes structures was found to accelerate together with the simulation temperature.

These findings provide useful explanation on the enhancement of composites properties due to the reinforcement of SWNTs. According to the experimental results, it is known that there was no significant chemical bonding between SWNTs and epoxy matrix, however, the improvement of materials properties was remarkable with the addition of SWNTs. Through the results of thermal analysis, the augmentation in the properties of composites can be accounted for the structural variation in nanotubes which would lead to micromechanical interlocking with the polymer matrix inside the structures. And this geometrical alteration in nanotubes can be created during the composites fabrication when nanotubes were processed under different temperature conditions i.e. solution mixing process, curing process. Under such circumferences, the nanotubes may allow to deviate from its cylindrical shape due to the energy gain from the thermal environment.

CHAPTER 5

SUMMARY AND FUTURE WORK

5.1 SUMMARY

This research has undertaken a systematic investigation into the material properties enhancement due to the reinforcement of carbon nanotubes. Single-walled carbon nanotubes were the major interested as the reinforcement in this study while epoxy was selected to be the matrix polymer due to its high availability nowadays. Both purified and functionalized SWNTs were employed to examine the effect of surface modification on nanotube dispersion and also interfacial adhesion to the polymer matrix. Besides, various weight percentages, i.e. 1%, 2%, 3%, 4%, 5%, of SWNTs and FSWNTs were introduced for manufacturing the composite, thus to study the mechanical improvement of polymer due to the application of nanotubes.

The fabrication procedures of nanotube/epoxy composites were developed to achieve the evaluation on properties improvement due to the addition of nanotubes. The nanotubes were dispersed throughoutly inside the epoxy resin via the solution mixing process. And sonication was employed to facilitate the mixing process. Although the sonication time was directly related to the dispersion of nanotubes inside the polymer matrix in liquid state, the excessive sonication process would damage the nanotube structure. Hence, three hours of

operation with sonication was utilized as the best processing duration in this work. Moreover, the usage of solvent was omitted during the composite fabrication to avoid the ductile behavior in the final product due to the solvent employed. Heating and degassing processes were also involved in the preparation of composites, and the nanocomposites were obtained after the completion of curing in the oven and then room temperature for about a week of time.

In order to investigate the properties augmentations of the nanotube based composites, a series of experiments and characterization methods tests i.e. tensile property test, flexural property test, impact test, microhardness test, dynamics mechanical analysis, thermogravimetric analysis, and scanning electron microscopy were conducted. Experimental evidences have shown that the reinforcement of SWNTs gave attractive improvement in the material properties over the neat epoxy. Also, the functionalization on nanotubes was revealed to provide remarkable enhancement in properties which were superior to the purified nanotubes as filler in composites. Mechanical properties, such as elastic modulus, flexural modulus, impact strength, hardness, of the composites were found to enhance due to the addition of nanotubes. However, such enhancements were varied according to the amount of nanotubes applied.

The outcomes from the tensile property test and flexural property test indicated that there was a significant improvement in mechanical properties due to the addition of nanotubes. The increments in material properties, i.e. ultimate strength, tensile modulus, and flexural modulus, reached the maximum when 5wt% of nanotube was employed. And the reinforcement of FSWNTs gave a superior enhancement in material properties to that of SWNTs. On the other hand, the results from impact test indicated a different behavior than in

any other tests. The peak impact strength of both types of nanotube based composites was obtained when 3wt% of nanotube was employed. This impact property was found to enhance by more than 50% over the neat epoxy when 3wt% of FSWNT was embedded inside the composite. Further filling of nanotubes in both kinds of composites was found to lower the impact value of composites and the impact strength showed a deterioration of approximately 21% when 5wt% of SWNT was used. Apart from this, through the microhardness test, the improvement in hardness property due to the reinforcement of nanotubes was observed and the peak value was concluded as 5wt% of nanotube was filled into the composite. However, in contrast to the results from other experiments, the introduction of SWNT was found to induce a better hardness value than that of FSWNT.

To facilitate the analysis on the performances of nanotube based composites, SEM was used to examine the failure mechanism of the composites after mechanical property tests and to inspect the dispersion of carbon nanotubes inside the composite. Through the micrographs obtained from SEM, it is demonstrated that the SWNTs tended to form agglomerates insides the composites, and these agglomerates showed poor wetting of epoxy and were parallel to the fracture surface. However, opposing to SWNTs, FSWNTs present a uniform dispersion in the composites. Besides, they showed a good wetting of epoxy and most of them were perpendicular to the fracture surface. The variation in nanotube distribution and interaction in different types of composites gave an alternative explanation on the deviation of load transferability due to different variety of nanotube reinforcement.

Apart from the mechanical property tests, thermal analysis, i.e. DMA and TGA, were also conducted to investigate the effect on the epoxy properties due to the addition of SWNT and FSWNT. The results showed that the interaction between purified SWNTs and epoxy

matrix was comparatively poor while strong cross-linking was formed between the FSWNTs and neat epoxy. In the analysis of DMA, the glass transition temperature of composites was found to shift to the lower value with the addition of nanotubes, and the FSWNT/Epoxy composites nanotubes demonstrated the dramatic decrement in the temperature value when compared to others. Furthermore, the storage modulus of composites was revealed to provide either enhanced or adverse effect due to the reinforcement of nanotubes. The filling of FSWNTs was shown to cause an enhancement in storage modulus no matter the temperature was below or above the $T_{g.}$ Apart from this, the viscosity of the composites was also determined to be increased induced by the addition of nanotubes. And the viscosity of FSWNT/Epoxy composites was found be higher than that of SWNT/Epoxy composites nanotubes in all reinforced content of nanotubes. The results from DMA implied the improved interfacial interaction was obtained between the functionalized nanotubes and epoxy matrix. Such improvement caused by the adsorption of epoxy prepolymer into the functionalized SWNTs, the induction of stiffening effect inside the composites, and also the limitation of molecular movement, which provided a superior thermal results over the SWNT/Epoxy composites and neat epoxy.

The enhancement of interfacial interaction between FSWNTs and epoxy matrix was further examined with the application of TGA. The outcomes of the TGA presented that the thermal decomposition temperature of the SWNT/Epoxy composite was closed to thermal value of epoxy while that of FSWNT/Epoxy composite was found to have the value higher than that of SWNT/Epoxy composite and neat epoxy. The raise of this thermal value was attributed to the increased thermal energy required to break the additional bonds which was formed between the functionalized nanotubes and the polymer matrix. Also, such enhancement can also contribute to the improvement in dispersion of SWNTs due to

functionalization. Therefore, the investigation though TGA given a convincing evidence of improved interfacial adhesion between nanotubes and epoxy matrix caused by functionalization.

Meanwhile, according to the experimental results, it is known that there was no significant chemical bonding between SWNTs and epoxy matrix, however, the improvement of materials properties was remarkable with the addition of SWNTs. The improvement in properties of SWNT/Epoxy composites was predicted to be caused by the micromechanical interlocking formed inside the structures. And the formation of physical interlocking was expected to induce by the change in shape of nanotubes caused by temperatures variation during composites fabrication. In order to examine the effect due to the alteration in temperature, molecular mechanics together with molecular dynamic simulations were used to investigate the structural variation of the carbon nanotube. A complete modeling of armchair and zig-zag type of SWNTs was under studied.

The results achieved from the simulation showed that the geometrical properties of the armchair and zig-zag nanotubes were subjected to change with temperature. And the alteration in nanotubes structures was found to accelerate together with the simulation temperature. These findings provided useful explanation on the enhancement of composites properties due to the reinforcement of SWNTs. Through the results of thermal analysis, the increase in material properties of composites can be accounted for the structural variation in nanotubes which would lead to micromechanical interlocking with the polymer matrix inside the structures. And this change in geometry of nanotubes can be created during the composites fabrication when nanotubes were processed under different temperature conditions. Under these conditions, the nanotubes may allow to deviate from its cylindrical

shape due to the energy gain from the thermal environment, forming the physical interlocking at least.

5.2 SUGGESTIONS FOR FUTURE WORK

The outcome from this study has indicated the enhancement of composite properties due to the reinforcement of nanotubes. And such improvement was found to accelerate when the nanotube has undergone the chemical functionalization. In order to entirely utilize the nanotubes as filler in composite structures, it is urged to understand the interaction between nanotubes and the polymer matrix. Though chemical functionalization is shown to provide an improvement on interfacial adhesion between nanotubes and epoxy matrix experimentally, the details on the chemical processes and the external influences such as temperature, pressure, and sonication frequency on such processes are still uncertain. Thus, it is essential to comprehend the chemistry involve in the whole composites fabrication process.

Apart from examining the chemical techniques require during composite production, the development of mass production method on nanotube based composites is crucial to fulfill the need of industrial application. And the duration of functionalization process also has to be taken into account to shorten the production time of composite. Moreover, the control of nanotube alignment inside the composites is also another important topic in the composite making.

In order to achieve the efficient production method of composites, experiments together with molecular modeling are required. Before any experiment to be carried out,

molecular simulation can be adopted to predict the behavior of the composite in different loading conditions and can provide a better understanding on effects cause by the external circumstance. As the extension of this research, a bulk simulation with disordered nanotubes embedding in the polymer chain should be developed. This simulation would help in identifying the influence induces by the polymer chain and nanotubes themselves inside the composite structure. Moreover, since the resin flow is important for nanocomposite manufacturing, thus molecular simulation involving the external pressure gradient will facilitate the understanding in the flow through the nanopores inside the epoxy polymer and how it relates to the final product obtain.

REFERENCES

[1]S. Iijima. Helical Microtubules of Graphitic. *Carbon, Nature 354: 56-58 (1991)*

[2] M. M. J. Treacy, T. W. Ebbesen, J. M. Gibson. Exceptionally High Young's Modulus Observed for Individual Carbon Nanotubes. *Nature 381: 678 – 680 (1996)*

[3] P. Poncharal, Z. L. Wang, D. Ugarte, W. A. de Heer. Nanobeam Mechanics: Elasticity, Strength, and Toughness of Nanorods and Nanotubes. *Science 283: 1513-1517 (1999)*

[4] Erik T. Thostenson, Z. F. Ren, T. W. Chou. Advances in the Science and Technology of Carbon Nanotubes and Their Composites. *Composites Science and Technology 61: 1899-1912 (2001)*

[5] B S. Files. Applications of Carbon Nanotube for Human Space Exploration. *Proceedings of NanoSpace 98, November 1998, Houston, TX*

[6] http://flightprojects.msfc.nasa.gov/fd02_elev.html. *NASA Marshall Space Flight Center, Flight Projects Directorate, FD02 Advanced Projects Office, Huntsville, AL 35812*

[7] B. C. Edwards, K. M. Jones, T. A. Bekkedahl, C. H. Kiang, D. S. Bethune, M. J. Heben. Storage of Hydrogen in Single-Walled Carbon Nanotubes. *Nature 47 (10): 735-44 (2000)*

[8] D. Qian, E. C. Dickey, R. Andrews, T. Rantell. Load Transfer and Deformation Mechanisms in Carbon Nanotube-Polystyrene Composites. *Applied Physics Letter 76: 2868–2870 (2000)*

[9] P. M. Ajayan, L. S. Schadler, C. Giannaris, A. Rubio. Single-Walled Carbon Nanotube-Polymer Composites: Strength and Weakness. *Advanced Materials 12: 750 – 753 (2000)*

[10] H. W. Kroto, J. R. Heath, S. C. O'Brien, R. F. Curl, R. E. Smalley. C_{60}: Buckminster -fullerene. *Nature 318: 162–163 (1985)*

[11] D. T. Colbert. Single-Walled Nanotubes: A New Option for Conductive Plastic and Engineering Polymers. *Plastic Additives and Compounding, 5 (1): 18-25 (2003)*

[12] http://www.iljinnanotech.co.kr/en/material/2.html. *ILJIN Nanotech Company, Carbon Nanotube (2002)*

[13] R. Saito, G. Dresselhaus, M. S. Dresselhaus. Physical Properties of Carbon Nanotubes. *Imperial college press 1998*

[14] M. S. Dresselhaus, G. Dresselhaus, R. Saito. Carbon Fibers based C_{60} and their Symmetry. *Physical Review B 45: 6234-6242 (1992)*

[15] M. S. Dresselhaus, G. Dresselhaus, R. Saito. Physics of Carbon Nanotubes. *Carbon 33: 883-891 (1995)*

[16] J. W. G. Wildoer, L. C. Venema, A. G. Rinzler, R. Smalley, C. Dekker. Electronics Structure of Atomically solved Carbon Nanotubes. *Nature 391: 59-62 (1998)*

[17] D. H. Robertson, D. W. Brenner, J. W. Mintmire. Energetics of nanoscale graphitic tubules. Physical Reviews B 45: 12592 - 12595 (1992)

[18] B. I. Yakobson, C. J. Brabec, J. Bernholc. Nanomechanics of Carbon Tubes: Instabilities Beyond Linear Range. *Physical Review Letters 76 (14): 2511-2514 (1996)*

[19] B. I. Yakobson, G. Samsonidze. Atomistic Theory of Mechanical Relaxation in Fullerene Nanotube. *Carbon 38 (11-12): 1675-1680 (2000)*

[20] B. I. Yakobson. Mechanical Relaxation and ''Intramolecular Plasticity'' in Carbon Nanotubes. *Applied Physics Letters 72 (8): 918-920 (1998)*

[21] M. B. Nardelli, B. I. Yakobson, J. Bernholc. Brittle and Ductile Behavior in Carbon Nanotubes. *Physical Review Letters 81 (21): 4656-4659 (1998)*

[22] Z.W. Pan, S. S. Xie, L. Lu, B. H. Chang, L. F. Sun, W. Y. Zhou, G. Wang, D. L.Zhang. Tensile Tests of Ropes of Very Long Aligned Multiwalled Carbon Nanotubes. *Applied Physics Letters, 74 (21): 3152-3154 (1999)*

[23] http://www.physics.berkeley.edu/research/zettl/projects/imaging.html *University of California at Berkeley, Department of Physics, Zettle Research Group, TEM and SEM Imaging of Nanostructures.*

[24] A. Thess, R. Lee, P. Nikolaev, H. Dai, P. Petit, J. Robert, C. H. Xu, Y. H. Lee, S. G. Kim, A. G. Rinzler, D. T. Colbert, G. E. Scuseria, D. Tomanek, J. E. Fischer, R. E. Smalley. Crystalline Ropes of Metallic Carbon Nanotubes. *Science 273: 483-487 (1996)*

[25] G. H. Gao, T. Cagin, W. A. Goddard III. Energetics, Structure, Mechanical and Vibrational Properties of Single Walled Carbon Nanotubes (SWNT). *The Fifth Foresight Conference on Molecular Nanotechnology, Nov. 5-8, Palo Alto, CA, USA (1997)*

[26] C. Journet, W. K. Maser, P. Bernier, A. Loiseau, M. L. de la Chapelle, S. Lefrant, P. Deniard, P. Lee, J. E. Fischer. Large-Scale Production of Single-Walled Carbon Nanotube by the Electric-Arc Technique. *Nature 388: 756-758 (1997)*

[27] D. S. Bethune, C. H. Kiang, M. DeVries, G. Gorman, R. Savoy, J. Vazquez. Cobalt-Catalysed Growth of Carbon Nanotubes with Single-Atomic-Layer Walls. *Nature 363: 605-607 (1993)*

[28] C. Journet, P. Bernier. Production of Carbon Tubes. *Applied Physics A 67: 1-9 (1998)*

[29] A. G. Rinzler, J. Liu, H. Dai, P. Nikolaev, C. B. Huffman, F. J. Todriguez-Macias, P. J. Boul, A. H. Lau, D. Heymann, D. T. Colbert, R. S. Lee, J. E. Fischer, A. M. Rao, P. C. Eklund, R. E. Smalley. Large-Scale Purification of Single-Walled Carbon Nanotubes: Process, Product, and Characterization. *Applied Physics A 67: 29-37 (1998)*

[30] T. Guo, P. Nikolaev, A. Thess, D. T. Colbert, R. E. Smalley. Catalytic Growth of Single-Walled Nanotubes by Laser Vaporization. *Chemical Physics Letters 243: 49-54 (1995)*

[31] F. Bonaccorso, C. Bongiorno, B. Fazio, P. G. Gucciardi, O. M. Marago, A. Morone, C. Spinella. Pulsed Laser Deposition of Multiwalled Carbon Nanotubes Thin Films. *Applied Surface Science 254 (4): 1260-1263 (2007)*

[32] M. Endo, K. Takeuchi, K. Kobori, K. Takahashi, H. W. Kroto, A. Sarkar. Pyrolytic Carbon Nanotubes from Vapor Growth Carbon Fibers. *Carbon 33: 873-881 (1995)*

[33] M. Kumar, Y. Ando. Carbon Nanotubes from Camphor: An Environment-Friendly Nanotechnology. *Journal of Physics: Conference Series 61: 643–646 (2007)*

[34] Z. F. Ren, A. P. Huang, J. W. Xu, D. Z. Wang, J. G. Wen, J. H. Wang, L. Calvet, J. Chen, J. F. Klemic, M. A. Reed. Growth of a Single Freestanding Multiwall Carbon Nanotube on Each Nanonickel Dot. *Applied Physics Letters 78 (8): 1086-1088 (1999)*

[35] Z. F. Ren, A. P. Huang, J. W. Xu, J. H. Wang, P. Bush, M. P. Siegal, P. N. Provencio. Synthesis of Large Arrays of Well-Aligned Carbon Nanotubes on Glass. *Science 282: 1105-1107 (1998)*

[36] Z. P. Huang, J. W. Xu, Z. F. Ren, J. H. Wang, M. P. Siegal, P. N. Provencio. Growth of Highly Oriented Carbon Nanotubes by Plasma-Enhanced Hot Filament Chemical Vapor Deposition. *Applied Physics Letters 73 (26): 3845-3847 (1998)*

[37] T. W. Ebbesen, P. M. Ajayan. Large-Scale Synthesis of Carbon Nanotubes. *Nature 358: 220-222 (1992)*

[38] B. I. Yakobson, R. E. Smalley. Fullerene Nanotubes: $C_{1,000,000}$ and Beyond. *American Scientist 85: 324-337 (1997)*

[39] P. G. Collins, P. Avouris. Nanotubes for Electronics. *Scientific American Magazine, December 2000*

[40] L. C. Qin, D. Zhou, A. R. Krauss, D. M. Gruen. Growing Carbon Nanotubes by Microwave Plasma-Enhanced Chemical Vapor Deposition. *Applied Physics Letters 72 (26): 3437-3439 (1998)*

[41] M. Terrones, N. Grobert, J. Olivares, J. P. Zhang, H. Terrones, K. Kordatos, W. K. Hsu, J. P. Hare, P. D. Townsend, K. Prassides, A. K. Cheetham, H. W. Kroto, D. R. M. Walton. Controlled Production of Aligned-Nanotube Bundles. *Nature 388: 52-55 (1997)*

[42] P. Nikolaev , M. J. Bronikowski, R. K. Bradley, F. Fohmund, D. T. Colbert, K. A. Smith, R. E. Smalley. Gas-Phase Catalytic Growth of Single-Walled Carbon Nanotubes from Carbon Monoxide. *Chemical Physics Letters 313: 91-97 (1999)*

[43] M. Ge, K. Sattler. Bundles of Carbon Nanotubes Generated by Vapor-Phase Growth. *Applied Physics Letters 64 (6): 710-711 (1994)*

[44] G. Che, B. B. Lakshmi, C. R. Martin, E. R. Fisher, R. S. Ruoff. Chemical Vapor Deposition Based Synthesis of Carbon Nanotubes and Nanofibers using a Template Method. *Chemistry of Materials 10 (1): 260-267 (1998)*

[45] W. Z. Li, S. S. Xie, L. X. Qian, B. H. Chang, B. S. Zhou, W. Y. Zho, R. A. Zhao, G. Wang. Large-Scale Synthesis of Aligned Carbon Nanotubes. *Science 274: 1701-1703 (1996)*

[46] X. X. Zhang, Z. Q. Li, G. H. Wen, K. K. Fund, J. Chen, Y. Li. Microstructure and Growth of Bamboo-Shaped Carbon Nanotubes. *Chemical Physics Letters 333 (6): 509-514 (2001)*

[47] C. Bower, W. Zhu, S. Jin, O. Zhou. Plasma-Induced Alignment of Carbon Nanotubes. *Applied Physics Letters 77 (6): 830-832 (2000)*

[48] S. Fan, M. Chapline, N. Franklin, T. Tombler, A. Cassell, H. Dai. Self-Oriented Regular Arrays of Carbon Nanotubes and their Field Emission Properties. *Science 283: 512-514 (1999)*

[49] H. Dai, J. Kong, C. Zhou, N. Frankin, T. Tombler, A. Cassell, S. Fan, M. Chapline. Controlled Chemical Routes to Nanotube Architectures, Physics and Devices. *Journal of Physical Chemistry 103: 11246-11255 (1999)*

[50] H. Dai. Controlling Nanotube Growth. *Physicsworld 13: 43-47 (2000)*

[51] N. R. Franklin, H. J. Dai. An Enhanced CVD Approach to Extensive Nanotube Networks with Directionality. *Advanced Materials 12 (12): 890-893 (2000)*

[52] M. M. J. Treacy, T. W. Ebbesen, T. M. Gibson. Exceptionally High Young's Modulus Observed for Individual Carbon Nanotubes. *Nature 381: 678-680 (1996)*

[53] E. W. Wong, P. E. Sheehan, C. M. Lieber. Nanobeam Mechanics: Elasticity, Strength, and Toughness of Nanorods and Nanotubes. *Science 2777: 1971-1975 (1997)*

[54] P. Poncharal, Z. L. Wang, D. Ugarte, W. A. De Heer. Electrostatic Deflections and Electromechanical resonances of Carbon Nanotubes. *Science 283: 1513-1516 (1999)*

[55] J. P. Salvetat, G. A. D. Briggs, J. M. Bonard, R. R. Bacsa, A. J. Kulik, T. Stockli, N. A. Burnham, L. Forro. Elastic and Shear Modulo of Single-Walled Carbon Nanotube Ropes. *Physical Review Letter 82 (5): 944-947 (1999)*

[56] M. F. Yu, O. Lourie, M. Dyer, K. Moloni, T. F. Kelly, R. S. Ruoff. Strength and Breaking Mechanism of Multi-Walled Carbon Nanotubes under Tensile Load. *Science 287: 637-639 (2000)*

[57] M. F. Yu, B. S. Files, S. Arepalli, R. S. Ruoff. Tensile Loading of Ropes of Single Wall Carbon Nanotubes and their Mechanical Properties. *Physical Review Letter 84 (24): 5552-5555 (2000)*

[58] G. Overney, W. Zhong D. Tomanek. Structural Rigidity and Low Frequency Vibrational Modes of Long Carbon Tubules. *Zeitschrift Fur Physik D-Atoms Molecules and Clusters 27 (1): 93-96 (1993)*

[59] J. P. Lu. Elastic Properties of Single and Multilayered Nanotubes. *Journal of the Physics and Chemistry of Solids 58 (11): 1649-1652 (1997)*

[60] E. Hernandez, C. Goze, P. Bernier, A. Rubio. Elastic Properties of C and $B_xC_yN_z$ Composite Nanotubes. *Physical Review Letters 80 (20): 4502-4505 (1998)*

[61] V. N. Popov, V. E. V. Doren, M. Balkanski. Elastic Properties of Crystals of Single-Walled Carbon Nanotubes. *Solid State Communications 114: 395-399 (2000)*

[62] L. Vaccarini, C. Goze, L. Henrard, E. Hernandez, P. Bernier, A. Rubio. Mechanical and Electronic Properties of Carbon and Boron-Nitride Nanotubes. *Carbon 38 (11-12): 1681-1690 (2000)*

[63] B. I. Yakobson, M. P. Campbell, C. J. Brabec, J. Bernholc. High Strain Rate Fracture and C-Chain Unraveling in Carbon Nanotubes. *Computational Materials Science 8 (4): 341-348 (1997)*

[64] J. Bernholc, C. J. Brabec, M. Nardelli, A. Maiti, C. Roland, B. I. Yakobson. Theory of Growth and Mechanical Properties of Nanotubes. *Applied Physics A-Materials Science and Processing 97 (1): 39-46 (1998)*

[65] D. Qian, E. C. Dickey, R. Andrews, T. Rantell. Load Transfer and Deformation Mechanisms in Carbon Nanotube-Polystyrene Composites. *Applied Physics Letters 76 (20): 2868-2870 (2000)*

[66] C. Q. Ru. Effective Bending Stiffness of Carbon Nanotubes. *Physical Review B 62 (15): 9973-9976 (2000)*

[67] C. Q. Ru. Degraded Axial Buckling Strain of Multiwalled Carbon Nanotubes due to Interlayer Slip. *Journal of Applied Physics 89: 3426-3433 (2001)*

[68] A. N. Kolmogorov, V. H. Crespi. Smoothest Bearings: Interlayer Sliding in Multiwalled Carbon Nanotubes. *Physical Review Letters 85 (22): 4727-4730 (2000)*

[69] J. W. Mintmire, C. T. White. Electronic and Structural Properties of Carbon Nanotubes. *Carbon 33, 7, 893-902 (1995)*

[70] M. S. Dresselhaus, G. Dresselhaus, P. C. Eklund. Science of Fullerenes and Carbon Nanotubes.*London: Academic Press, 1996.*

[71] J.A. Stroscio, W. J. Kaiser. Scanning Tunneling Microscopy. *New York: Academic Press 1993*

[72] Ti W. Odom, J. L. Huang; P. Kim, C. M. Lieber. Atomic Structure and Electronic Properties of Single-Walled Carbon Nanotubes. *Nature 391: 6662, 62-64 (1998)*

[73] S. J. Tans, M. Devoret, H. Dai, A. Thess, R. Smalley, L. Geerligs, C. Dekker. Individual Single-Wall Carbon Nanotubes as Quantum Wires. *Nature 386: 474-477 (1997)*

[74] M. Bockrath, D. Cobden, P. McEuen, N. Chopra, A. Zettl, A. Thess, R. Smalley. Single-Electron Transport in Ropes of Carbon Nanotubes. *Science 275: 1922-1925 (1997)*

[75] A. Cassell, N. Franklin, T. Tombler, E. Chan, J. Han, H. Dai. Directed Growth of Free-Standing Single-Walled Carbon Nanotubes. *Journal of the American Chemical Society 121: 7975-7976 (1999)*

[76] H. Dai, J. Hafner, A. Rinzler, D. Colbert, R. Smalley. Nanotubes for Nanoprobes. *Nature 384: 147-150 (1996)*

[77] S. Frank, P. Poncharal. Carbon Nanotube Quantum Resistors. *Science 280 : 5370, 1744 (1998)*

[78] B. Q. Wei, R. Vajtai, P. M. Ajayan. Reliability and Current Carrying Capacity of Carbon Nanotubes. *Applied Physics Letters 79 (8): 1172-1174 (2001)*

[79] M. Nardelli, J. Bernholc. Mechanical Deformations and Coherent Transport in Carbon Nanotubes. *Physics Reviews B 60: R16338-16341 (1998)*

[80] A. Rochefort, D. Salahub, P. Avouris. The Effect of Structural Distortions on the Electronic Structure of Carbon Nanotubes. *Chemical Physics Letters 297: 45-50 (1998)*

[81] A. Rochefort, F. Lesage, D. Salahub, P. Avouris. Conductance of Distorted Carbon Nanotubes. *Physics Reviews B 60: 13824-13830 (1999)*

[82] T. Tombler, C. Zhou, L. Alexeyev, J. Kong, H. dai, L. Liu, C. Jayanthi, M. Tang, S. Wu. Reversible Nanotube Electro-Mechanical Characteristics under Local Probe Manipulation. *Nature 405: 769- 772 (2000)*

[83] J. Hone, M. Whitney, A. Zettle. Conductivity of Single-Walled Carbon Nanotube. *Synthetic Metals 103: 2498-2499 (1999)*

[84] J. W Che, T. Cagin, W. A. Goddard III. Thermal Conductivity of Carbon Nanotubes. *Nanotechnology 11 (2): 65-69 (2000)*

[85] Y. K. Kwon, S. Berber, D. Tomanek. Unusually High Thermal conductivity of Carbon Nanotubes. *Physics. Review Letters 84 (20): 4613-4616 (2000)*

[86] M. Fujii, X. Zhang, H. Q. Xie, H. Ago, K. Takahashi, T. Ikuta, H. Abe, T. Shimizu. Measuring the Thermal Conductivity of a Single Carbon Nanotube. *Physics Review Letters 95, 065502-1 – 065502-4 (2005)*

[87] P. Kim, L. Shi, A. Majumdar, P. L. McEuen. Thermal Transport Measurements of Individual Multiwalled Nanotubes. *Physics Review Letters 87 (21): 215502-1 - 215502-4 (2001)*

[88] G. Zhang, B. W. Li. Thermal Conductivity of Nanotubes Revisited: Effects of Chirality, Isotope Impurity, Tube Length, and Temperature.*The Journal of Chemical Physics 123: 114714-1 - 114714-4 (2005)*

[89] Y. Yosisa. High Temperature Shrinkage of Single-Walled Carbon Nanotube Bundles up to 1600 K. *Journal of Applied Physics 87 (7): 338-3341. (2000)*

[90] Y. Maniwa, R. Fujiwara, H. Kira, H. Tou, H. Kataura, S. Suzuki, Y. Achiba, E. Nishibori, M. Takata, M. Sakata, A. Fujiwara, H. Suematsu. Thermal Expansion of Single-Walled Carbon Nanotube (SWNT) Bundles: X- ray Diffraction Studies. *Physical Review B 64: 241402-1 - 241402-3 (2001)*

[91] N. R. Raravikar, P. Keblinski, A. M. Rao, M. S. Dresselhaus, L. S. Schandler, P. M Ajayan. Temperature Dependence of Radial Breathing Mode Raman Frequency of Single-Walled Carbon Nanotubes. *Physical Review B 66: 235424-1 - 235424-9 (2002)*

[92] Y. Kyun, S. Berber, D. Tomanek. Thermal Contraction of Carbon Fullerenes and Nanotubes. *Physical Review Letters 92 (1): 015901-1 – 015901-4 (2004)*

[93] H. Jiang, B. Liu, Y. Huang, K. C. Hwang. Thermal Expansion of Single Wall Carbon Nanotubes. *Journal of Engineering Materials and Technology 126 (3): 265-270(2004)*

[94] N. Chandra, H. Ghonem. Interfacial Mechanics of Push-Out Test: Theory and Experiments.*Composites: Part A, 32 (3-4): 575-584 (2001)*

[95] P. M. Ajayan, T. W. Ebbesen, T. Ichihashi, S. Iijima, K. Tanigaki, H. Hiura. Opening Carbon Nanotubes with Oxygen and Implications for Filling. *Nature 362: 522-525 (1993)*

[96] T. W. Ebbesen. Wetting, Filling and Decorating Carbon Nanotubes. *Journal of Physics and Chemistry of Solids 57 (6-8): 951-955 (1996)*

[97] K. Hernadi, A. Siska, L. Thien-Nga, L. Forro, I. Kiricsi. Reactivity of Different Kinds of Carbon during Oxidative Purification of Catalytically Prepared Carbon Nanotubes. *Solid State Ionics 141-142: 203-209 (2001)*

[98] C. Sekar, C. Subramanian. Purification and Characterization of Buckminsterfullerene, Nanotubes and their Byproducts. *Vacuum 47 (11): 1289-1292 (1996)*

[99] Y. C. Feng, G. M. Zhou, G. P. Wang, M. Z. Qu, Z. L. Yu. Removal of some Impurities from Carbon Nanotubes. *Chemical Physics Letters 375 (5-6): 645-648 (2003)*

[100] T. Jeong, W. Y. Kim, Y. B. Hahn. A New Purification Method of Single-Wall Carbon Nanotubes using H_2S and O_2 Mixture Gas. *Chemical Physics Letters 344 (1-2): 18-22 (2001)*

[101] M. Yumura, S. Ohshima, K. Uchida, Y. Tasaka, Y. Kuriki, F. Ikazaki, Y. Saito, S. Uemura. Synthesis and Purification of Multi-Walled Carbon Nanotubes for Field Emitter Applications. *Diamond and Related Materials 8: 785-791 (1999)*

[102] S. Iijima, T. Ichihashi. Single-Shell Carbon Nanotubes of 1-nm Diameter. *Nature 363: 603-605 (1993)*

[103] K. Esumi, M. Ishogami, A. Nakajima, K. Sawada, H. Honda. Chemical Treatment of Carbon Nanotubes. *Carbon 34 (2): 279- 281 (1996)*

[104] C. Y. Moon, Y. S. Kim, E. C. Lee, Y. G. Jin, K. J. Chang. Mechanism for Oxidative Etching in Carbon Nanotubes. *Physical Reviews B 65: 155401-1 - 155401-4 (2002)*

[105] D. J. Mann, W. L. Hase. Direct Dynamics Simulations of the Oxidation of a Single Wall Carbon Nanotube. *Physical Chemistry Chemical Physics 3 (19): 4376-4383 (2001)*

[106] S. Gajewski, H. E. Maneck, U. Knoll, D. Neubert, I. Dorfe, R. Mach, B. Strausz, J. F. Friedrich. Purification of Single Walled Carbon Nanotubes by Thermal Gas Phase Oxidation. *Diamond and Related Materials 12 (3-7): 816-820 (2003)*

[107] Z. Xu, X. Chen, X. H. Qu, S. J. Dong. Electrocatalytic Oxidation of Catechol at Multi-Walled Carbon Nanotubes Modified Electrode. *Electroanalysis 16 (8): 684-687 (2004)*

[108] A. Leonhardt, M. Ritschel, R. Kozhuharova, A. Graff, T. Mühl, R. Huhle, I. Monch. Synthesis and Properties of Filled Carbon Nanotubes. *Diamond and Related Materials 12 (3-7): 790-793 (2003)*

[109] N. Zhang, J. Xie, V. K. Varadan. Functionalization of Carbon Nanotubes by Potassium Permangante Assisted with Phase Transfer Catalyst. *Journal of Smart Materials and Structures 11: 962-965 (2002)*

[110] C. A. Dyke, M. T. James. Overcoming the Insolubility of Carbon Nanotubes Through High Degrees of Sidewall Functionalization. *Chemistry - A European Journal 10 (4): 812-817 (2004)*

[111] A. Hirsch. Functionalization of Single-Walled Carbon Nanotubes. *Angewandte Chemie International 41(11): 1853-1859 (2002)*

[112] H. S. Kang. Organic Functionalization of Sidewall of Carbon Nanotubes. *Journal of Chemical Physics 121 (14): 6967-6971 (2004)*

[113] S. Banerjee, T. Hemraj-Benny, S. S. Wong. Covalent Surface Chemistry of Single-Walled Carbon Nanotubes.*Advanced Materials 17 (1): 17-29 (2005)*

[114] X. F. Wu, G. Q. Shi. Synthesis of a Carboxyl-Containing Conducting Oligomer and Non-Covalent Sidewall Functionalization of Single-Walled Carbon Nanotubes. *Journal of Materials Chemistry 15 (18): 1833-1837 (2005)*

[115] M. Holzinger, O. Vostrowsky, A. Hirsch, F. Hennrich, M. Kappes,R. Weiss, F. Jellen, Frank. Sidewall Functionalization of Carbon Nanotubes. *Angewandte Chemie, International Edition 40 (21): 4002–4005 (2001)*

[116] N. Tagmatarchis, V. Georgakilas, M. Prato, H. Shinohara. Sidewall Functionalization of Single-Walled Carbon Nanotubes Through Electrophilic Addition. *Chemical Communications 18: 2010-2011 (2002)*

[117] H. P. Peng, L. B. Alemany, J. L. Margrave, V. N. Khabashesku. Sidewall Carboxylic Acid Functionalization of Single-Walled Carbon Nanotubes. *Journal of the American Chemical Society 125 (49): 15174-15182 (2003)*

[118] E. T. Mickelson, I. W. Chiang, J. L. Zimmerman, P. J. Boul, J. Lozano, J. Liu, R. E. Smalley, R. H. Hauge, J. L. Margrave. Solvation of Fluorinated Single-Wall Carbon Nanotubes in Alcohol Solvents. *Journal of Physical Chemistry B 103 (21): 4318–4322 (1999)*

[119] K. N. Kudin, H. F. Bettinger, G. E. Scuseria. Fluorinated Single-Wall Carbon Nanotubes.*Physical Reviews B 63: 045413-1 - 045413-8 (2001)*

[120] K. H. An, K. G. Jeon, D. J. Bae, C. Jo, C. Y. Yang, C. Y. Park, Y. H. Lee. X-Ray Photoemission Spectroscopy Study of Fluorinated Single-Walled Carbon Nanotubes. *Applied Physics Letters 80(22): 4235-4237, (2002)*

[121] N. G. Lebedev, I. V. Zaporotskova, L. A. Chernozatonskii. Fluorination of Carbon Nanotubes within the Molecular Cluster Method. *Microelectronic Engineering, Volume 69 (2-4): 511-518 (2003)*

[122] A. Hamwi, H. Alvergnat, S. Bonnamy, F. Beguin. Fluorination of Carbon Nanotubes. *Carbon 35 (6): 723-728 (1997)*

[123] H. Touhara, F. Okino. Property Control of Carbon Materials by Fluorination. *Carbon 38 (2): 241-267 (2000)*

[124] N. Khare, P. Wilhite, M. Meyyappan. The Fluorination of Single Wall Carbon Nanotubes Using Microwave Plasma. *Nanotechnology, 15: 1650-1654 (2004)*.

[125] S. Kawasaki, K. Komatsu, F. Okino, H. Touhara, H. Kataura. Fluorination of Open- and Closed-End Single-Walled Carbon Nanotubes. *Physical Chemistry Chemical Physics 6(8): 1769-1772 (2004)*

[126] S. Meisha. Nanotube Reinforced Thermoplastic Polymer Matrix Composites. *Diss. Rice University 2003.*

[127] B. Ni, S. B. Sinnott. Chemical Functionalization of Carbon Nanotubes Through Energetic Radical Collisions. *Physical Review B 61: R16343-R16346 (2000)*

[128] H. Lim, H. J. Jung, S. K. Joo. Control of Carbon Nanotube's Shape by Ion Bombardment. *Microelectronic Engineering 69 (1): 81-88 (2003)*

[129] J. A. V. Pomoell, A. V. Krasheninniko, K. Nordlund, J. Keinonen.Ion Ranges and Irradiation-Induced Defects in Multiwalled Carbon Nanotubes. *Journal of Applied Physics 96(5): 2864-2871 (2004)*

[130] *Engineered Materials Handbook, Volume 1, Composites, ASM International, 1987*

[131] K. El-Hami, K. Matsushige. Covering Single Walled Carbon Nanotubes by the Poly(VDF–co–TrFE) Copolymer. *Chemical Physics Letters 368, 1-2, 168-171 (2003)*

[132] H. Murakami, T. Nomura, N. Nakashima. Noncovalent Porphyrin-Functionalized Single-Walled Carbon Nanotubes in Solution and the Formation of Porphyrin–Nanotube Nanocomposites. *Chemical Physics Letters 378 (5-6): 481-485 (2003)*

[133] J. Y. Kwon, H. D. Kim. Preparation and Properties of Acid-Treated Multiwalled Carbon Nanotube/Waterborne Polyurethane Nanocomposites.*Journal of Applied Polymer Science 96 (2): 595-604 (2005)*

[134] B. Philip, J. I. Xie, J. K. Abraham, V. K. Varadan. A New Synthetic Route to Enhance Polyaniline Assembly on Carbon Nanotubes in Tubular Composites. *Smart Materials & Structures. 13(6):N105-N108 (2004)*

[135] B. Safadi, R. Andrews, E. A. Grulke. Multiwalled Carbon Nanotube Polymer Composites: Synthesis and Characterization of Thin Films.*Journal of Applied Polymer Science 84 (14): 2660-2669 (2002)*

[136] L. S. Schadler, S. C. Giannaris, P. M. Ajayan. Load Transfer in Carbon Nanotube Epoxy Composites.*Applied Physics Letters 73: 3842-3844 (1998)*

[137] R. J. Moraa, J. J. Vilatelaa, A. H. Windle.Properties of Composites of Carbon Nanotube Fibres. *Composites Science and Technology, Article in Press (2009)*

[138] J. K. W. Sandler, S. Pegel, M. Cadek, F. Gojny, M. van Es, J. Lohmar, W. J. Blau, K. Schulte, A. H. Windle, M. S. P. Shaffer. A Comparative Study of Melt Spun Polyamide-12 Fibres Reinforced with Carbon Nanotubes and Nanofibres. *Polymer 45 (6): 2001-2015 (2004)*

[139] P. Pötschke, M. Abdel-Goad, I. Alig, S. Dudkin, D. Lellinger. Rheological and Dielectrical Characterization of Melt Mixed Polycarbonate-Multiwalled Carbon Nanotube Composites. *Polymer 45 (26): 8863-8870 (2004)*

[140] Z. Jin, K. Pramoda, G. Xu, S.H. Goh. Dynamic Mechanical Behavior of Melt-Processed Multi-Walled Carbon Nanotube/Poly(methyl methacrylate) Composites. *Chemical Physics Letters 337: 43-47 (2001)*

[141] P. Potschke, A. R. Bhattacharyya, A. Janke, H. Goering. Melt Mixing of Polycarbonate/Multi-Wall Carbon Nanotube Composites. *Composite Interf 10: 389–404 (2003)*

[142] J. C. Kearns, R. L. Shambaugh. Polypropylene Fibers Reinforced with Carbon Nanotubes. *Journal of Applied Polymer Science 86: 2079–2084 (2002)*

[143] B. Wang, J. M. Li, H. P. Wang, J. M. Jiang, Y. Q. Liu. Rheological Behavior of Spinning Dope of Multiwalled Carbon Nanotube/Polyacrylonitrile. *Composites. Macromolecular Symposia 216 (1): 189-194 (2004)*

[144] S. J. Park, M. S. Cho, S. T. Lim, H. J. Choi, M. S. Jhon. Synthesis and Dispersion Characteristics of Multi-Walled Carbon Nanotube Composites with Poly(methyl methacrylate) Prepared by In-Situ Bulk Polymerization. *Macromolecular Rapid Communications .24 (18): 1070-1073 (2003)*

[145] W. Feng, X. D. Bai, Y. Q. Lian, J. Liang, X. G. Wang, K. Yoshino. Well-Aligned Polyaniline/Carbon-Nanotube Composite Films Grown by In-Situ Aniline Polymerization. *Carbon 41 (8): 1551-1557 (2003)*

[146] B. H. Chang, Z. Q. Liu, L. F. Sun, D. S. Tang, W. Y. Zhou, G. Wang, L. X. Qian, S. S. Xie, J. H. Fen, M. X. Wan. Conductivity and Magnetic Susceptibility of Nanotube/Polypyrrole Nanocomposites. *Journal of Low Temperature Physics 119 (1/2): 41-48 (2001)*

[147] Y. S. Oh, C. S. Kim, D. S. Lim, D. S. Cheong. Fracture Strengths and Microstructures of Si3N4/SiC Nanocomposites Fabricated by In-Situ Process. *Scripta Materialia 44 (8-9): 2079-2081 (2001)*

[148] D. Y. Wang, C. A. Wilkie. In-Situ Reactive Blending to Prepare Polystyrene–Clay and Polypropylene–Clay Nanocomposites. *Polymer Degradation and Stability 80 (1): 171-182 (2003)*

[149] C. Velasco-Santos, A.L. Martinez-Hernandez, F. T. Fisher, R. Ruoff, V. M. Castano. Improvement of Thermal and Mechanical Properties of Carbon Nanotube Composites through Chemical Functionalization.*Chemistry of Materials 15: 4470–4475 (2003)*

[150] K. W. Putz, C. A. Mitchell, R. Krishnamoorti, P. F. Green. Elastic Modulus of Single-Walled Carbon Nanotube/Poly(methyl methacrylate) Nanocomposites. *Journal of Polymer Science Part B: Polymer Physics 42: 2286–2293 (2004)*

[151] M. S. P. Shaffer, A. H. Windle. Fabrication and Characterization of Carbon Nanotube/poly(vinyl alcohol) composites. *Advanced Materials 11 (11): 937–41 (1999)*

[152] M. Cadek, J. N. Coleman, V. Barron, K. Hedicke, W. J. Blau. Morphological and Mechanical Properties of Carbon-Nanotube-Reinforced Semicrystalline and Amorphous Polymer Composites. *Applied Physics Letters 81 (27): 5123–5 (2002)*

[153] S. J. V. Frankland, A. Caglar, D. W. Brenner, M. Griebel. Molecular Simulation of the Influence of Chemical Cross-Links on the Shear Strength of Carbon Nanotube–Polymer Interfaces. *Journal of Physical Chemistry B 106 (12): 3046–8 (2002)*

[154] R. Haggenmueller, H. H. Gommans, A. G. Rinzler, J. E. Fischer, K. I. Winey. Aligned Single-Wall Carbon Nanotubes in Composites by Melt Processing Methods. *Chemical Physics Letters 330: 219-225 (2000)*

[155] X. Y. Gong, J. Liu, S. Baskarn, R. D. Voise, J. Yong. Surfactant-Assisted Processing of Carbon Nanotube/Polymer Composites. *Chemistry of Materials 12: 1049-1052 (2000)*

[156] M. C. Paiva, B. Zhou, K. A. S. Fernando, Y. Lin, J. M. Kenndey, Y. P. Sun. Mechanical and Morphological Characterization of Polymer-Carbon Nanocomposites from Functionalized Carbon Nanotubes. *Carbon 42 (14): 2849-2854 (2004)*

[157] A. P. Yu, H. Hu, E. Bekyarova, M. E. Itkis, J. Gao, B. Zhao, R. C. Haddon. Incorporation of Highly Dispersed Single-Walled Carbon Nanotubes in a Polyimide Matrix. *Composites Science and Technology 66 (9): 1190-1197 (2006)*

[158] D. Qian, E. C. Dickey. In-Situ Transmission Electron Microscopy Studies of Polymer-Carbon Nanotube Composite Deformation. *Journal of Microscopy 204: 39-45 (2001)*

[159] H. D. Wagner, O. Lourie, Y. Feldman, R. Tenne. Stress-Induced Fragmentation of Multiwall Carbon Nanotubes in a Polymer Matrix. *Applied Physics Letters 72 (2): 188-190 (1998)*

[160] O. Lourie, D. M. Cox, H. D. Wagner. Buckling and Collapse of Embedded Carbon Nanotubes. *Physical Review Letters 81: 1638-1641 (1998)*

[161] V. G. Hadjiev, M. N. Live, S. Arepalli, P. Nikolaev, B. S. Files. Raman Scattering Test of Single-Wall Carbon Nanotube Composites. *Applied Physics Letters 78: 3193-3195 (2001)*

[162] J. R. Wood, Q. Zhao, H. D. Wanger. Orientation of Carbon Nanotubes in Polymers and its Detection by Raman Spectroscopy. *Composites: Part A 32: 391-9 (2001)*

[163] C. A. Cooper, R. J. Young, M. Halsall. Investigation into the deformation of Carbon Nanotubes and their Composites through the Use of Raman Spectroscopy. *Composites: Part A 32: 401-411 (2001)*

[164] L. Jin, C. Bower, O. Zhou. Alignment of Carbon Nanotubes in a Polymer Matrix by Mechanical Stretching. *Applied Physics Letters 73 (9): 1197-1199 (1998)*

[165] B. Vigolo, A. Penicaud, C. Coulon, C. Sauder, R. Pailler, C. Journet, P. Bernier, P. Poulin. Macroscopic Fibers and Ribbons of Oriented Carbon Nanotubes. *Science 290: 1331-1334 (2000)*

[166] D. A. Walters, M. J. Casavant, X. C. Qin, C. B. Huffman, O. J. Boul, L. M. Ericson, E. H. Haroz, M. J. O'Connell, K. Smith, D. T. Colbert, R. E. Smalley.In-Plane-Aligned Membranes of Carbon Nanotubes. *Chemical Physics Letters 338: 14-20 (2001)*

[167] http://www.nanotubes.com.cn/ *Shenzhen Nanotech Port Company Limited (NTP)*

[168] J. Chen, M. A. Hamon, H. Hu, Y. Chen, A. M. Rao, P.C. Eklund, R. C. Haddon. Solution Properties of Single-Walled Carbon Nanotubes. *Science 282: 95-99 (1998)*

[169] K. T. Lau, M. Lau, C. K. Lam, H. Y. Cheung, F. L. Sheng, H. L. Li. Thermal and Mechanical Properties of Single-Walled Carbon Nanotube Bundle-Reinforced Epoxy Nanocomposites: The Role of Solvent for Nanotube Dispersion. *Composites Science & Technology 65: 719-725 (2005)*

[170] K. Mukhopadhyay, C. D. Dwivedi, G. N. Mathur. Conversion of Carbon Nanotubes to Carbon Nanofibers by Sonication. *Carbon 40: 1369 –1383 (2002)*

[171] http://www.internationalequipmentsindia.com/ *International Equipments*

[172] K. P. Menard.Dynamic Mechanical Analysis: A Practical Introduction. *Boca Raton: CRC Press (1999)*

[173] M. W. Marshall, S. Popa-Nita, J. G. Shapter. Measurement of Functionalised Carbon Nanotube Carboxylic Acid Groups using a Simple Chemical Process. *Carbon 44: 1137-1141 (2006)*

[174] I. M. Ward, J. Sweeney. The Mechanical Properties of Solid Polymers. *Wiley (2004)*

[175] G. X. Chen, H. S. Kim, B. H. Park, J. S. Yoon. Multi-Walled Carbon Nanotubes Reinforced Nylon 6 Composites. *Polymer 47: 4760-4767 (2006)*

[176] K. Kitaura. A Procedure to Generate Ab Initio Intermolecular Potential Function. *Fluid Phase Equilibria 1995; 104(1): 57-69 (1995)*

[177] Y. P. Liu, K. Kim, B. J. Berne, R. A. Friesner, S. W. Rick. Constructing Ab Initio Force Fields for Molecular Dynamics Simulations. *The Journal of Chemical Physics 108(12): 4739-4755 (1998)*

[178] F. Gygi. Ab Initio Molecular Dynamics in Adaptive Coordinates. *Physical Review B 51(16): 11190-11193 (1995)*

[179] S. Hammes-Schiffer, H. C. Andersen. Ab Initio and Semiempirical Methods for Molecular Dynamics Simulations based on general Hartree–Fock Theory. *The Journal of Chemical Physics 99(1): 523-532 (1993)*

[180] A. K. Mazur. Quasi-Hamiltonian Equations of Motion for Internal Coordinate Molecular Dynamics of Polymers. *Journal of Computational Chemistry 18(11): 1354-1364 (1997)*

[181] H. Tanaka. Critical Dynamics and Phase-Separation Kinetics in Dynamically Asymmetric Binary Fluids: New Dynamic Universality Class for Polymer Mixtures or Dynamic Crossover? *The Journal of Chemical Physics 100(7): 5323-5337 (1994)*

[182] S. F. Edwards, K. F. Freed. Theory of the Dynamical Viscosity of Polymer Solutions. *The Journal of Chemical Physics 61(3): 1189-1202 (1974)*

[183] S. Trohalaki. Molecular dynamics simulation of a single-component molecular composite: poly(*p*-phenylene benzobisthiazole)/*meta*-poly(aryl ether ketone) block copolymer *Polymer 37(10): 1841-1845 (1996)*

[184] R. Szorek. A Dynamic Model for Locally Stiff Straight Chain Polymers *The Journal of Chemical Physics 83(3): 1421:1423 (1985)*

[185] P. L. Bonate. A Brief Introduction to Monte Carlo Simulation. *Clinical Pharmacokinetics 40(1): 15-22 (2001)*

[186] B. Tombuyses, P. R. DeLuca, C. Smidts. Backward Monte Carlo for Probabilistic Dynamics. *Mathematics and Computers in Simulation1998; 47(2-5): 493-505 (1998)*

[187] U. Ravaioli, C. H. Lee, M. B. Patil. Monte Carlo Simulation of Microwave Devices. *Mathematics and Computer Modelling 23(8-9): 167-179 (1996)*

[188] D. Kumar, S. J. Thomson. Implementing Direct Mongd-Carlo Simulation in Batch Mode. *Computer and Electronics in Agriculture 12(2): 163-171 (1995)*

[189] C. Y. Li, T. W. Chou. A Structural Mechanics Approach for the Analysis of Carbon Nanotubes. *International Journal of Solids and Structures 40(10): 2487-2499 (2003)*

[190] K. Sakakibara, K. Shimazaki, K. H. Chen, J. H. Li. Molecular Mechanics (MM3) Calculations on Phosphonamidate Compounds. *Journal of Molecular Structure 556(1-3): 283-291 (2000)*

[191] Z. J. Wang, M. Chen, Z. Y. Guo, C. Yang. Molecular Dynamics Study on the Liquid–Vapor Interfacial Profiles. *Fluid Phase Equilibria 183-184: 321-329 (2001)*

[192] R. W. Harrison. Integrating Quantum and Molecular Mechanics. *Journal of Computational Chemistry 20(15): 1618-1633 (1999)*

[193] N. L. Allinger. MM2 - Hydrocarbon Force-Field Utilizing V1 and V2 Torsional Terms. *Journal of the American Chemical Society 99: 8127-8134 (1977).*

[194] N. L. Allinger, Y. H Yuh. *Quantum Chemistry Program Exchange, Bloomington, Indiana, Program# 395.*

[195] U. Burkert, N. L. Allinger. Molecular Mechanics. *ACS Monograph 177, American Chemical Society, Washington, D.C. (1982).*

[196] D. Frenkel, B. Smit. Understanding Molecular Simulation From Algorithms to Applications. *Academic Press (1996)*

Vita

Wai-Yin Tam was born in Hong Kong on September 07, 1977. Fifth of the six daughters in her family. She was awarded with a Bachelor degree (with Honor) in Mechanical Engineering from the Hong Kong Polytechnic University in year 2000. And in the same year, she received the degree of Master of Engineering in Mechanical Engineering from the same university as she started her master program on the third year in her undergraduate studies.

After the graduation, she was working as an engineer trainee in a construction company and, later, as a research assistant in a University for almost two years. Soon after, she moved to New Orleans to pursue her PhD in Engineering and Applied Sciences at the Mechanical Engineering Department of University of New Orleans. She worked as a Graduate Research Assistant at the Mechanical Engineering Department at this university until fall 2004 and then moved to Hong Kong to continue her research work. Currently, she is working for the Department of Mechanical Engineering in The Hong Kong Polytechnic University as a research assistant.